VIBRATIONAL AND ELECTRONIC PROPERTIES OF IMPURITIES IN SEMICONDUCTORS

James M. Noras

A Thesis Submitted for the Degree of PhD
at the
University of St Andrews

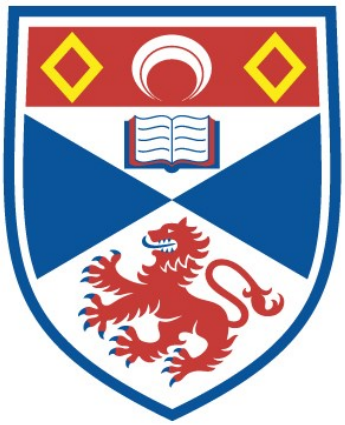

1978

Vibrational and Electronic Properties of Impurities in Semiconductors

A Thesis

presented by

James M Noras BSc

to the

University of St Andrews

in application for the

Degree of Doctor of Philosophy

ProQuest LLC.
789 East Eisenhower Parkway
P.O. Box 1346
Ann Arbor, MI 48106 – 1346

Abstract

Properties of impurities in semiconductors have been investigated by means of absorption spectroscopy. The studies have concentrated not on one topic but on a range of types of impurity behaviour: they may be summarized under three main headings.

(1) Fine Structure in Absorption Bands.

The shapes and temperature-dependent widths of absorption bands of impurities may be understood qualitatively in terms of vibrational coupling with the lattice. The spectra studied show evidence of Jahn-Teller coupling, one particular form of such an interaction, and it has been found possible in most cases to relate the fine structure observed to features in the phonon spectra of the host lattices.

(2) Antiresonances.

Since the materials studied are such that in some cases a clear and complete ascription of spectral fine structure can be made in terms of Jahn-Teller coupling, it is possible unambiguously to identify certain other features not previously observed in any systems. These are vibronic anti-resonances, resulting from interference between vibrational levels of the lattice and impurity states of mixed electronic-vibrational nature. In the absence of adequate models, these features are discussed phenomenologically.

An electronic analogue of these effects, involving spontaneous ionization of excited impurities, has been looked for, but no convincing instances have been found.

(3) Photoionization.

The charge state and electronic configuration of an impurity depend not only on bonding requirements at the lattice site, but on other factors such as the position of the Fermi level in the bulk medium, and may be

changed by photo-excitation. Electrons or holes being removed from an impurity and released into crystal bands results in intense absorption. The form of the absorption cross-section for these processes follows a simple power law near the threshold of ionization, so the value of the ionization energy may be determined quite readily.

In this way the positions of a deep level of nickel in zinc selenide and in zinc sulphide have been determined with respect to the conduction and valence bands of these materials. This important information has not been obtained directly for any other transition metal impurity.

In addition, fine structure has been seen near the ionization thresholds in these materials. This is due to the coulomb potential of the ionized centre, charged with respect to the lattice, being able to bind holes in hydrogenic orbits. The phonon coupling to this shallow level is found to be much stronger than is observed in absorption bands due to photoionization.

Declaration

I hereby certify that this thesis has been composed by me, and is a record of work done by me, and has not previously been presented for a Higher Degree.

The research was carried out in the Wolfson Institute of Luminescence, within the School of Physical Sciences in the University of St Andrews, under the supervision of Mr J W Allen.

J M Noras

Certificate

I certify that James M Noras, BSc, has spent nine terms at research work in the Wolfson Institute of Luminescence, within the School of Physical Sciences in the University of St Andrews under my direction, that he has fulfilled the conditions of the Resolution of the University Court, 1967, No.1, and that he is qualified to submit the accompanying thesis in application for the Degree of Doctor of Philosophy.

Research Supervisor

Career

After matriculating in the University of St Andrews, in October 1969, I studied Mathematics and Physics, and in 1972 was awarded the William D. Brodie Prize for Physics. In 1973 I obtained the Degree of Bachelor of Science with First Class Honours in Physics, and was awarded the Neil Arnott Prize for Physics and the Miller Prize of the Faculty of Science.

In October 1973, following the award of a Carnegie Scholarship, I was enrolled as a Research Student under Resolution of the University Court, 1967, No.1, as a candidate for the Degree of Doctor of Philosophy.

Acknowledgements

Firstly I thank the Carnegie Institute for the Universities of Scotland for providing me with financial support.

Secondly I must confess my debt to Dr J M Baranowski, and warmly express my gratitude to him for the knowledge and expertise that he transmitted to me during my first few postgraduate terms. He was closely involved in the early research and in no small way determined the course of the project.

Most of all I thank my supervisor, John Allen, for his unfailing support and encouragement. It has been a great privilege to work with him, and to benefit from both his advice and his example.

Rows of books around me stand,
Fence me round on either hand;
Through that forest of dead words
I would hunt the living birds —

Great black birds that fly alone
Slowly through a land of stone,
And the gulls who weave a free
Quilt of rhythm on the sea.

Gavin Maxwell
"Raven Seek Thy Brother"

Contents

Chapter Six : Titanium in ZnSe and ZnS

Chapter Seven : Nickel in ZnSe and ZnS

Chapter Eight : Discussion

CHAPTER ONE

INTRODUCTION

Chapter One

Introduction

> "Hem," said the badger.
> He immediately became paralysed with shyness, and sat blushing at his papers, unable to begin.
>
> "Go on," said the Wart.
>
> "It is not very good," he explained coyly. "It is just a rough draft, you know. I shall alter a lot before I send it in."
>
> "I am sure it must be interesting."
>
> "Oh no, it is not a bit interesting. It is just an odd thing I threw off in an odd half-hour, just to pass the time. But still, this is how it begins."
>
> T H White, "The Sword in the Stone" ch.XXI.

This thesis describes experimental research into the optical properties of semiconductors. It is concerned chiefly with effects due to impurities.

The materials investigated are II-VI compounds containing transition metal ions. Some materials of this type are useful technologically, but those chosen for this project have not yet found any particular application. Instead interest lies in studying their fundamental properties, particularly effects which although seen clearly in these compounds had not been discovered before or which did not have a satisfactory interpretation.

The results may be viewed in a wider context. A recent review shows that systematic examination can reveal many underlying trends and similarities in the behaviour of a large class of solids that appear at first sight to have quite disparate properties [1]. The processes studied in this thesis are expected to occur quite generally and may be of more than academic interest in some cases.

A large amount of information about such materials already exists. Chapter two outlines the models used to account for the main aspects of their optical properties. Only a brief discussion is given but concepts are presented which are fundamental to later sections, including those

dealing with interpretation of results.

Effects that may be neglected in a general treatment often become important when behaviour is studied in detail. For example it is found that the static lattice model of chapter two does not account for the temperature dependence of optical spectra nor for the shape and structure of absorption and emission bands. These can be explained only in terms of dynamic coupling of impurities to lattice vibrations. Many of the processes studied in this work involve this type of interaction, so it is useful, in chapter three, to review the relevant theory.

Chapter four describes the phenomenon of antiresonance. This can be important when a discrete localized state is degenerate with a continuum of extended states. Such a situation can be envisaged easily as occurring in solids, where the localized state might be due to an impurity electronic level or to a local mode of vibration. Interesting effects may arise when these levels interact with electronic band states and phonon continua respectively, as the experimental sections will show.

Most of the results were obtained by standard techniques of absorption spectroscopy, using high resolution at low temperatures. Some details of the apparatus and procedures are given in chapter five together with notes on the preparation of samples.

The results of experiments on crystals containing titanium are contained in chapter six. Much of the evidence presented indicates the effects of vibrational coupling on the energy levels of these systems. Many of the details are interpretedin terms of Jahn-Teller coupling, but there are in addition features which are shown to involve antiresonance between vibrational modes.

Previous work has suggested that in such materials there is a

fairly strong resonant interaction between excited electronic impurity states and the host energy bands [2,3], but the present work does not support this interpretation.

Chapter seven deals with samples containing nickel impurities, and begins by considering the influence of vibrational coupling. There are many similarities in this respect to the systems of the preceding chapter although the interpretation is sometimes less complete.

Apart from transitions of electrons between internal energy levels of the nickel impurity, absorption bands due to photoionization of this centre are seen also. These give valuable information about the positions of impurity energy levels with respect to the energy bands of the solid. Not much experimental work has been done in this area, although there is growing interest in it.

Chapters six and seven are intended to be largely complete on their own, and constitute the original contribution of this thesis. Their main findings are summarized in the final chapter, together with more general discussion and some concluding suggestions.

CHAPTER TWO

ENERGY LEVELS

Chapter Two

Introduction

The properties of solids are changed in many different ways by the addition of dopants or impurities. Perhaps the most important result is that localized energy levels may be introduced. Such energy levels can be classified usefully into two groups: shallow levels and deep levels.

Defects with shallow levels may bind electrons or holes with energies of a tenth of an electron volt or less. Since the charged particles may be liberated quite easily, many of the centres will be emptied at room temperature by thermal excitation. The resulting free carriers may dominate the bulk electrical properties. For this reason, materials containing such impurities have widespread technological importance.

Other impurities bind electrons or holes in deep levels. Although these defects affect the bulk behaviour of the host to some extent, and in ways different from impurities with shallow levels, it is the very existence of deep, localized levels and their special properties that is often of greater importance. With deep centres it is the properties of the impurity, perturbed by its environment, that are of most interest, whereas the opposite applies in the case of shallow levels. For example, if transitions between internal states of an impurity are possible at energies below that of the host band-gap, it may be feasible to prepare doped material with useful optical properties which are dictated by even very small amounts of the particular impurity. Such systems find applications in many areas including the production of luminescent devices, sub-nuclear particle detectors and computer memories.

This thesis is concerned with semiconductors doped with transition metals, which produce deep levels. These materials constitute a large group with a considerable literature devoted to them. Much current work concerns specific details of their properties, such as vibrational effects in optical spectra, and may involve sophisticated treatments. Before approaching these, however, it is necessary to appreciate their more general characteristics. This chapter will acount for these using simple models, and will review concepts used extensively in later sections.

Doping

The formation of the II-VI compounds requires the contributions of the two outer electrons of the cation to the establishment of bonding orbitals. Thus zinc, in zinc sulphide, will donate both 4s electrons, leaving an outer shell of ten d electrons i.e. $3d^{10}$. The doubly ionized iron group elements, consisting of the row in the periodic table from scandium to copper, have the outer shell $3d^n$, where n = 1, ..., 9. Thus any of the transition metal ions may be substituted for zinc in this type of compound, and still satisfy bonding requirement, though perhaps with different force constants. The resulting impurity centre is isoelectronic with respect to the lattice.

Doping of cadmium compounds is possible for similar reasons.

The importance of the substitution is that the incomplete d-shell of the dopant has energy levels not available to the zinc or cadmium atom. Because there are empty states in the d-shell, rearrangement of the electrons may take place into configurations with differing energy. In a free atom the level separations would depend, in the absence of external fields, on electron interaction and spin-orbit coupling. At a crystal site there is an additional perturbation of the d-levels due to charge distribution in the lattice.

Crystal Field

With the exception of cadmium oxide all the II-VI compounds have wurzite or zinc blende structure. Thus in a compound MX, each M atom is surrounded by four X nearest neighbours, lying at the vertices of a perfect or slightly distorted tetrahedron. Any charge distribution must have the periodicity of the crystal so the resulting electrostatic field at a lattice site has tetrahedral symmetry. This field, acting on the d-shell of a substitutional impurity may produce shifts and splittings of the internal energy levels. A calculation of these perturbations from first principles still remains to be done but if the crystal field strength is taken as an experimentally determinable quantity then the measured level scheme can be shown to follow from the theoretical splittings of the d-shell.

With this empirical approach the origin of the electric field is irrelevant, the most important factor being the point symmetry of the impurity site. For this reason the system can be described in terms of a point-ion model, although there may be considerable covalency in the materials involved. Indeed the crystal field splittings tend to be larger for the more covalent crystals, being determined by the position and amount of electric charge in the bonds between atoms rather than by the charges of ions on lattice sites. [4]

Site Symmetry

The Hamiltonian of the localized electrons must have the transformation properties of the point group of the impurity site in the crystal. A system with tetrahedral symmetry has the point group Td, so the electronic wavefunctions are basis functions of this group. Interactions mixing d-states and any other states are much weaker than intra-shell effects, so impurity wavefunctions still remain similar to free ion orbitals.

For a system with tetrahedral symmetry the five-fold orbital degeneracy of the independent electronic d-states is removed by the crystal field, leaving two energy levels, one triply and one doubly degenerate. Wave functions for these levels are basis functions of the irreducible representations T_2 and E respectively. When only one electron is in the d-shell these levels are separated by 10 Dq, where Dq is a parameter giving the strength of the electric potential energy due to the crystal field. With more electrons present, permutations among the levels give multi-electron states which differ in energy by multiples of 10 Dq. These states are further split by spin-orbit coupling and electron correlation.

Spin-orbit coupling has usually a minor effect on the positions of energy levels so the level scheme may be accurately constructed from only three parameters: Dq , B and C. The last two arise from electron interaction and are known as Racah parameters. They differ from their free ion values but are still proportional so that

$$C/B \simeq 4.5 \qquad [5].$$

This is a further constraint on the choice of parameters to describe experimentally obtained spectra, which makes the success of the model even more satisfactory.

Selection Rules

Atomic d-states have even parity and electric dipole transitions between them are forbidden. Such processes do occur in impurity atoms of the types considered here and provide the main features of absorption and emission spectra, rather than magnetic dipole or electric quadrupole transitions which are allowed even in free atoms. This is a direct consequence of the lack of inversion symmetry in the T_d group.

Both p-states, which have odd parity, and the triply degenerate d-levels span T_2. An odd parity component of the crystal field couples the two manifolds so that a proper basis function of T_2 must be a linear combination of the two types of state. These functions have no definite parity, and thus electric dipole transitions between the corresponding levels are not forbidden.

The p-states which are coupled to the d-levels by the crystal field may be impurity states, but interaction with orbitals originating on the ligand atoms is greater. In the latter case the impurity wavefunctions may become more diffuse, with the possibility of charge transfer between the impurity and its surroundings. Doubly degenerate d-states do not interact so strongly with the ligands and so have a different radial distribution. This increases the number of parameters since Dq, B and C will be different for doublet and triplet states. Since the effect of the correction is small, it is generally neglected.

Spin conservation gives another selection rule which is useful in identifying observed transitions, since transitions between levels predominantly of the same spin tend to be strongest and most easily seen. However spin-orbit coupling mixes states with different spins so that otherwise forbidden transitions may occur.

Low symmetry fields or random strains tend to modify states so that more transitions become possible. Also, lattice vibrations which reduce the site symmetry by displacing neighbouring atoms, can induce or strengthen otherwise weak transition probabilities.

Thus selection rules are not strongly obeyed but are useful as guides to the interpretation of spectra. Measurements of transition strengths can give information about weak and high-order perturbations.

Basic Texts

The previous sections set out an account of the main characteristics of transition metal impurity spectra using physical ideas rather than mathematical techniques. More detailed accounts of the theory are given in many papers and in some longer reviews. There is a brief but interesting discussion by Martin [6] while the article by McClure is particularly useful and goes into more theoretical detail than is given here [7]. Much more information is contained in the book by Griffith [8].

Detailed calculations of the energy matrices for ions with configurations $3d^2$ or $3d^8$ are given by Liehr and Ballhausen [9]. Figures 1 and 2 show the energy level schemes for d^2 and d^8 ions respectively, in a tetrahedral crystal field. The results of including spin-orbit effects are shown in figures 3 and 4. Such diagrams form the basis for the interpretation of the spectra discussed in later chapters of this work.

Photoionization

In addition to transitions which result in the rearrangement of electrons within internal impurity levels, it is also possible for the charge state of impurities to be altered, and for electrons or holes to be transferred into bands of the host crystal [10]. Such processes can be important, for example in the production of luminescence by electron-impact ionization.

It is known that some transition metals may have more than one stable charge state in II-VI compounds, but calculation of the energy separation of the impurity levels and the crystal bands is more difficult than an evaluation of internal level splittings. This is because the entire Hamiltonian has to be used, not just the part that describes the d-shell interactions [11]. At present little is known about these effects and relevant experimental data are not available for most of the materials of interest.

Since some of the excited states of the d-shell may be degenerate with crystal band states, a resonance or interaction between the two may

result in an ionization process known as autoionization. This effect is considered in chapter four.

Summary

For the type of system considered here the crystal field theory does not provide a complete model, but it does permit the organisation of a large amount of data using only a few experimental parameters. Energy levels may be identified and their symmetries, transition probabilities and other properties such as spin resonance behaviour can be predicted on this basis.

What has been described, therefore, is the essential framework within which experimental results may be simplified and classified before more subtle physical problems are considered.

FIGURES FOR CHAPTER TWO

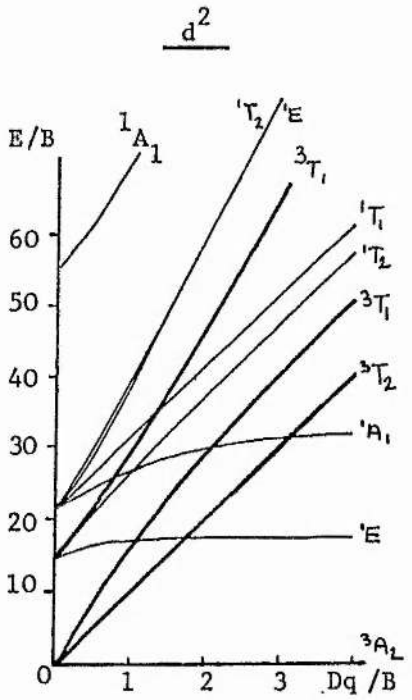

Figure 1

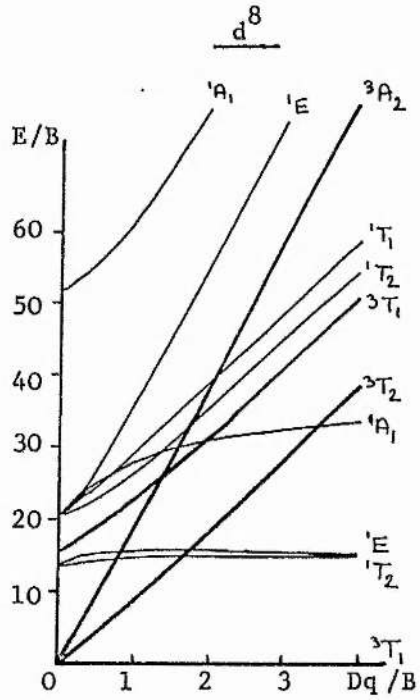

Figure 2

Figure 1: Energy level curves for a d^2 electronic system in a tetrahedral field. C/B = 4.71

Figure 2: Energy level curves for a d^8 electronic system in a tetrahedral field. C/B = 4.42

No account is taken of spin-orbit splitting of the above levels. The diagrams are taken from reference [7].

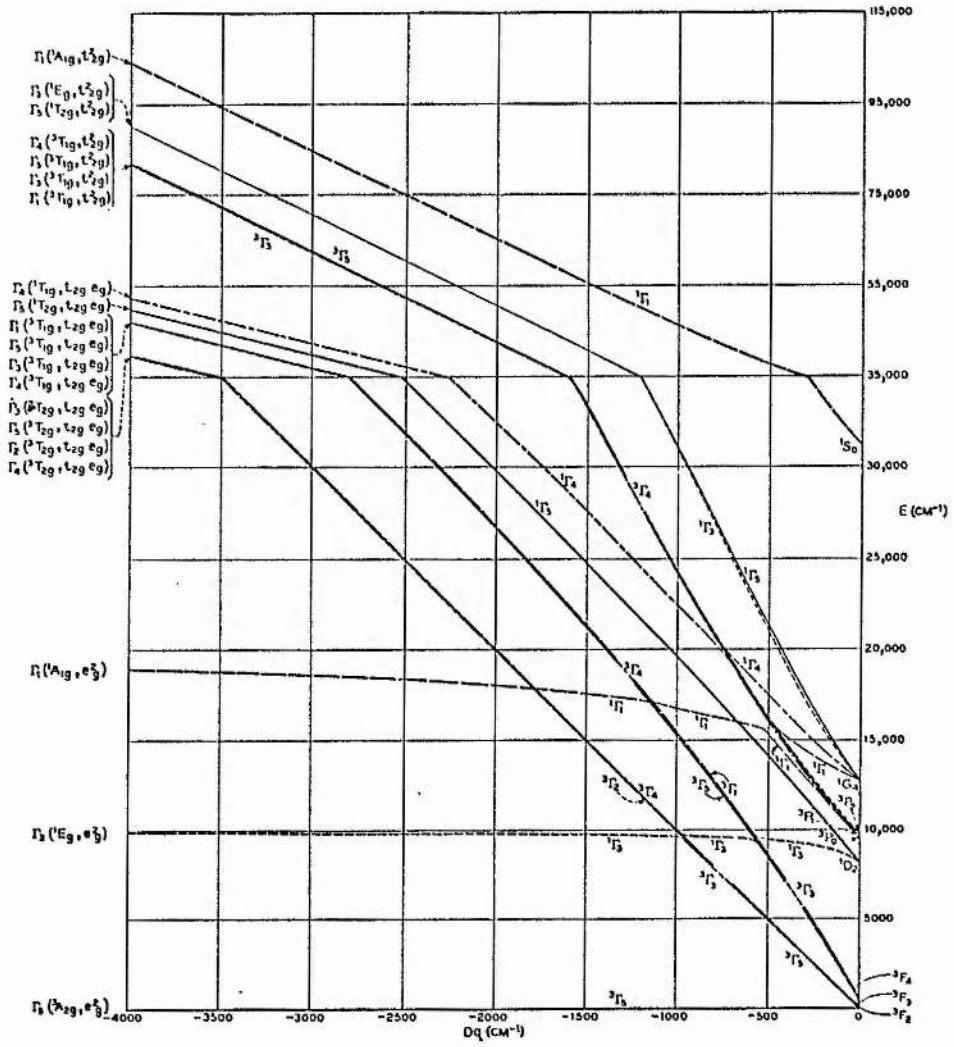

Figure 3:
Energy level curves for a d^2 electronic system immersed in a field of tetrahedral symmetry. Spin-orbit effects are included; $\lambda = 65\ cm^{-1}$. In this case $B = 630\ cm^{-1}$

$C/B = 3.89$

The diagram is due to Liehr and Ballhausen [9].

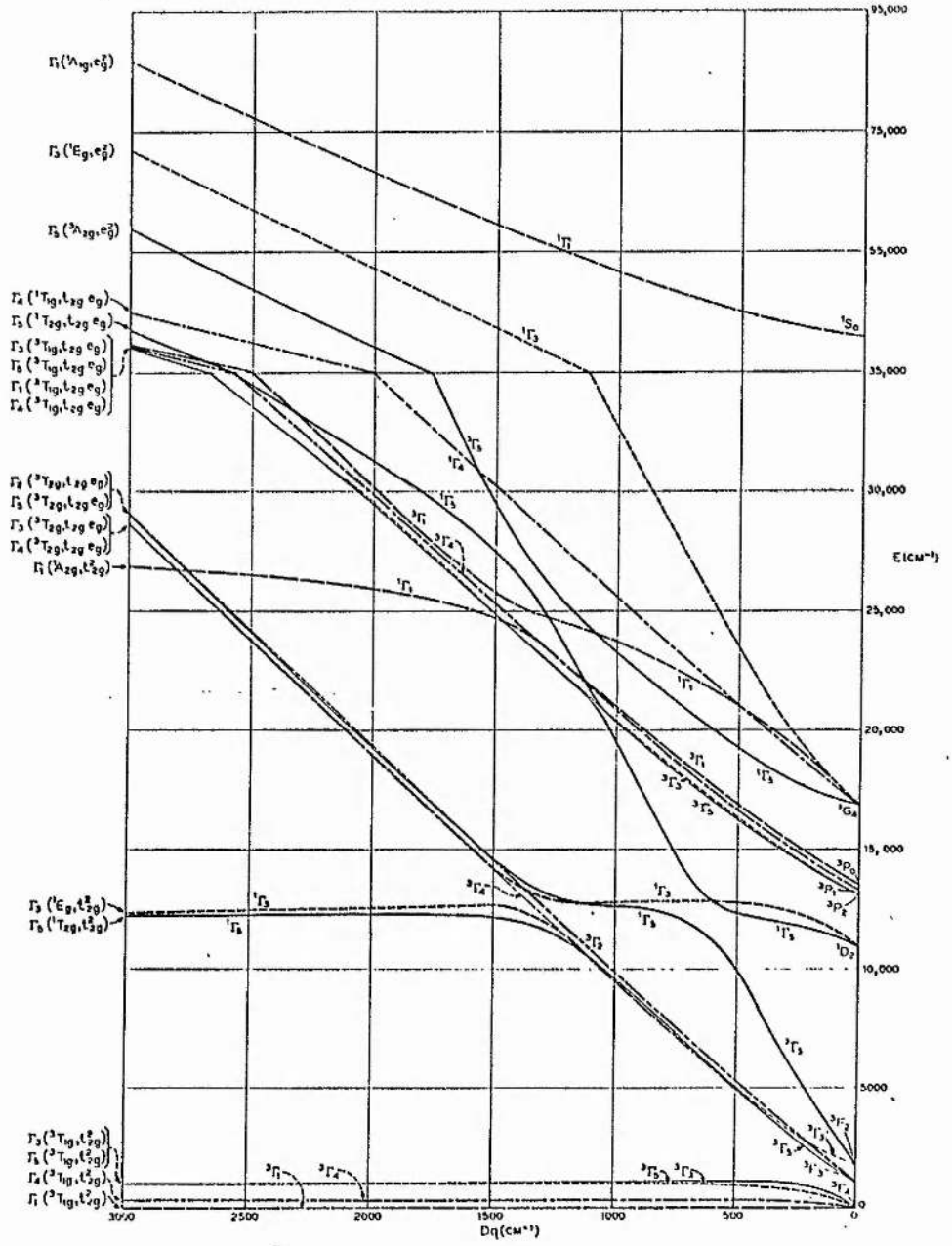

Figure 4: Energy level curves for a d^8 electronic system immersed in a field of tetrahedral symmetry. Spin-orbit effects are included; $\lambda = -275$ cm^{-1}. $B = 810$ cm^{-1} $C/B = 3.89$.

The diagram is due to Liehr and Ballhausen [9].

CHAPTER THREE

THE JAHN-TELLER EFFECT

Chapter Three

Introduction

Crystal field theory predicts the spin and orbital degeneracy of the electronic energy levels arising from perturbed d-states of transition metal ions. It also gives good agreement with recorded spectra for the energy separations of these states. It does not explain why optical transitions produce wide bands, often with fine structure, which alter their appearance with variation of temperature. A theory of these effects hinges on the dynamic interactions of impurity and lattice which make possible the exchange of energy between the electronic states of the impurity and the vibrational modes, or phonons, of the surrounding crystal.

This chapter gives an account of the origin of the electron-phonon interaction and explains the important consequences for crystal impurities. In particular it discusses the Jahn-Teller effect and its influence on absorption and emission spectra.

Dynamic Impurity-Lattice Coupling

When an impurity is introduced into a crystal the lattice vibrations in its vicinity are generally changed from those of the pure material. This happens when the mass of the impurity is different from that of the atom it replaces, creating what is known as a "mass defect", or when the interatomic forces between the atom on the site of the impurity and the neighbouring atoms are changed by the substitution. These forces will be altered if the impurity differs in size from the atom it replaces or if it contributes differently to the formation of bonds. Any of these circumstances produce local changes in the frequencies and amplitudes of vibrations of the crystal, which may

be investigated by Raman scattering or infra-red absorption [12].

When transition metals are added to semiconductors the above-mentioned effects may have to be considered. However their importance for optical properties is secondary to the changes that lattice vibrations produce in the electronic states of the impurities. Even so it must be stressed that in the following sections the spectrum of interacting phonons is not that of the pure material, but of the lattice perturbed by the presence of the defect.

The nature of the alteration of electronic states depends on whether the states are degenerate, or are well separated in energy from other levels. The former case is that met with most frequently in the systems with which this thesis is concerned. It is convenient to approach a description of this situation by analogy with the latter, which is more straightforward and yet illustrates many of the ideas relevant to the more general theory of impurity-phonon coupling.

Coupling to Non-degenerate Electronic Levels

The energy of an electron bound to an impurity is in part a function of the coordinates of the atoms or ions in the surrounding crystal. This will be altered by displacements of those coordinates either because the charge distribution in the crystal will be affected and thus the electric field at the impurity will change, or because the exclusion principle results in a correlation of the positions of impurity and ligand electrons. Since the thermal energy of a crystal is contained in lattice vibrations, keeping the atoms in constant motion, the energy of these oscillations and the energy of the electrons are coupled.

The Hamiltonian for a system without impurities is

$$H = T_N + V_N (\{\underline{Q}\}) \qquad (1)$$

T_N is the kinetic energy of the crystal and the second term represents the

interatomic potential, where $\{\underline{Q}\}$ is the set of coordinates of all the atoms in the crystal. It is assumed that the main role of the electrons in this system is to modify the internuclear potential and that this effect is included in $V_N\ (\{\underline{Q}\})$.

When an impurity is present the Hamiltonian becomes

$$H = T_N + T_e + V_N\ (\{\underline{Q}\}) + V_e\ (\underline{r},\{\underline{Q}\}) \qquad (2)$$

T_e is the electronic kinetic energy and the final term is the impurity electron-lattice interaction.

A first solution may be found in which the wave-functions of the impurity states are

$$\psi_{e,N} = \phi_e\ (\underline{r},\{\underline{Q}^o\})\ \chi_N\ (\{\underline{Q}\}) \qquad (3)$$

χ_N is the vibrational part and ϕ_e is the electronic part of the wave function. This represents a situation where the lattice has relaxed to a new equilibrium configuration $\{\underline{Q}^o\}$ because of the change in potential due to the impurity, but no account is taken in the electronic wavefunction of the changes due to the vibrational motion of the lattice.

A better solution is found in the adiabatic approximation [13] where the zero order wavefunctions are

$$\psi_{e,N} = \phi_e\ (\underline{r},\{\underline{Q}\})\ \chi_N(\{\underline{Q}\}) \qquad (4)$$

This applies when the electronic levels of the impurity are separated in energy by an amount large compared with the energy of a phonon of the crystal. Because the electron is a light, rapidly moving particle the slowly moving, heavier atoms appear to detect only the mean electronic position. Thus the vibrational part of the wavefunction, χ_N, has no $\underline{r}$ dependence.

The actual positions of the electrons result in an instantaneous interaction which is averaged over the whole orbit to give the effective electron-lattice coupling. The electronic distributions depend on the atomic

displacements, but deform adiabatically as the lattice vibrates.

In electronic states of different energy the interaction may be different since the charge distribution in the different levels need not be the same. In general, excited states have a greater spatial spread than lower energy states. Hence the equilibrium positions of atoms around an impurity may be different before and after an electronic transition. Since relaxation of the lattice to the new potential minimum involves motion of the atoms around the impurity, the crystal may be set into oscillation. The vibration may be localised, or phonons may be emitted into the crystal. The symmetry of the modes involved depends on the nature of the electronic levels involved in the transition.

Configuration Coordinates

The prediction of which modes of lattice distortion are active and produce experimentally measurable effects will be left until later, as this lies at the heart of the Jahn-Teller theorem. For the present the idea of configuration coordinates or normal modes of a cluster of atoms will be set out.

Electron-lattice interactions may be short or long range and thus may involve the positions of many or few atoms [14]. It is possible to construct from sums of atomic coordinates modes which transform as irreducible representations of the point group of the impurity. When the interaction is expressed in terms of these modes the range of the coupling is seen not to be of primary importance, since the effects of the interaction are due very largely to the symmetry of the modes involved. In fact it is possible to derive reasonable results from molecular models in which only the vibrational modes of the impurity-nearest-neighbour cluster are considered explicitly. However the strength of the interaction may be parameterised and found experimentally, so that the effects of more distant atoms are taken into account in this way.

It is important to note that the interaction mode of a cluster is mono-energetic whereas in a crystal there will be a range of energies in which modes of the relevant symmetry occur. In many cases it is adequate to take the mean energy of all the active modes as the important parameter.

If a transition between non-degenerate electronic states is allowed and the vibrational coupling is different in the two levels, then the spectrum of the transition will consist not of one line corresponding to the difference between the electronic terms, but will contain other lines differing in energy by multiples of the frequency of the interaction mode.

In a reasonable approximation, the interaction is taken to be linear in displacement of the lattice, and the lattice vibrations assumed harmonic. In this case the spectrum can be described in terms of a transition between two displaced potential wells in which harmonic oscillations occur [15]. See figure 1.

For coupling with degenerate electronic levels the adiabatic approximation is inadequate, and the situation is not at all so straightforward.

Electrons in Degenerate Levels

Useful reviews relevant to the following sections are given by Englman [13] and Sturge [16].

The customary starting point for the treatment of the general electron-lattice problem is a formulation with the interaction switched off, both the crystal and the impurity being in an unperturbed state. The interaction is then introduced, in the linear approximation as

$$V = \sum_k \frac{\partial V}{\partial Q_k} Q_k \qquad (5)$$

The summation runs over all different modes, defined so that Q_k transforms as the k'th irreducible representation of the point group of the impurity in the crystal, Γ_k. Since V is a term in the total Hamiltonian it must itself transform as the completely symmetric irreducible representation, usually written Γ_1 [17]. $\frac{\partial V}{\partial Q_k}$ then appears as a generalised force which also transforms as Q_k.

Consider an electronic impurity state ψ_i, which must be a basis function of some representation of the point group of the system, say Γ_i. Then this state will interact with modes of symmetry Γ_k if

$$\langle \psi_i | \frac{\partial V}{\partial Q_k} | \psi_i \rangle \neq 0 \qquad (6)$$

This is only possible if Γ_1 is contained in the product $\Gamma_i \otimes \Gamma_k \otimes \Gamma_i$, which means that $[\Gamma_i^2]$ contains Γ_k.

It is now clear why the case of non-degenerate electronic levels is especially simple, since they may couple only with breathing modes.

Jahn-Teller Theorem

If a degenerate electronic level couples to a vibrational mode there is no obvious reason why such degeneracy should be preserved. In fact it has been shown by Jahn and Teller that in crystals, with only the exception of Kramers degeneracy, for any degenerate electronic state of an impurity, of any symmetry, there exists at least one type of distortion which will remove the electronic degeneracy and split the level [18].

The ensuing situation is much more complex than in the case of breathing mode coupling. Not only can more than one symmetry species of mode interact with a given configuration, but their coupling strengths will in general be different. Furthermore the split electronic levels may still lie close together in energy and thus be strongly interacting. This means

that any eigenfunctions for the resulting states are an intimate mixture of electronic and vibrational terms which cannot be separated easily. These states are called "vibronic states". All the consequences of vibrational coupling in degenerate electronic systems are classified as examples of the "Jahn-Teller effect". The following sections will consider some of the physical effects on impurities.

Table 1 lists the products $[\Gamma_i^2]$ for the group T_d. It is easily seen that more than one mode can be active in many cases, so that Jahn-Teller effects are likely to be significant for transition metals in crystals with this point group, such as the II-VI compounds.

Types of Jahn-Teller Systems

The representation of the electron-lattice interaction as a linear function of the mode displacement is often quite adequate. The presence of elastic restoring forces between the atoms in the lattice prevents the system from undergoing arbitrarily large distortion. As shown in figure 2, an equilibrium degree of distortion is reached when the tendency for further distortion to reduce the energy of the electronic state is balanced by the harmonic restoring forces.

In the linear approximation, the Jahn-Teller effect is always what is known as a dynamic effect. For example, if the interaction mode is tetragonal so that there are three equivalent axes along which the system may spontaneously undergo a distortion, then no direction is favoured: the system passes smoothly from one position to any of the others. This continual reorientation occurs for a linear Jahn-Teller interaction, regardless of how strong it is, so that the oscillations of the system between equivalent distortions may be very large, even in the lowest vibrational state. However because of the large amplitudes these oscillations would have, such systems are extremely sensitive to anharmonic effects or external perturbations

If such effects are present then the system may adopt a fixed direction of displacement. Even a very small shift in energy can make one particular orientation overwhelmingly favourable, and make the probability of tunnelling into another potential well almost negligible [25].

This is especially true if the Jahn-Teller coupling is strong. When the potential barriers between the equivalent wells are greater than the average energy in vibrational modes of the crystal, the distortion is permanent. Such an effect is called the static Jahn-Teller effect [19].

Since anharmonic processes, or lattice strains which may also induce this effect, are present in most cases, strong Jahn-Teller coupling usually produces a static effect. The strong and static Jahn-Teller effects are not synonomous however: it is the presence of other than linear coupling that makes the static effect possible. With increasing temperature transitions between wells become more likely, so that a static distortion at low temperature may disappear, and the system exhibit a dynamic effect.

A dynamic situation may appear to be static if the reorientation time for jumps between equivalent distortions is long compared with the time taken to make an experimental measurement on the system [20].

Consequences of the Jahn-Teller Effect

If the linear Jahn-Teller coupling is weak then at sufficiently low temperatures a narrow zero phonon line appears in absorption or emission spectra, corresponding to transitions between different electronic levels, without the creation or absorption of phonons. Processes that do involve a net change in the energy of the phonon system give rise to additional peaks in the energy spectrum, of varying intensity and generally increasing width as their energy separations from the purely electronic line

increase [21]. These peaks, called "phonon replicas" or "multi-phonon lines", may correspond to the energies of peaks in the density of states of phonons in the pure material [22]. These often occur at critical points of the Brillouin zone. In such a case it is possible to determine the symmetry of the modes involved in the coupling, if the lattice dynamics of the pure material are known.

Sometimes the fine structure may appear at irregularly spaced energies which cannot be interpreted directly as being due to phonons. This may be the result of interactions between the different electronic states which, although not degenerate, may lie close in energy to each other, and may not be orthogonal. Very uneven spacings make it necessary to find the nature of the active modes by calculation rather than inspection.

Spin-orbit coupling also may produce irregular structure, as may low symmetry fields, due either to the crystal structure or to random strains. These interactions may broaden and split a zero phonon line into several components.

In some cases the observed phonon structure in optical spectra is not simply related to lattice modes but instead is produced by coupling to localized vibrations. Even if predominantly lattice modes are active, the intensity with which they appear in a spectrum is not due solely to the density of states, but depends also on the mode interaction strength, which varies with frequency of vibration [14].

When impurity-lattice coupling is strong then the discrete components of an absorption or emission band due to the creation or annihilation of integral numbers of phonons may not be strong or sharp enough to be seen. Instead broad bands appear. In the case of breathing mode coupling a transition occurs as a Gaussian band with a width which increases with temperature and is proportional to the strength of the vibrational interaction.

Strong Jahn-Teller coupling produces bands which are split into two or three Gaussian components, lying at different energies. The widths and separations of these components are themselves increasing functions of temperature and are larger for stronger coupling. Additional information in such cases is obtained by moments analysis [23].

Since the Jahn-Teller effect results in the originally degenerate electronic states being separated in energy and to some extent being differently orientated in space, any matrix elements of interactions between these states are strongly affected. In particular the off-diagonal operators of spin-orbit coupling may be attenuated considerably. Hence the separation of spin-orbit split levels may be much less in the presence of even weak Jahn-Teller coupling than otherwise expected [13]. This is an example of the Ham effect [24], and is noted extensively in the spectra of impurities. Interpretation is complicated by the fact that covalency can produce similar effects, again by reducing the overlaps between different electronic states.

Summary

The Jahn-Teller effect is very important in determining many of the details of the behaviour of impurities in crystals. The mixing of electronic and vibrational states determines the peculiar and otherwise inexplicable shapes of absorption bands, and one consequence, the Ham effect, explains the very strong quenching of spin-orbit splitting which is often observed.

Unfortunately many applications of the theory have to be qualitative, since calculations of optical spectra or of spin resonance effects are very complicated even if only a few modes of interaction are important. It is not possible to include the effects of dispersion in phonon frequencies in calculations from first principles.

These limitations on the application of the Jahn-Teller theorem do not greatly diminish its effectiveness as a guide to interpreting spectra. Later chapters will show that much information may be derived from data using even simple models.

Table for Chapter Three

Table 1

The symmetric product $[\Gamma_i^2]$ in the Td group. *

$$[A_1^2] = [A_2^2] = A_1$$

$$[E^2] = A_1 \oplus E$$

$$[T_1^2] = A_1 \oplus E \oplus T_2$$

$$[T_2^2] = A_1 \oplus E \oplus T_2$$

* taken from Hollas [128], p91.

Figures for Chapter Three

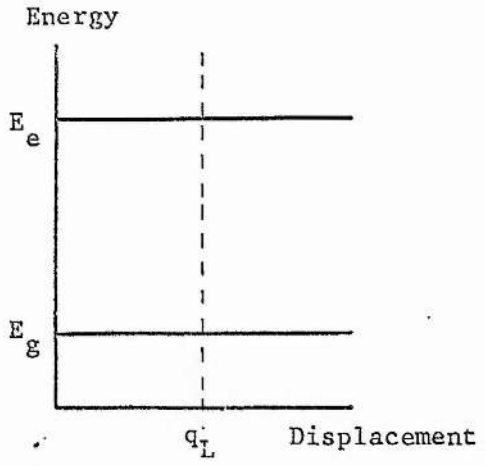

Figure 1(a)

In the absence of electron-lattice coupling, the energy of a localised state is independent of lattice distortion.

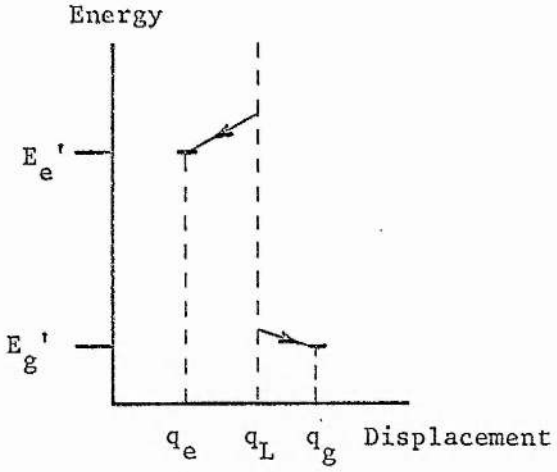

Figure 1(b)

With electron-lattice coupling localised states relax in energy to new minima involving lattice displacements.

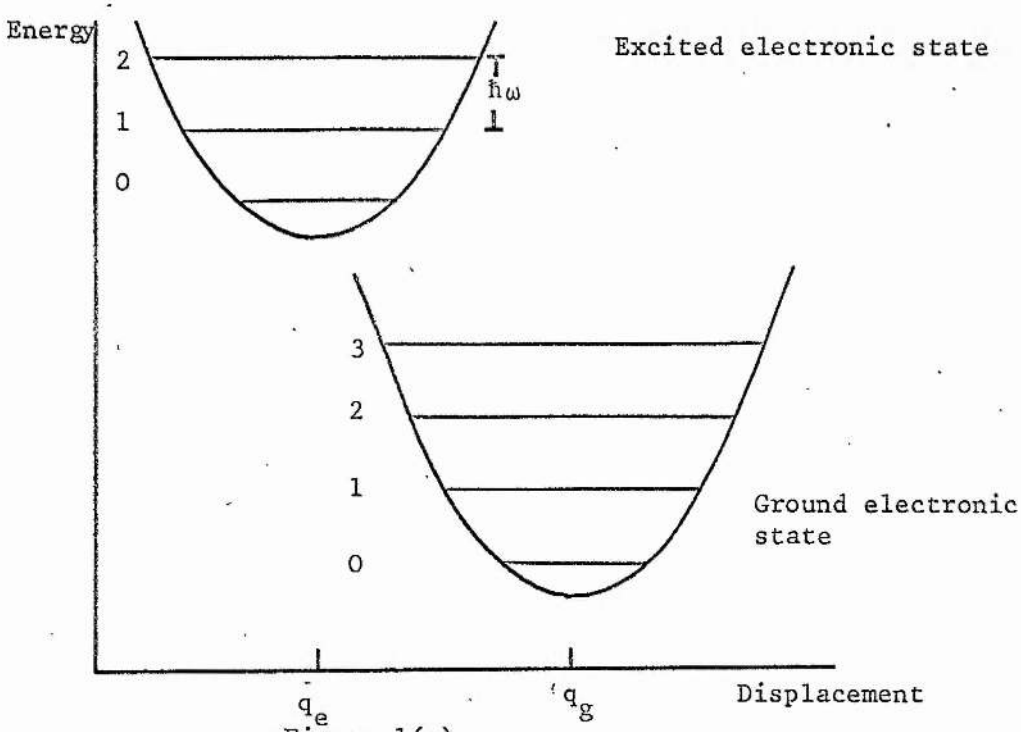

Figure 1(c)

In figure 1(b), E_e' and E_g' are the energies of the electronic states in the static lattice. Vibrational excitation may occur into higher levels, so that each electronic state has associated with it many vibronic states.

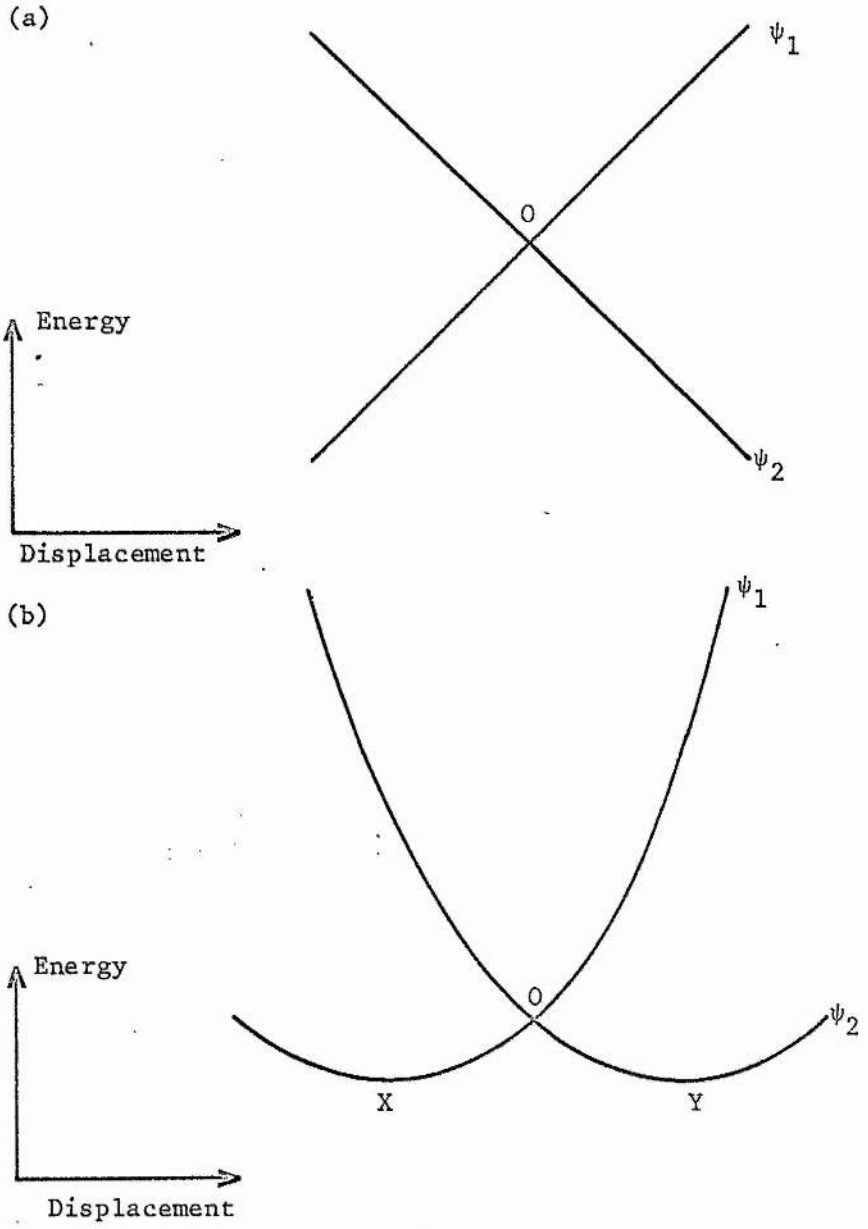

Figure 2

(a) At O the electronic states ψ_1 and ψ_2 are degenerate. With a linear Jahn-Teller coupling, a displacement will split the levels as shown.

(b) Elastic restoring forces in the lattice stabilize the distortion at X or Y. The energies of these two configurations are equal. In a dynamic coupling case the distortion will oscillate between X and Y, and the electronic state will be a mixture of ψ_1 and ψ_2.

CHAPTER FOUR

ANTIRESONANCE

Chapter Four
Introduction

In the vocabulary of high energy physicists, resonances are particles that exist only a short time (perhaps as little as 10^{-23} seconds) before decaying into two or more other particles. They are frequently formed in experiments by the collision of two particles which, at particular values of kinetic energy, interact to form a bound state. The lifetime of this state depends on the strength of interaction between the initial particles and on the number and transition probabilities of different decay channels. These short-lived bodies are detected by resonances in the scattering cross-sections of the interacting particles [26].

A feature of such systems is that neither a state in which the particles are bound nor in which they are free is a complete description of the physical situation. A full wavefunction would be a mixture of the two: this would be more obvious if, after the decay, the emitted particles were not allowed to escape but were "reflected back" to interact again and again.

The existence of states which involve close coupling of particles but which are not stable bound states is not exclusive to esoteric sub-nuclear physics. For example, anharmonic coupling may combine two phonons into a single quasi-particle which exists for a short time and then decays into another two modes. The intermediate state can be thought of as a scattering resonance.

In atomic physics information about high energy states may be found by measuring electron-atom or electron-ion scattering cross-sections. Whenever the energy of the incident electron is such that a resonance may be possible, the cross-section shows a peak or other, more complex variations. Similar information can be found from studying ionization. If sufficient energy is put into an atom or ion an electron may be emitted. However, it may also be possible to excite two electrons simultaneously so that the

energy is shared between them and both are bound. Since there will be some interaction between the two electrons, one may drop into a lower bound state donating its energy to the other which is then released. There is interference between these two mechanisms of ionization, which leads to peculiarities in scattering probabilities and optical absorption of the atoms or ions concerned [27].

This chapter will show that similar effects may be important in impurity behaviour. Some relevant theory is presented.

Configuration Interaction

The following elementary example illustrates some of the aspects of inter-state mixing that are of interest in systems with resonance states. Consider the model shown in figure 1:
T is an operator inducing transitions; to be specific it may represent light absorption. All other symbols are standard.

From these equations the absorption spectrum consists of one line at energy (E_2-E_o).

Now suppose there is an interaction V between states 1 and 2 such that

$$\langle\psi_2|V|\psi_1\rangle = V_o \neq 0 \qquad (5)$$

Then ψ_1 and ψ_2 are no longer stationary states. Instead suitable functions are ψ_1^1 and ψ_2^1 where

$$\psi_1^1 = (1 - \alpha^2)^{\frac{1}{2}}\ \psi_1 - \alpha\psi_2 \qquad (6)$$

$$\psi_2^1 = (1 - \alpha^2)^{\frac{1}{2}}\ \psi_2 + \alpha\psi_1 \qquad (7)$$

where $\alpha = |V_o / (E_2-E_1)|$, is small and

and ψ_1, ψ_2 are not degenerate.

ψ_2^1 and ψ_1^1 are orthogonal, and the energies E_1^1, E_2^1 of these states are given by

$$E_1^1 = (1 - \alpha^2)^{\frac{1}{2}}\ E_1 - \alpha E_2$$

$$\simeq E_1 - |V_o E_2/(E_2-E_1)| \qquad (8)$$

and $$E_2^1 \simeq E_2 + |V_o E_1/(E_2 - E_1)| \qquad (9)$$

Thus the presence of configuration interaction V_o has the following results:

(a) The total transition probability is not changed.

(b) The energies of states ψ_1^1 and ψ_2^1 differ from those of the unperturbed states by amounts proportional to V_o.

(c) The absorption spectrum is no longer monochromatic.

An example of this kind of mixing would be spin-orbit coupling between d-states with different spin quantum numbers [chapter two].

Fano Theory

The examples of resonances given in the introduction involve not only bound states, but also delocalised states. Thus a model is required to describe the situation where instead of having two discrete states E_1, E_2, we have a discrete state E_1 (in the absence of interaction) and a continuum of levels. The notation generally used derives from Fano's classic paper [28].

In this he considers a discrete state ϕ,with energy E_ϕ, and a continuum of states ψ_E. There is an interaction V_E between these states so that the states are mixed; the orthogonal wavefunctions are then Ψ_E

$$\text{where } \Psi_E = a(E)\phi + \int b(E,E')\ \psi_{E'}\ dE'. \qquad (10)$$

Where V_E is not too strong, near E_ϕ a and b are such that Ψ_E is very similar to ϕ, while far from resonance it resembles the unperturbed states of the continuum. On finding Ψ_E, Fano shows that

$$\frac{|\langle\Psi_E|T|i\rangle|^2}{|\langle\psi_E|T|i\rangle|^2} = \frac{(q+\varepsilon)^2}{1+\varepsilon^2} \qquad (11)$$

which is the ratio of the transition probabilities from an initial state i to the perturbed and unperturbed continuum when the continuum density of states is constant. The function on the right hand side of equation (11) is plotted for various values of q in figure 2. ε is a reduced energy parameter, defined by

$$\varepsilon = \frac{E - E_\phi - F}{\frac{1}{2}\Gamma} \qquad (12)$$

where $\Gamma = 2\pi |V_E|^2$

Γ gives an indication of the broadening introduced into the state ϕ by the interaction, and F is the energy by which the resonance is shifted from E_ϕ. q is related to the ratio of transition probabilities to the perturbed discrete state and to a band width Γ of unperturbed continuum states. When the transition to the perturbed discrete state is forbidden, $q = 0$.

There are several assumptions made in the derivation of these results, including that of a smooth variation in the properties of the continuum states.

The main conclusions of this theory are:

(A) The total probability of transitions to both discrete and continuous states is not changed by coupling of the states.

(B) The energy of the discrete state is altered by an amount proportional to the strength of the configuration interaction. The continuum states also have their energies shifted but since they form a continuous spectrum this is less significant.

(C) The transition to the discrete state is broadened by the interaction so that the oscillator strength for the absorption is diluted into the continuum states over a range of energy. This may be thought of as a life-time effect; the stronger the interaction the more rapidly can the discrete state decay into the continuum.

A, B and C are very similar to a, b and c of the previous section. This follows from the similarity of the underlying physics. In addition the Fano theory predicts:

(D) In general the absorption spectrum will not be symmetric about the resonance energy.

(E) At some energy near that of the discrete state the transition probability

becomes exactly zero (unless there is some background absorption due to non-interacting states). This is an interference produced by cancellation of the transition probability to the discrete state by that to the continuum states. It is this apparent reduction in absorption that leads to the mixing process being called antiresonance.

Experimental Detection of Antiresonance

The three most characteristic signs of antiresonances are broadening of lines, skewness in spectra and the presence of absorption dips.

The first two may be ambiguous since other processes may cause broadening, and unresolved structure can make a line appear asymmetric. However the occurrence of minima in absorption spectra is clear evidence of antiresonances.

Fano has calculated the line shapes to be expected in simple cases andthe class of curves where antiresonance produces large dips in a spectrum can usually be fitted to experimental data quite confidently. [The physical significance of the parameters obtained when there may be other broadening processes and rapid changes in background are discussed in chapter six. Modifications to the predicted line shapes may result].

The observation of shifts in the position of energy levels may also suggest the presence of the effect but in general it is the detection of spectral minima and demonstration of the typical "Fano lineshape" that provides most satisfactory evidence of the presence of antiresonance.

Occurrence in Solids

From the above it may be expected that in any situation where discrete and continuum states are degenerate antiresonance will be possible. This will often be the case in solids and it is not hard to find some instances. A few are given below, but a more complete review is made in

chapter eight.

(a) Friedel Virtual Bound States.

These occur when transition metal impurities in metal solutions have d-shell levels degenerate with conduction - band states. These levels are therefore resonance states mixing with free band states, with notable consequences for magnetic and electrical properties [29] .

It has been suggested that in a similar way excited states of transition metal ions in semiconductors may be resonance states. This would arise when the localised states were degenerate with bands of the host crystal and could result in ionization of the impurity. This could be detected, in suitable cases, by photoconductivity measurements or Fano characteristics in absorption spectra.

(b) Electronic-Vibronic Degeneracy

If an electronic transition is degenerate with a band of absorption associated with phonon creation then the two mechanisms may interfere, the states mixing through electron-lattice coupling. This has been clearly seen in both absorption and Raman scattering experiments [30] .

(c) Purely Vibronic Antiresonance

A Jahn-Teller interaction may involve more than one mode of distortion. The resulting correlation between the modes, together with the presence of large local oscillations which may induce anharmonic effects may result in coupling between vibronic states. It is already well known that Jahn-Teller distortions may produce scattering of lattice modes [31] .

It can be expected therefore that transitions between states coupled to different vibrational modes will show signs of antiresonance in some cases, either because of interference of localised modes among themselves or also involving lattice modes. Examples of this will be reported in later chapters.

Conclusion

The phenomenon known as antiresonance can occur whenever bound and free states are degenerate, or even when continua due to different states overlap. In solids this may arise when there is coupling between localised levels and band states, whether of electronic or vibrational origin.

The fact that antiresonance in solid systems has not been considered in many cases in the past may merely reflect the fact that it is hard to detect and identify unambiguously. Thus, where it is not obscured by other spectral details it may simply be overlooked.

Figures for Chapter Four

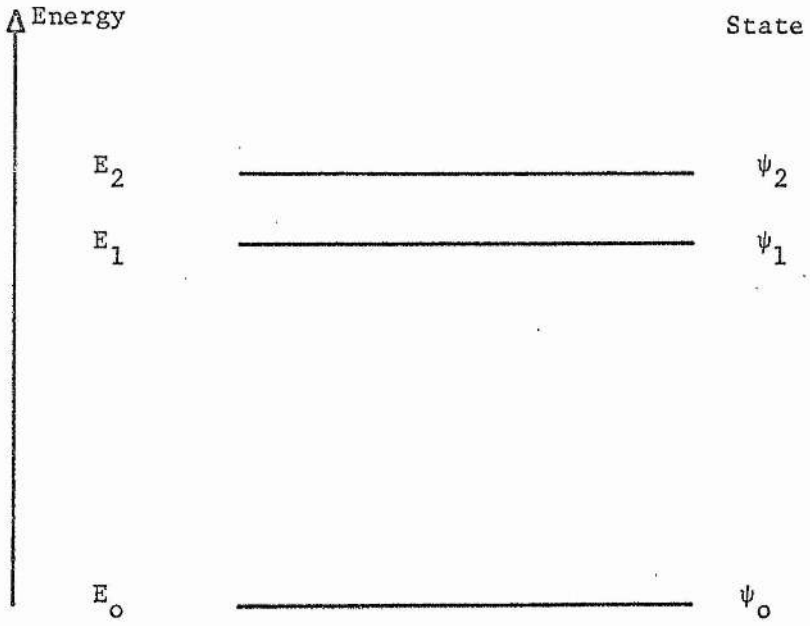

$$H|\psi_i\rangle = E_i|\psi\rangle \quad (1)$$

$$\langle\psi_i|\psi_j\rangle = \delta ij \quad (2)$$

$$\langle\psi_2|T|\psi_o\rangle = 1 \quad (3)$$

$$\langle\psi_1|T|\psi_o\rangle = 0 \quad (4)$$

Figure 1

The above diagram and equations provide a simple model with which to demonstrate configuration interaction.

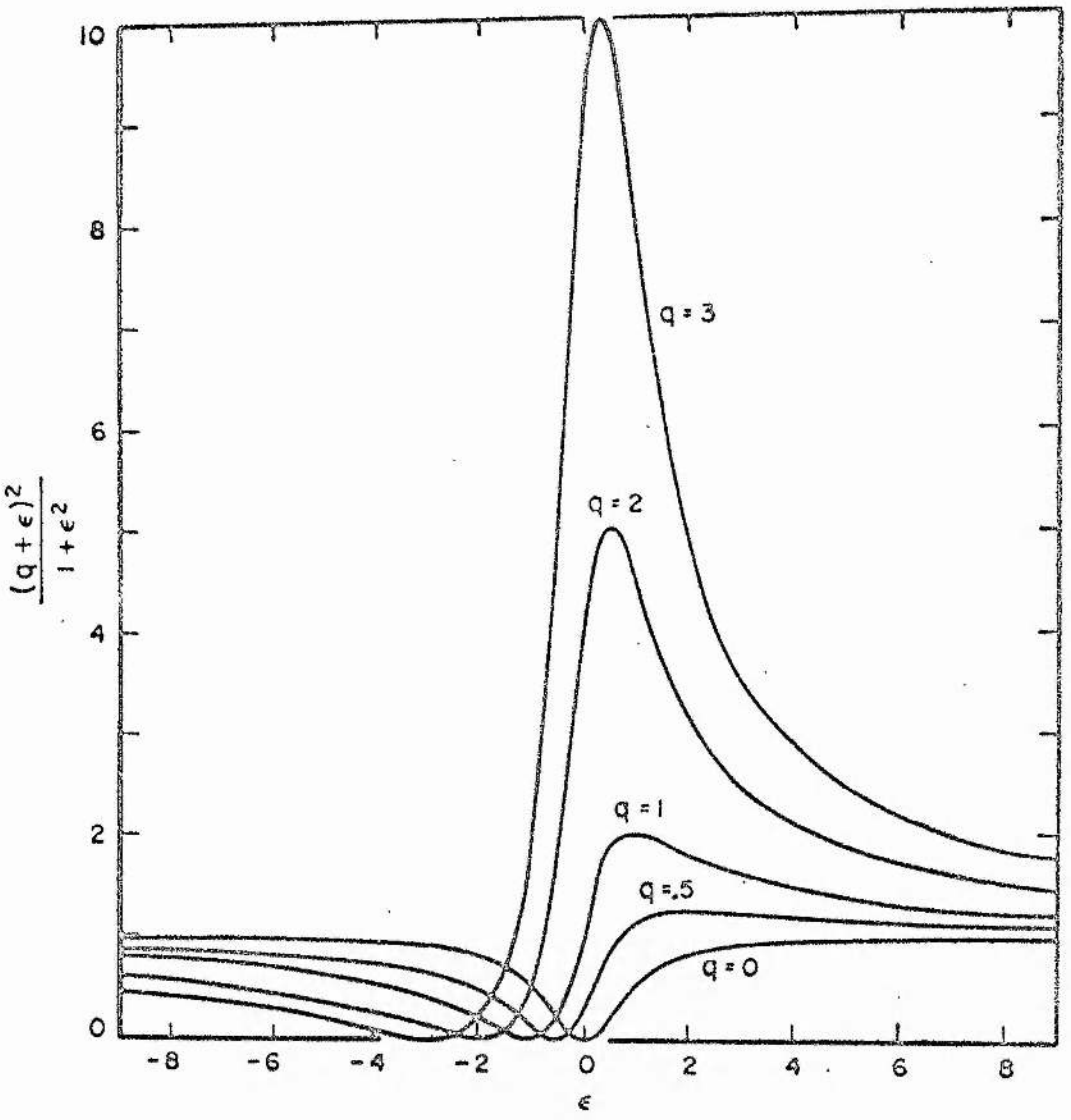

Figure 2

This figure, taken from reference [28], shows how the function on the right hand side of equation (11) varies with q. This function, which is related to the line-shape, is plotted against ϵ, a reduced energy parameter (see equation (12)).

CHAPTER FIVE

EXPERIMENTAL DETAILS

Experimental Details

Most of the experimental results were obtained by absorption spectroscopy. The methods used are standard and need little description beyond an indication of the experimental conditions and equipment used. It is useful also to record here some information about the preparation of samples and about the form in which the data were recorded.

Preparation of Undoped Material

Polycrystalline ZnSe and ZnS were grown from powder by sublimation in sealed evacuated quartz glass tubes. These were about fifteen centimetres long. In the case of ZnSe the hot part of the tube was set at 960°C, with the growth point some 100°C colder. To ensure transport of ZnS some iodine had to be added to the powder. The growth of ZnS crystals required a lower temperature, 800°C, with a temperature difference along the tube of about 50°C.

Ingots twenty millimetres long and fifteen millimetres in diameter could be grown under these conditions. The time required was four days for ZnSe and up to twenty days for ZnS.

Incorporation of Impurities

It is possible to make material containing transition metal impurities by adding the metal to the powder and continuing the growth as described above. In this case HgCl also has to be added to make sure that the metal transports down the tube. It is simpler and more flexible to grow undoped material and incorporate the impurity subsequently by either of the following two methods.

Metal Coating

After the surfaces were cleaned and etched (see under "Final Preparation") specimens were coated by evaporation of the metal in high

vacuum. The samples were held under vacuum for several days at 800°C. This ensured diffusion of the metal into the substrate. To minimise the effects of sublimation the tube was positioned in the furnace so that the sample lay at the coolest point. A special design of silica-glass container (figure 1) kept the enclosing volume down to a minimum, to reduce further the effects of temperature gradients.

Doping from a Zinc Bath

The n-type conductivity of ZnSe or ZnS is increased by immersion of the material in molten zinc [32]. If a transition metal is added to the zinc then a small fraction will diffuse into the solid. Since the segregation coefficient is of the order of one part in a thousand the doping level obtained with this technique is lower than with the previous method. A small amount of selenium or sulphur may be added to reduce the extent that the solid dissolves in the liquid metal.

One feature of this method of doping which may be useful is that the samples obtained may still be highly conducting electrically.

Final Preparation

Specimens were cut to the required shape by a diamond wire or carborundum disc saw, and then were hand-polished with diamond paste to a one micron finish. Before being coated with metal or when a clean surface was required for any reason specimens were etched by a solution of bromine in methanol, then immersed in carbon disulphide.

Specimen sizes were at best six millimetres thick, with a fifteen millimetre diameter, but pieces one millimetre thick by two to three millimetres across had to be used sometimes.

Apparatus and Experimental Techniques

Samples were mounted on a copper cold finger attached to a reservoir of liquid helium or liquid nitrogen. Both the copper and the sample were painted with G.E. 7031 varnish to ensure good thermal contact. Although temperatures of 4 to 5°K could be reached by pumping on liquid helium, usually 6°K, which was attainable without pumping, was found adequate. This temperature could be sustained for six to seven hours on one charge of liquid helium. The cold finger was perforated and the cryostat had transparent windows to let light pass through the samples.

The light source was a 50 watt tungsten filament bulb. The samples were illuminated by undispersed light so that the intensity of incident light was constant in time at all wavelengths. This avoids a difficulty in the use of monochromatic light, where it is possible for the occupancy of energy levels to alter considerably if the wavelength corresponds to a strong absorption resulting, for example, in ionization of a centre. By using undispersed light, the occupancy of energy levels is allowed to reach a steady state condition which does not alter in time.

The transmitted light was chopped mechanically and passed into a Monospek 1000 monochromator with a dispersion of 8Å per millimetre. The resolution used depended on sample quality and wavelength region, but was typically 2Å. Where required, up to 0.5Å could be used. The monochromator was calibrated with a mercury lamp and could be filled with nitrogen to minimise absorption due to atmospheric water-vapour. Scattered light inside the instrument was 0.1% of incident radiation.

A variety of detectors were available to monitor the dispersed radiation. Early work was done using a lead sulphide cell, but an S20 or liquid nitrogen cooled S-1 photomultiplier were used for greater sensitivity. In the infra-red a cooled indium antimonide cell was used.

The detector signal was amplified by a lock-in device and displayed on a chart recorder.

Processing of Data

With no sample in the system the recorded signal I_B is given by

$$I_B = I_o B \qquad (1)$$

where I_o is an intensity determined by the tungsten filament and B represents the combined effects of filters, dispersion in the monochromator, detector response, etc. (All quantities are functions of wavelength). With a sample present the signal is I_s where

$$I_s = I_o B R e^{-\alpha d} \qquad (2)$$

and where α is the absorption coefficient

d is the sample thickness

and R is a quantity related to light scattering and reflection by the sample.

Thus

$$x = \ell n [I_B/I_s] = \alpha d - \ell nR \qquad (3)$$

R is expected to be slowly varying with wavelength of light and so may be removed by extrapolation, being regarded as a background signal to the important information which is contained in αd.

Most of the spectra contained in later chapters are displayed as αd or x plotted against energy, and thus are given in terms of relative numbers of photons absorbed per unit energy range.

This concludes the discussion of experimental procedures.

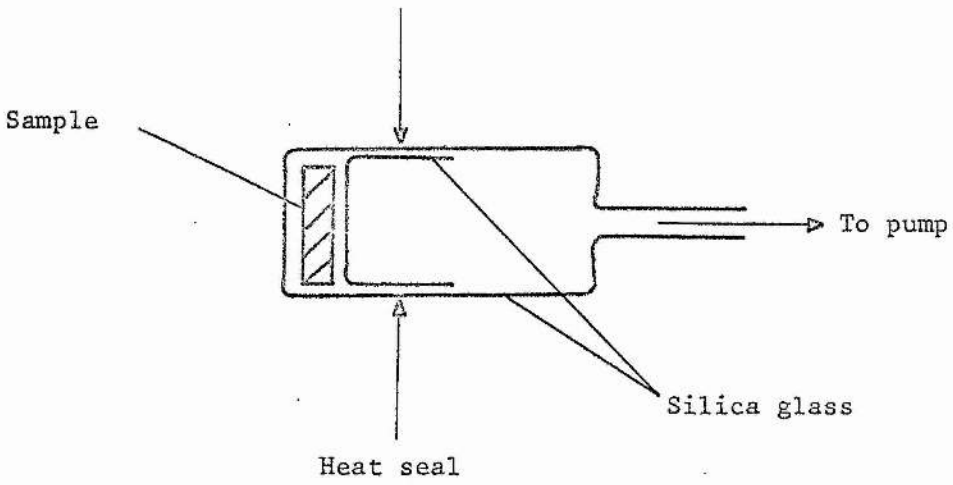

Figure 1

Tube design to minimise volume containing sample.

Chapter Six
Titanium in ZnSe and ZnS

Chapter Six

Introduction

This chapter reports experiments carried out on II-VI compounds containing titanium. The systems studied most closely in the present work were ZnSe:Ti and ZnS:Ti.

These were chosen because they had not been examined previously in detail at low temperatures, and because reports had been made of autoionization of excited titanium levels in the corresponding cadmium compounds [2,33]. When the absorption spectra recorded in this chapter were first obtained it was seen that they were rich in fine structure, the study of which raised many interesting points.

The following sections deal, first with these spectral details, and discuss the applicability of models involving vibrational interactions. Subsequently the role of electronic antiresonance in the materials studied here will be considered. Comparisons with other systems will be made.

ZnSe:Ti and ZnS:Ti - General Features

Atomic titanium has the electronic configuration

$$(Ar)3d^2\ 4s^2.$$

When one of the II-VI compounds is doped with a 3d transition metal, there are several possible kinds of site that the impurity ion might occupy. The impurity can replace a zinc atom on a lattice site, or become an interstitial in either of two distinct locations. In the zinc-blende structure one interstitial position has tetrahedral symmetry, while the other is octahedral. The following section presents the evidence for the impurities being substitutional in the systems of interest here.

Ludwig and Woodbury have obtained electron spin resonance data for several tetrahedrally bonded materials [135]. They propose the following model to explain their results. If an impurity has a free atom con-

figuration (Ar) $3d^n\ 4s^m$, then when it is in a substitutional site and is neutral with respect to the lattice, the s-electrons go into bonding orbitals, together with as many of the d-electrons as are necessary to satisfy the bonding requirements. The remaining d-electrons constitute the d-shell of the impurity. For example, if a free atom has the configuration (Ar) $3d^n\ 4s^2$, and if it is substituted for the Group II element in a II-VI compound then the resulting impurity will have a $3d^n$ configuration. Different charge states then correspond to an increase or decrease in the number of electrons in the d-shell. When an impurity occupies an interstitial site, then the s-electrons collapse into the d-shell. Thus an impurity with free atom configuration (Ar) $3d^n\ 4s^2$ would have the configuration $3d^{n+2}$ as a neutral interstitial.

This model has subsequently been verified by many workers for many combinations of impurity and host crystal, investigated both by electron spin resonance and by optical absorption.

In particular, e.s.r. measurements have been reported for titanium impurities in ZnS, CdTe, CdS and CdSe. It is found that the titanium is present, in the uncharged state, with two d-shell electrons, and is substitutional for a Group II atom [136 and references therein]. Optical absorption measurements in the cadmium compounds reveal energy level separations consistent with those calculated from the crystal field matrices for d^2 states [7]. Parameters are given in table 18. It thus seems probable that titanium in ZnS and ZnSe also should occur as substitutional $3d^2$.

Figure 1 shows the room temperature absorption spectrum of ZnSe:Ti. Two broad bands are visible. If the metal impurity were interstitial it would have a d^4 configuration and whether in tetrahedral or octahedral coordination, only one strong absorption band would be found.

It is possible that charge compensation could produce electronic configurations of substitutional titanium other than d^2 [135]. A d^1 shell would give only one absorption band, and would not give rise to the observed spectrum. A d^3 shell might produce this kind of absorption; for the case of ZnSe:Ti the necessary parameters have been calculated. (ZnS:Ti would be similar). Two ascriptions of the absorption bands are possible, since there are several spin-allowed transitions within the d^3 configuration. The results in each case are given in table 19.

In case (a) the value of B is small compared with other impurities in ZnSe. The value of B for a given transition metal is always found to be less for the impurity in the crystal than for the free ion. It is useful to define a parameter β, such that

$$\beta = \frac{B(\text{impurity})}{B(\text{free ion})} .$$

Values of β for impurities in ZnSe are 0.6 for $V(d^3)$, 0.8 for $Mn(d^5)$, 0.5 for $Co(d^7)$ and 0.5 for $Ni(d^8)$ [11]. All of these are impurities uncharged with respect to the lattice, so the data may not be directly comparable with the results of ascription (a), which implies β is 0.1 for ZnSe:Ti. However β for ZnSe:$V(d^2)$ is 0.7, which lies within the range of the above values. Thus ascription (a) is improbable.

The second possibility, (b), is unlikely because of the value of the crystal field parameter Δ which it requires. Szawelska and Allen observe that the value of Δ for charged impurities is larger by a factor of 1.5-2. than for neutral impurities [83]. This is supported by data for ZnSe:V; $\Delta(d^3)$ is 3350 cm^{-1}, while $\Delta(d^2)$ is 5150 cm^{-1} [11].

In those systems which have been investigated previously, it is found that for a given impurity the values of Δ in cadmium compounds are close to the values in zinc compounds. Crystal field parameters for cadmium compounds containing titanium are given in table 18. It has been verified by e.s.r. that in these materials titanium is present in the d^2

configuration. If the titanium in the ZnS or ZnSe were in a d^3 configuration, Δ would be expected to lie in the range 4500-6000 cm^{-1}, which is in disagreement with the observed value if ascription (b) is correct.

The possibilities that titanium is interstitial or is in a d^1 or d^3 configuration can therefore be ruled out. The observed spectra are however consistent with the titanium being substitutional in a d^2 configuration. Fitted crystal field parameters are given in table 1, and in table 18 for comparison with cadmium compounds. Figures 2(a) and 2(b) show the calculated and experimental spectra schematically. Since only two bands were detected, it is not possible to find more than two parameters.

Low Temperature Spectra

Figures 3a, b and 4a,b show the absorption bands of ZnSe:Ti and ZnS:Ti taken with specimens at $6^{o}K$. These had not previously been measured at low temperatures with high resolution. (ZnSe:Ti had been recorded near $4.2^{o}K$, but with poorer resolution [5]). A great deal of fine structure is seen.

For comparison, measurement on cadmium compounds containing titanium were also made. Figures 5a,b,c show the low temperature spectra of CdS:Ti, CdSe:Ti and CdTe:Ti. Of these, other workers had previously published that of CdS:Ti [2] and subsequently reported that of CdSe:Ti [34]. In all these materials the absorption bands show only broad features, even at liquid helium temperatures. An interpretation of the form of these bands in terms of vibrational coupling has been made by Boyn and co-workers [34].

It is interesting to study the fine structure in the zinc compounds. Although both bands have been recorded here for each material, this work will deal mainly with the higher energy bands which are easier to record and to interpret.

Near Infra-red Absorption Band $^3A_2 - {}^3T_1 ({}^3P)$.

In each material, at sufficiently low temperatures this band may be seen to consist of many components. A sharp line at low energy is followed by uniformly spaced replicas at higher energy which become progressively broader. Somewhere near the third or fourth component of this sequence is superimposed a second sharp line, itself followed by a set of equally spaced repetitions. As shown in figures 4a and 4b, the spacing is different for each series. The widths of the two sharp lines are given in table 2. In this, Δ_1 and Δ_2 refer to the widths of the low and high energy sharp lines respectively.

The sharpness of these lines suggests that they are zero phonon lines arising from purely electronic transitions: the widths should be compared with the value of kT which at $6^\circ K$ is some 3 cm^{-1}.

There are several mechanisms which may produce more structure due to electronic transitions than is predicted by the simple crystal field model of a d^2 configuration within a site of tetrahedral symmetry. The following have to be considered:

(a) Trigonal and other low symmetry electrostatic fields.

(b) Spin-orbit splitting.

(c) The possible presence of transitions involving low-spin states, due to the relaxation of the spin-selection rule.

(d) Jahn-Teller coupling.

(e) The results of (b) and (d) simultaneously.

Low Symmetry Crystalline Fields

Zinc sulphide occurs in two distinct forms. The phase stable at high temperatures is hexagonal, while the cubic phase is stable below $1020^\circ C$. Crystals at room temperature may contain regions of both types.

If the crystals of ZnS:Ti contained hexagonal regions, then the crystal field at the impurity sites in such regions would not be tetrahedral but would have a trigonal component. The lower symmetry would split the degeneracy of the levels and thus produce additional zero phonon lines in the absorption spectrum. The absorption bands would also be split if the impurities were near stacking faults, where again the symmetry would be lowered [139,140,141].

The crystals of ZnS used in the present study were grown at temperatures not greater than 850^{o} centigrade, using an iodine transport technique (see page 29). Thus they are expected to be in the cubic phase. However to test whether the doped samples did contain any non-cubic regions, they were examined between crossed Nicol prisms, using a petrological microscope. Although a very small fraction did appear to be non-cubic, and there was some evidence of optical activity induced by strain, in general the material was cubic and of good quality. Samples of ZnSe:Ti were also observed and found to be of high quality, with little sign of strain fields and no stacking faults.

From this evidence, the impurity atoms must in each material be present predominantly at sites of cubic symmetry. This conclusion is further supported by e.s.r. data for titanium in several materials, including ZnS, showing that the impurity site symmetry is either cubic or it is hexagonal, depending on the structure of the crystal [136].

Spin-orbit Splitting

Spin-orbit effects can split electronic levels. Inspection of the d^2 energy matrices, extended by Liehr and Ballhausen to include spin-orbit effects [9], reveals that the $^3T_1$ (^3P) state splits into four, giving three separate levels in first order:

Symmetry	Energy (relative to zero splitting)
Γ_5	$+\lambda$
Γ_3	$+\lambda$
Γ_4	$-\lambda$
Γ_1	-2λ

where λ is the spin-orbit coupling parameter. The symmetry labels are those of the joint spin-coordinate classification of Bethe [142], such that there are neither spin-orbit nor electron correlation interactions between the states listed [9]. However there are higher order interactions between each of these states and others of the same symmetry, so that the degeneracy of Γ_3 and Γ_5 is lifted, and the energy variation with λ is more complicated. Figure 6 shows how the mutual separation of the four $^3T_1$ (^3P) components varies with λ in ZnSe:Ti.

The electric dipole operator in Td symmetry has the representation Γ_5 [11], so that since the ground electronic state $^3A_2$ also belongs to Γ_5, transitions to all four levels of $^3T_1$ may be expected, since

$$\Gamma_5 \otimes \Gamma_5 = \Gamma_1 \oplus \Gamma_3 \oplus \Gamma_4 \oplus \Gamma_5 \quad [17].$$

Clearly this model does not agree with the experimental observation of two zero phonon lines.

Transitions to States of Lower Spin

So far, only spin triplet levels have been considered, because the ground state is a triplet and electric-dipole transitions between states of different spin are forbidden. However, in the presence of spin-orbit coupling, spin is no longer a good quantum number, and transitions to lower-spin levels must be considered as a possible source of extra lines.

As has been stated, spin-orbit coupling not only splits the $^3T_1$ (^3P) state but also induces an interaction between the different components of this multiplet and other states of the same symmetry. This may result in

the transfer of intensity between allowed triplet-triplet bands and otherwise forbidden triplet-singlet bands. Although from figure 2 it does not seem that there are any spin-forbidden transitions close to the $^3A_2 - {}^3T_1$ (^3P) band in either material, this is not certain, since only A and B have been determined. Also, when λ is of the order of 100 cm^{-1}, the nearest $\Gamma_1(^1A_1)$ and $\Gamma_4(^1T_1)$ states approach the triplet levels. The configuration interaction between these spin-singlet levels and the spin-triplet levels of $^3T_1$ in the same Bethe classification might result in significant intensity transfer.

It is possible to find the degree of mixing from the d^2 energy matrices by calculating not only the eigenvalues but also the eigenvectors. The following results are obtained:

Material	State	% triplet admixture	λ (cm^{-1})
ZnS:Ti	$^1A_1(\Gamma_1)$	8.4	100
	$^1T_1(\Gamma_4)$	0.34	100
ZnSe:Ti	$^1A_1(\Gamma_1)$	8.6	100
	$^1T_1(\Gamma_4)$	0.43	100

Thus the perturbed $^1A_1$ state has about 10% triplet character. Since the "borrowed intensity" is proportional to the square of the admixture coefficient, this would lead to triplet-singlet bands with intensities of one-hundredth of the triplet-triplet bands. With the stated values of crystal field parameters, these bands would lie some 700-800 cm^{-1} below the lowest energy parts of the triplet-triplet bands.

There is considerable disagreement between the predicted and measured intensities and separations (see figures 4(a) and 4(b)), so an explanation based on this model is unlikely.

Jahn-Teller Coupling

The ground state of substitutional Ti (d^2) in II-VI compounds is an

orbital singlet, $^3A_2$. The arguments given in chapter three imply that this state should be unaffected by Jahn-Teller coupling. This is not true of the excited state $^3T_1(^3P)$, an orbital triplet.

Since $$[T_1^2] = A_1 \oplus E \oplus T_2 \qquad (1)$$

this level could couple to lattice distortions of symmetry ε or τ_2.

The previous paragraphs show that the observed spectra cannot be explained solely in terms of spin-orbit coupling. In the next section the effects of the simultaneous interaction of Jahn-Teller and spin-orbit effects will be discussed.

Combined Spin-Orbit and Jahn-Teller Interactions

The general problem of a triplet state in a tetrahedral environment is mathematically intractable unless various assumptions are made, or the physical situation is similar to one of two limiting cases. These arise from Jahn-Teller coupling being much stronger than spin-orbit coupling, or vice versa.

(A) Jahn-Teller Coupling much stronger than Spin-Orbit Coupling

In this case, the theory of Ham may be applied [24], which predicts that various orbital operators may be reduced. In particular, there is an exponential reduction (or quenching) of the spin-orbit interaction in first order. In this case it is reasonable to diagonalise the interaction Hamiltonian neglecting spin-orbit effects, introducing these afterwards as perturbations on the resulting basis functions.

(B) Spin-Orbit Coupling much stronger than Jahn-Teller Coupling

When spin-orbit interactions are much greater than Jahn-Teller coupling, it is permissible to solve the spin-orbit problem first and to ignore vibronic interactions. In this case J is taken to be a good quantum number. Jahn-Teller matrix elements, which couple levels of different J, may be introduced later as perturbations [24].

Physically, this situation is typified by measured vibrational coupling much weaker than would otherwise be expected. Since the distortions of the lattice around the impurity are also reduced, this effect is known as spin-orbit stabilisation [19].

The intermediate situation, where vibronic and spin-orbit effects are comparable, necessitates the simultaneous inclusion of both effects in the diagonalisation of the Hamiltonian. This problem is tackled numerically, and the finding of a solution generally requires several simplifying assumptions to be made. For example, it is often found that an approximate fit to an observed spectrum can be made with a model of coupling to only one representative frequency of vibration, with a particular symmetry, rather than to the continuum of lattice phonons. This is true even in situations similar to that being considered here, where the state involved is a triplet and might couple to more than one symmetry type of mode.

Jahn-Teller Coupling to Orbital Triplets

Some justification for this is given by M C M O'Brien who has considered the coupling of a triplet state to ε and τ_2 vibrations simultaneously [143,144]. This treatment is most easily applied when there is equal coupling to both types of mode, but it is also shown, for example, that the ground vibronic state is always a triplet regardless of the strengths of coupling involved. Further, by considering the various orbital reduction factors, it is seen that even a slightly stronger interaction with one type of mode leads to a physical situation where it appears that only coupling to that type of mode is important. Thus if coupling to ε modes is stronger than to τ_2 modes, the energy level scheme will be closely approximated by a model involving only $T \otimes \varepsilon$ interactions. In particular, the minima of energy will correspond to three equivalent tetragonal distortions.

Consequences for Transition Metals

The values of the atomic spectral parameters B, C and λ for the transition metal atoms are known [8]. In particular, for the doubly ionised ions of the 3d transition metal group, the magnitude of λ increases monotonically with atomic number, from 40 cm^{-1} for Sc^{2+} to 415 cm^{-1} for Cu^{2+}. (In reference 8, page 437, Griffith gives ζ, the Condon and Shortley spin-orbit coupling constant, which is twice the value of $|\lambda|$ [9]).

Where λ has been determined for divalent transition metal impurities in II-VI compounds, it is found to be reduced by some 10-20% from its free ion value, by covalent effects. It is mainly spin-orbit coupling and Jahn-Teller coupling that give rise to the fine structure seen in the absorption or emission spectra of many impurity-systems, but as yet no complete systematic study has been made of these effects, so that their relative influences are not yet clear.

One group of materials that has been studied in this light consists of chromium (d^4) doped II-VI's, namely, ZnS, ZnSe, ZnTe, CdS and CdTe [145]. The ground state of the impurity in these materials is $^5T_2$, and in all cases a static distortion is found to be present. Coupling is to ε-mode phonons, with a Jahn-Teller energy of 470-600 cm^{-1}. However for the ^5E excited state, the strength of vibronic coupling is zero, or very small. Thus in the ground state strong quenching of first-order spin-orbit splitting is expected.

In these systems there is no first-order splitting in the excited state.

A brief look at the spectra of other systems shows that Jahn-Teller energies of a few hundred wave-numbers may be typical, as indicated by the widths of the various absorption or emission bands. In many cases zero phonon lines are seen. Thus it is probable that in general the

spectrum of an impurity will not correspond to either of the limiting cases, but will belong to the intermediate regime. In this situation it is clearly desirable to have as complete a model as possible, and to study systems not in isolation, but in comparison with several others.

Parameters for $^3A_2 - {}^3T_1\ (^3P)$ Band in ZnS:Ti and ZnSe:Ti

In each case there appear to be two zero phonon lines, each with an equally spaced series of vibrational sidebands at higher energy. Table 3 lists the energies of separation of the replicas in the various series. These lie very close to the energies of certain phonons at critical points of the Brillouin zones of the host materials. Properties of these lattice modes are given in table 4. From equation 1, both of these modes might be coupled to the excited level of titanium by the Jahn-Teller interaction.

Simple Interpretation

Two assumptions are made:

(1) that the lower energy series of TA(L) phonon replicas is due to coupling to ε-mode vibrations, while the higher energy lines result from coupling to τ_2 or ε-active TA(X) phonons;

(2) that spin-orbit splitting is quenched by the Ham effect. To justify this the following arguments are advanced: if the spin-orbit coupling is weak compared with the Jahn-Teller energy, E_{JT}, then any spin-orbit splitting is reduced by a factor γ, where

$$\gamma = \exp[-3E_{JT}/2\hbar\omega] \qquad (2a)$$

for ε-mode coupling, and

$$\gamma = \exp[-9E_{JT}/4\hbar\omega] \qquad (2b)$$

for τ_2-mode coupling [24,10].

Now within the assumptions of this model, $E_{JT} \simeq 200\ cm^{-1}$ for ZnSe:Ti (see later sections) so that $\gamma = 10^{-3}$. Thus any spin-orbit structure would be

compressed within the width of a zero phonon line.

Jahn-Teller Coupling Parameters

Figure 7 shows a typical configuration co-ordinate model diagram which might apply in a simple case of vibronic interaction with one mode [15]. Using this model it is possible to show that at sufficiently low temperature the intensity of the transition into the n'th vibrational state of the upper electronic level is given by I_n, where

$$I_n = I_o \, e^{-S} \, S^n/n! \qquad (3)$$

where I_o = total intensity of the absorption band

and $S = E_{JT}/\hbar\omega$, the Huang-Rhys factor [38]. Thus, where this relation is applicable, it is possible to find the parameters S and E_{JT} from ratios of the intensities of the observed phonon replicas.

It should be possible to find these values for the ε-mode series in each compound quite readily since the zero phonon line and three replicas are visible. A rough calculation shows that for both ZnSe and ZnS, relation (3) holds with a Huang-Rhys factor of approximately 4.

It is not possible to improve very much on this value because of the rapid increase in halfwidth of the phonon replicas with vibrational quantum number. This means that they overlap considerably and that only the intensities of the first two lines in the ε-mode series may be used confidently. Not only is there a loss of accuracy because only two lines may be taken, but also the calculated variation of intensity of these particular lines is not so great as for higher levels, in the possible ranges of values of Huang-Rhys factor (see table 5).

In ZnSe:Ti the ratio of I_0 and I_1 leads to

$$S_\varepsilon = 4.2 \pm 0.1$$

and $$E_{JT\varepsilon} = 205 \pm 5 \text{ cm}^{-1}$$

The shape of the ε-mode zero phonon line of ZnSe:Ti is close to being Gaussian (see figure 8). For comparison the first and second lines of this series are plotted together, with height and halfwidth normalised. Values of these are given in table 6. It seems that the first phonon replica departs from true Gaussian behaviour at low energy: this may reflect some spread in the energy of the interaction mode, in that the participating mode need not be a critical point phonon but may be a weighted average of the lattice modes of appropriate symmetry.

Table 6 shows that the first phonon replica in ZnS:Ti is wider than that in ZnSe:Ti. This may be due to the greater dispersion of vibrational modes in ZnS, where the highest energy acoustic and optical modes have energies of 220 cm^{-1} and 350 cm^{-1} respectively; in ZnSe the corresponding values are 190 cm^{-1} and 250 cm^{-1}.

In ZnS:Ti, S_ε is close to 4, so that

$$E_{JT\varepsilon} \simeq 276 \text{ cm}^{-1}.$$

Configuration-Co-ordinate Model

With these parameters for the ε-mode series it is possible to sketch a model to represent the interaction of both modes. This is shown in figure 9. Using this it is possible to find the Jahn-Teller parameters for the τ_2 series, as shown on the figure. The values are given in table 7.

If it is assumed that the intensities in the τ_2 series again conform to the Poisson distribution of equation (3) with $S\tau_2$ obtained from $E_{JT}/\hbar\omega$, then the measured strengths of the various replicas should be as given in table 8. When this is compared with figures 4a and 4b, it is seen that the observed spectra consist of many strong replicas which do not fall in intensity as rapidly as the predicted values. Thus the values of $S\tau_2$ required to fit equation (3) to the observed series would have to be much larger than the values given by $S\tau_2 = E_{JT}/\hbar\omega$.

For ZnSe:Ti the value of $S\tau_2$ required to make up the total intensity of the band, less that part due to the ε-mode series was found according to the relation:

$$I_{total} = I_{(Z.P.L)\varepsilon}\, e^{S_\varepsilon} + I_{(Z.P.L.)\ \tau_2}\, e^{S\tau_2} \qquad (4)$$

Here $I_{(Z.P.L.)\varepsilon}$ and $I_{(Z.P.L.)\tau_2}$ are the intensities of the zero phonon lines of the ε and τ_2 series respectively. This leads to a value for $S\tau_2$ of 4.1. (Note that $S\tau_2$ can not be found by comparing ratios of phonon replicas, since the components of the τ_2 series overlap not only the ε-mode series, but also overlap each other quite considerably.) A similar value would apply to ZnS:Ti. This calculation gives also the values of intensity of the ε and τ_2 series: for ZnSe:Ti the ratio is

$$\frac{\text{Total } \varepsilon\text{-series Intensity}}{\text{Total } \tau_2 \text{ series Intensity}} \simeq \frac{1}{32}$$

For a simple vibrational interaction model the mean energy $\bar{E}$ of an absorption band is given by

$$\bar{E} = E_{Z.P.L.} + (S \times \hbar\omega) \qquad (5)$$

For the $^3A_2 - {}^3T_1\ (^3P)$ transition in ZnSe:Ti, $\bar{E}$ is about 10140 cm^{-1}. This value is quite close to E*, where

$$E^* = E_{Z.P.L.} + (S_{\tau_2} \times \hbar\omega_{\tau_2})$$
$$= 9836 + (4.1 \times 71)\ \ cm^{-1}$$
$$= 10127\ cm^{-1}.$$

(The contribution of the ε-mode series to E* is neglected because of its low intensity).

This shows that it is possible to get good agreement with theory for each of the two series separately, assuming Poisson distributions and simple, independent vibrational coupling. However it is not possible to combine the two consistently on one diagram, such as that shown in figure 9.

Objections to Simple Model

Öpik and Pryce have studied the linear Jahn-Taller interaction of ε and τ_2 modes with a triplet electronic state [19]. They find that trigonal and tetragonal minima cannot coexist; if the equivalent minima in the potential energy correspond to tetragonal distortions, then trigonal distortions correspond to saddle points, not minima, and vice versa. This is confirmed by calculations for this situation for a wide range of coupling strengths [144]. Thus zero phonon levels would be found associated with only tetragonal minima, or trigonal minima, but not both.

Furthermore although a harmonic approximation might seem reasonable around the minima of energy, so that regularly spaced levels would be found below the cross-over point at $E_{JT} = S\hbar\omega$, a more complex behaviour is likely at higher energies. In the present experiments, values of S have been deduced which make it appear that Jahn-Teller coupling is not large. However equispaced phonon replicas are found well above the derived cross-over point, and for both series.

These objections render the simple model of linear coupling untenable. To retain some features of the interpretation, the consequences of higher order coupling have to be considered.

Quadratic Jahn-Teller Interaction

Bacci et al have investigated the quadratic Jahn-Teller interaction of a triply degenerate T electronic term in an O_h complex with ε_g and τ_{2g} modes. They show that for a range of interaction strengths tetragonal and trigonal minima may coexist [146,147]. It also appears that spin-orbit effects are quenched when the vibronic coupling is stronger than the spin-orbit coupling. It is therefore possible that the scheme for the absorption spectra of ZnS:Ti and ZnSe:Ti given above could be retained if the possibility of higher than linear Jahn-Teller coupling is admitted.

Bacci et al have studied only octahedral complexes, so the details of quadratic coupling for tetrahedral centres are not known. Also they have looked at the potential surfaces, and have not yet worked out the energy level scheme. However if the minima are sufficiently well separated, with a sufficiently high saddle point between them, it is plausible that for low-lying energy levels within each potential well, a harmonic approximation may be adequate. This would lead to equally spacdd levels. Quadratic effects would be important at higher energies and might account for the observed broadening of sidebands. The presence of quadratic interactions means that the values of S derived above would not be directly related to the depth of the Jahn-Teller minima.

Conclusions

The model advanced is a possible explanation of the observed spectra, but depends on non-linear Jahn-Teller coupling. This is not yet well understood or experimentally confirmed. Until the eigenfunctions of the quadratic system have been obtained theoretically, no firm statement for or against the model can be made.

However it should be stressed that the physical picture obtained by measuring the absorption bands in the ZnS:Ti and ZnSe:Ti studied here is clearer in some ways than that obtained for many other systems. Two examples demonstrate this:

(1) It is known that when trigonal and tetragonal modes interact with a triplet electronic state complex shapes are seen in absorption, even when individual phonon replicas are not seen [36]. For example a broad band may consist of two or three overlapping Gaussian bands. From the analysis above it seems that these individual bands are due to different modes. However it does not seem, from the literature, that any such ascription is made; indeed it seems that such a step has not been taken, just because individual replicas are not seen.

(2) Toyozawa and Inoue have studied an A-T_1 transition in KBr:Tl, and find that the structure of the absorption band is due to τ_2-mode coupling [39] . In contrast Fukuda et al have shown that ε-mode coupling dominates emission [40] . This is what would be expected by analogy with the systems studied in this work. The strong τ_2 coupling is most evident in the absorption band, while emission would occur from the low lying ε-coupled levels. However in the present work it is clear that the properties of transitions between such electronic states are due to simultaneous, fairly strong coupling to both types of mode.

Vibronic Antiresonance

Apart from the structure in the absorption spectra which has been shown to be due directly to Jahn-Teller coupling there are some other interesting details. These are clearly seen in figures 10 and 11, in which the zero of energy is taken to be the position of the ε-mode zero phonon line. It is apparent that these features are not simple absorption peaks but correspond to dips in absorption coefficient, or to fluctuations with positive and negative regions of absorption. The strongest dips occur at energies close to those of the host TO(Γ) phonons, while the others may be related to other critical point phonons (see appendix).

It is possible to extrapolate in these regions a background due mainly to absorption of the τ_2 series. This has been subtracted from the measured spectra in figures 12 and 13 to show the structure more clearly.

It seems that these features are correlated with vibronic levels of the impurity electrons. The presence of negative or asymmetric bands suggests antiresonance between states which are degenerate and arise from the coupling of different vibrational modes to the excited electronic level. In the particular cases of the strongest resonances in each material there are two interfering mechanisms of absorption; an electronic transition together with the excitation of a mode of vibration similar to a TO(Γ) phonon, and a transition into the Jahn-Teller coupled state corresponding to the creation of four ε-mode vibrational quanta. Table 9 shows that the TO(Γ)-coupled state lies close to the expected peak position of the fourth ε-mode replica in each material; in ZnS:Ti the coincidence of energies is exact.

The evidence for these spectral features being due to antiresonances is stronger than mere correlation with phonon energies. A further argument results from consideration of the line shapes.

The theory reviewed in chapter four applies in the case of a uniform

or slowly changing background. Sturge has extended this to allow for the effects of variations in the response due to background absorption [41]. The formulae are considerably more complicated than those of Fano, and calculations more lengthy. In order to discover some of the general properties of such a system, a computer model with variable parameters has been constructed. Numerical solutions enable the following general conclusions to be drawn:

(1) Where there is a uniform continuum of states so that the background absorption would be constant in the absence of any interaction, the shape parameter q (see chapter 4) gives an indication of whether the transition to the discrete state is allowed or forbidden. When the background absorption changes with energy, the shape of the antiresonance is affected not only by the probability of the transition to the discrete state, but also depends on the details of the shape of the background.

(2) When the transition to the unperturbed discrete state is forbidden the antiresonance band is totally negative only when the background is symmetric about the position of the unshifted resonance. In this case the antiresonance is most negative at the energy of the unperturbed discrete state, and is symmetric about this point.

In the systems studied experimentally in this work the background is due to Jahn-Teller coupling to TA(L) phonons. The absorption due to states coupled to these active modes is strong in comparison with that due to the totally symmetric TO(Γ) mode. Thus in the absence of interaction between the different vibronic states, the transition to a TO(Γ)-coupled level is expected to be forbidden. In ZnS:Ti, superposition of the TO(Γ) level with the centre of the fourth ε-mode replica, which is assumed to be approximately Gaussian and therefore symmetric about its centre, means that the resonance absorption is also symmetric, and is always negative.

Since the shape of the background is known, and it is known to be symmetric it is possible to analyse the antiresonance line-shape using the theory of Sturge [41].

Figure 13 shows the calculated fit to the relation

$$f(\omega) \alpha \; -\{1 + \gamma^2 \; (\omega - \omega_r)^2\}^{-1} \qquad (6)$$

$$\text{where } \gamma^2 = \gamma^2_{\,o} \exp \{- a^{-2} \; (\omega - \omega_r)^2\} \qquad (7)$$

Suitable parameters are

$$\omega_r = 276 \text{ cm}^{-1},$$

$$\hbar\gamma_o = 25 \text{ cm}^{-1},$$

$$\hbar a = 9 \text{ cm}^{-1}.$$

From the value of γ_o, it is possible to calculate that the lifetime of the TO(Γ)-coupled state before decay into the states of the Jahn-Teller series is 2×10^{-13} secs. This process need not go only in one direction. The Jahn-Teller states involve large local oscillations of the impurity and its close neighbours. It is not obvious that the TO(Γ) mode is localised however, so an alternative way of describing the antiresonance might be as a relaxation of vibrational energy of the impurity whereby four local quanta are destroyed and one optical phonon is emitted into the crystal.

The values of γ_o and a cannot be taken to be very significant as no account is taken in the above treatment of the width of the unperturbed TO(Γ)-coupled state, However $\hbar a$ is much less than any reasonable estimate of the width of the fourth phonon sideband.

This seems to indicate a selection rule in the interaction between the different vibronic states. The exact nature of the interaction is not known. Examples of such antiresonances as reported here have not previously been published, so there is no theory of vibronic antiresonance in impurity spectra.

Examples of multi-phonon resonances in the phonon spectra of some materials have been noticed: GaP [42], CdTe:S [43], CdSe:S [44],

$Ga_x In_{1-x}P$ [45] and $Al_x Ga_{1-x} As$ [46]. These resonances are detected by Raman scattering or infra-red absorption, and usually are discovered because of asymmetric optical phonon sidebands. No analysis of these in terms of Fano theory has been made, but Ruvalds and Zawadowski have proposed a model for such systems [47]. They suggest that "in the special case of a resonance consisting of two acoustic phonons, the hybridization of the resonance with a single optical phonon is possible." Their model applies to resonances with zero total momentum, but could be extended to resonances with small total momentum.

It is possible that the main resonances seen in the present work are due to the interaction of zone centre optical modes with continuum states formed from sums of four acoustic modes with total momentum equal to or nearly zero. This could explain why the parameter a, related to the spread in energy of the interacting continuum, is narrower than the total phonon sideband. It is reasonable that this interacting continuum is symmetric about the centre of the multiphonon sideband, so that the model of Sturge may be applied in the case of ZnS:Ti.

In general the nature of the interacting continuum may be observed by other absorption processes, for example the τ_2-mode series. The above theory cannot then be used with any confidence; however it is possible to find suitable empirical parameters by fitting to Fano's formula. It is clear that in a complicated spectrum only a strong absorption dip would suggest or justify this procedure.

The main antiresonance in ZnSe:Ti can be fitted to the Fano line-shape formula, with parameters as shown in table 10. The experimental and calculated curves are shown in figure 12.

Table 10 also gives parameters for the smaller antiresonances seen in the two materials. It is possible that these involve phonons from other critical points of the Brillouin zone, but the phonon dispersion

curves of the materials is not known with sufficient accuracy to make firm identifications. However these would be resonances with non-zero momentum, in contrast to the main resonances seen in these materials, and those seen in other systems. It is also possible that the resonances are due to the decay of localised vibrations into phonons from regions of the Brillouin zone with high densities of states. This point will be left to the following chapter, since similar effects are seen in ZnSe:Ni and ZnS:Ni.

Autoionization

All the properties of the absorption spectra described in previous sections relate to interactions between localised electrons and lattice vibrations or distortions. Autoionization is a purely electronic interaction; a mixing of bound impurity states and band states of the host material. This may lead to the release of electrons into the host material. Since this provides an extra decay channel for the excited state it will result in a decrease of the lifetime of the bound state, and may produce the typical antiresonance profiles.

A pre-requisite for the possibility of autoionization is that the excited impurity state lie within the conduction bands of the host material. It is expected that the ground state of titanium (d^2) should lie fairly close to the conduction band edge of II-VI compounds in which it is present [11]. Baranowski has shown that in ZnSe:Ti at least, the $^3T_1(^3P)$ state is degenerate with band states, although it seems to lie only 0.2eV above the band edge [3].

The zero phonon lines seen in the bands studied in this chapter are purely electronic lines, apart from weak high-order coupling with lattice vibrations. Effects such as lattice strain may broaden these lines inhomogeneously but the widths of the lines set lower limits for the lifetimes of the excited states:

$$\Delta t = h/\Delta E \qquad (8)$$

where ΔE = F.W.H.M.

These are shown in table 11.

An extra decay mode exists for the state corresponding to the zero phonon line of the τ_2 series, since it may decay into lower-lying ε states. The lifetime $\Delta t'$ of this inter-series decay, also shown in table 11, is calculated from the relation:

$$\Delta t' = [\,(\Delta t_{\tau_2})^{-1} - (\Delta t_{\varepsilon})^{-1}]^{-1} \qquad (9)$$

Δt_{ε} refers exclusively to the electronic transition, so that the decay of the excited state due to autoionization must take place in a time not less than 2×10^{-12} secs. This should be compared with autoionization times of 10^{-14} secs in free atoms and for s-d resonances in metallic solutions (Table 12).

It is apparent that autoionization is not important in determining the line widths of transitions in the materials investigated here. However the lifetimes of excited impurity states may be 10^{-6} to 10^{-8} secs, so that very weak coupling could still produce appreciable ionization, while not significantly broadening transition lines. It is not clear how this mechanism might be separated in practice from thermally induced transitions to degenerate ionized states. Indeed where the frequency of autoionization is lower than the frequency of zero point motion of the impurity, there will be no constant phase relation between impurity states and band states.

An earlier experiment on ZnSe:Ti suggested that there was autoionization from the $^3T_1$ (^3P) state [3]. The evidence is rather indirect, being based on the appearance of increased photoconductivity in the vicinity of the $^3A_2 - {}^3T_1$ transition. Ascriptions on similar arguments have been made for CdSe:Co, CdTe:Ti and CdTe:V [48]. However it was experiments carried out on CdS:Ti and CdSe:Ti, showing

anomalies in line widths that seemed to offer the clearest examples of autoionization [2,33].

Autoionization in CdS:Ti and CdSe:Ti

Figures 5a, b and c show absorption spectra of titanium impurities in cadmium compounds, obtained at liquid helium temperature. Other workers have investigated the transitions $^3A_2 - {}^3T_1\ (^3F)$ and $^3A_2 - {}^3T_1\ (^3P)$ in CdS:Ti and CdSe:Ti [2,33]. An analysis of the absorption bands by the method of moments [23] leads them to conclude that broadening of these bands is due not only to Jahn-Teller coupling, but also to strong autoionization, based on the following argument.

The second moment $\langle\overline{E^2}\rangle$ of an absorption band, broadened only by vibrational coupling, is given by

$$\langle\overline{E^2}\rangle = \sum_j S_j(\hbar\omega_j)^2 \coth(\hbar\omega_j/2kT) \qquad (10)$$

where j labels the different modes involved in coupling to the states. Thus at absolute zero of temperature there is a non-zero band width such that

$$\langle\overline{E^2}\rangle_{T=0} = \sum_j S_j(\hbar\omega_j)^2 \qquad (11)$$

This arises from zero point motion of the lattice. At high temperature it may be shown that

$$\langle\overline{E^2}\rangle \propto T. \qquad (12)$$

Thus extrapolation of the high temperature behaviour should pass through the origin.

Boyn and coworkers find that equation (10) is not adequate to fit the observed band shapes but require an additional constant term η, such that

$$\langle\overline{E^2}\rangle = \eta + \sum_j S_j(\hbar\omega_j)^2 \coth(\hbar\omega_j/2kT) \qquad (13)$$

In each case η is non-zero: values are given in table 13. In this table t_I is calculated from

$$t_I = \hbar/(\eta)^{\frac{1}{2}} \qquad (14)$$

It is argued that η arises from purely electronic processes and is in fact due to autoionization. This argument is supported by correlation with photoconductivity. t_I, the autoionization time, for each band is much shorter than the values found in this work for zinc compounds.

Thus for comparison the same methods have been applied in the present study, and table 14 lists various moments of the $^3A_2 - {}^3T_1(^3P)$ band of ZnSe:Ti at different temperatures. Low values of temperature were avoided as the fine structure would make it necessary to take very many experimental points to characterise the band accurately. At higher temperatures the band becomes much smoother.

Figure 14 shows the computed second moment as a function of temperature. The intercept on the moment axis is clearly not zero when the temperature is zero, so a value of "η" may be found. This is approximately 800 $(meV)^2$, so that the corresponding $t_I = 2.2 \times 10^{-14}$ secs. This is in strong disagreement with the value deduced from the width of the zero phonon line. Since the moment analysis for both zinc and cadmium compounds gives qualitatively similar results, it is reasonable to suggest that evidence for autoionization resulting from the analysis of moments is not conclusive.

Anomalous Second Moments

It is not clear where the extra factor η originates, but the following seem relevant to the problem:

(1) Cho shows that, with some simplifying assumptions, Jahn-Teller coupling to ε and τ_2 modes results in bands with two or three broad components (this is for strong coupling so individual phonon replicas are not resolvable) [36]. The peaks of these approximately Gaussian sub-bands are separated by energies which vary with temperature, becoming zero at low temperature. Boyn et al show this for CdS:Ti,

$^3A_2 - {}^3T_1\ (^3F)$, but find a non-zero separation for the corresponding band in CdSe:Ti. In the case of CdS:Ti, the fit is rather strained. Table 15 shows that, by inspection, the separation of the resolved components in all the bands of these materials may remain quite large.

In ZnSe:Ti also there appears to be an envelope with two broad peaks superimposed on the τ_2 series of the $^3A_2 - {}^3T_1\ (^3P)$ band; one peak is near the first or second phonon replica, the other near the sixth. The squared separation of these features is of the order of η for ZnSe:Ti.

This suggests that η might arise from some complexity of Jahn-Teller coupling. However Englman has stated that where the coupling to vibrations is not strong, the relevant temperature for such a system is an effective temperature T*. For τ_2 modes only coupling,

$$kT^* = \tfrac{1}{2}\,\hbar\omega_\tau \coth\,(\hbar\omega_\tau/2kT) \qquad (15),$$

which for T = 0, reduces to the zero point energy [13]. In analysis of band shapes for the $A_{1g} - T_{1u}$ transition, Nasu and Kojima find that equation (10) should hold for all strengths of linear coupling, and that even if quadratic effects are allowed, the high temperature behaviour of the second moment should still extrapolate to zero band width at zero temperature [49]. Thus it does not seem possible to relate η to the separations of the vibrational sub-bands.

(2) In 1964, Shionoya suggested that the width of several bands due to luminescent transitions in ZnS fitted a relation

$$W = B + A\,[\coth\,(h\nu/2kT)]^{\frac{1}{2}} \qquad (16).$$

A high energy mode, not activated at the temperatures used, was suggested to explain non-zero values of B[50]. Ermolovitch et al. have studied bands in CdS, and fit their data using an equation similar to (10), and seem to view the inclusion of B as an unjustified fitting parameter, at least in the case of CdS [51]. However their temperature

variation is rather small, so the fit is not very convincing.

Other authors have used Shionoya's model e.g. Williams [52], Iida [53] and Brandt [54]. In a study by Jones and Woods on luminescence of ZnSe:Mn, it is seen that the second moment of a band does not extrapolate to zero [55]. However equation (10) is the one most usually accepted: in the case of KBr:TL, which seems to have similarities with the systems of particular interest here, it is this formula that describes the behaviour of the emission band [56].

The presence of B seems to imply the existence of a highly energetic mode. It is not suggested that this is the explanation in the present cases, but it is interesting to note these examples of such behaviour.

Jahn-Teller Parameters : Cadmium Compounds

Before leaving the data for CdS:Ti and CdSe:Ti it is useful to compare the coupling parameters with those for ZnS:Ti and ZnSe:Ti. These are given in table 16, where

$$E_{vib}(x) = S_x \times \hbar\omega_x \qquad (17)$$

The values for the Cd compounds were found by fitting to the experimental data. In all materials the τ_2 modes have similar S values. However the fitting procedure does not allow for the disparity of intensities of the ε and τ_2-mode bands, evident in zinc compounds. This would have the effect of making S_ε in CdS and CdSe much larger, and closer to the zinc values.

The parameter $E_{vib}(\tau_2)$ is larger for cadmium compounds due to the higher energy found by fitting the experimental results for the τ_2-mode quanta: 107 cm^{-1} and 150 cm^{-1} for CdS and CdSe respectively. The dispersion curves for these materials are not known, but the higher values of dispersion apparent from these high acoustic phonon energies may, in part, explain why no discrete phonon structure is seen in the

cadmium compounds.

It is not surprising that the phonon coupling in the four materials reviewed here seem rather similar, since the degree of ionicity does not change markedly from one compound to another (see table 17). The coupling should be proportional, among other factors, to the crystal field parameter Δ, which is itself proportional to the ionicity [4].

Figures for Chapter Six

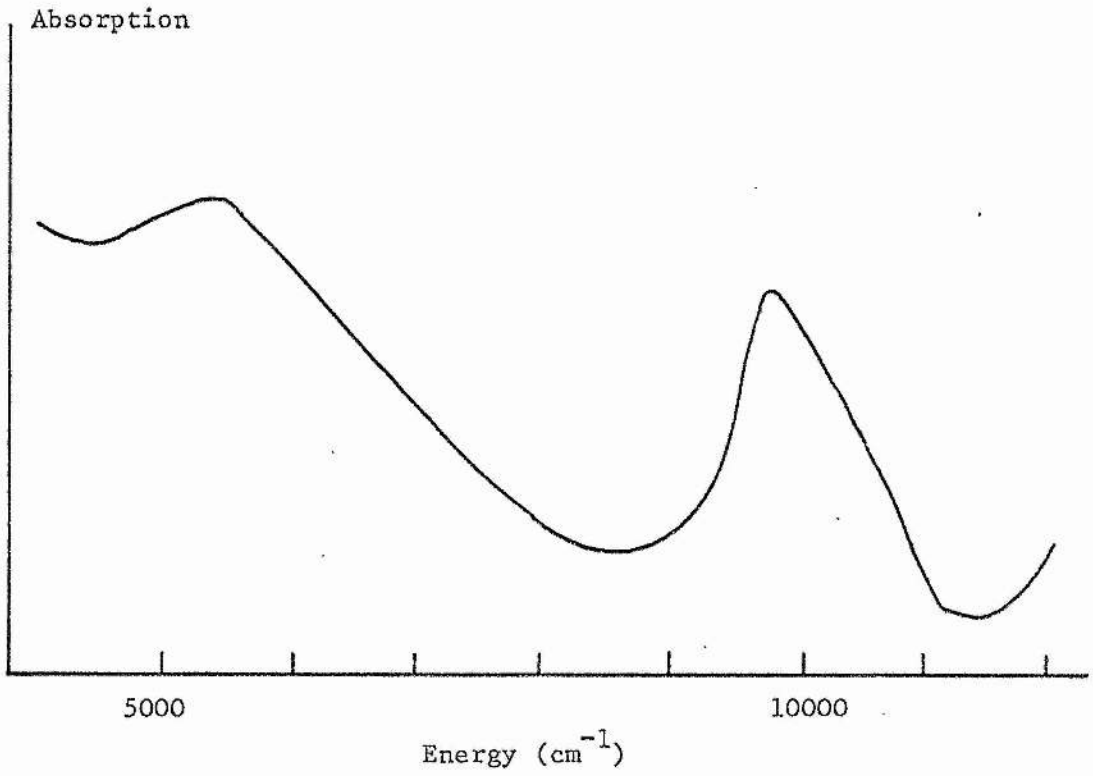

Figure 1

Absorption spectrum of ZnSe:Ti at room temperature (taken from trace of double-beam spectrophotometer.) The rising absorption at low energies is much weaker at low temperatures, and may be due to conduction band electrons.

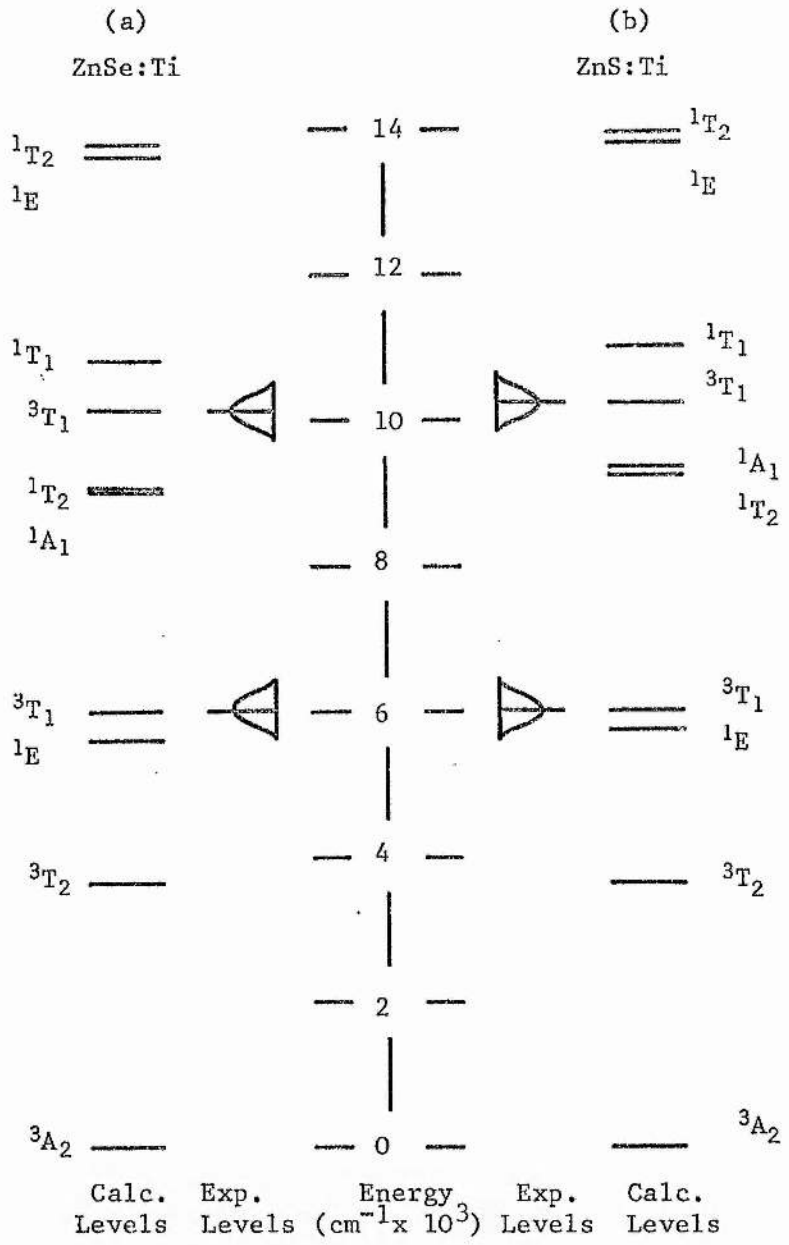

Figure 2

Calculated and experimental levels of ZnSe:Ti and ZnS:Ti. The crystal field parameters come from table 1, with C = 4.5B. The widths of the measured bands are indicated schematically; these and the positions are taken from spectra at liquid helium temperatures.

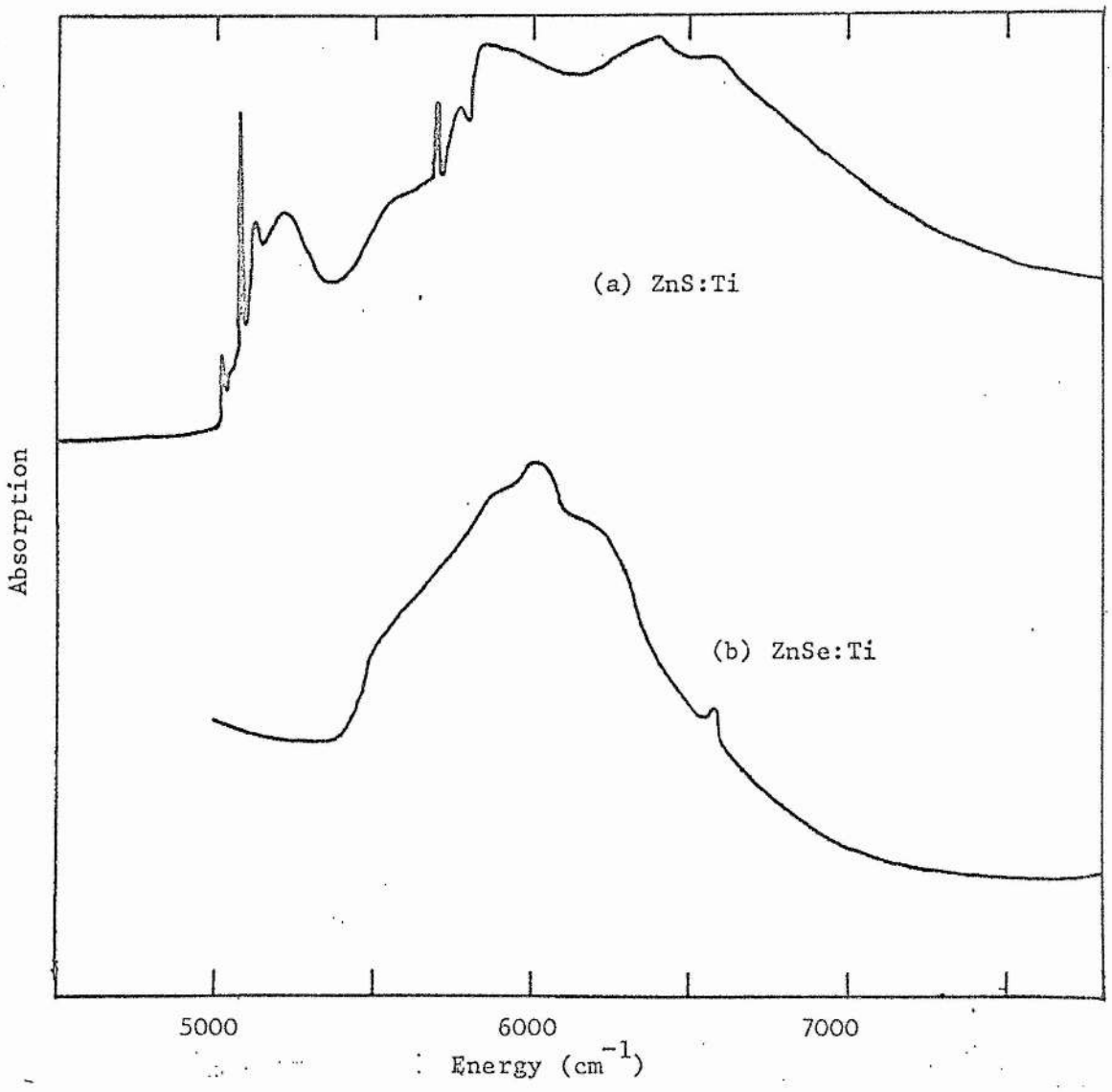

Figure 3
The $^3A_2 - {}^3T_1$ (^3F) bands of ZnS:Ti and ZnSe:Ti at 6°K.

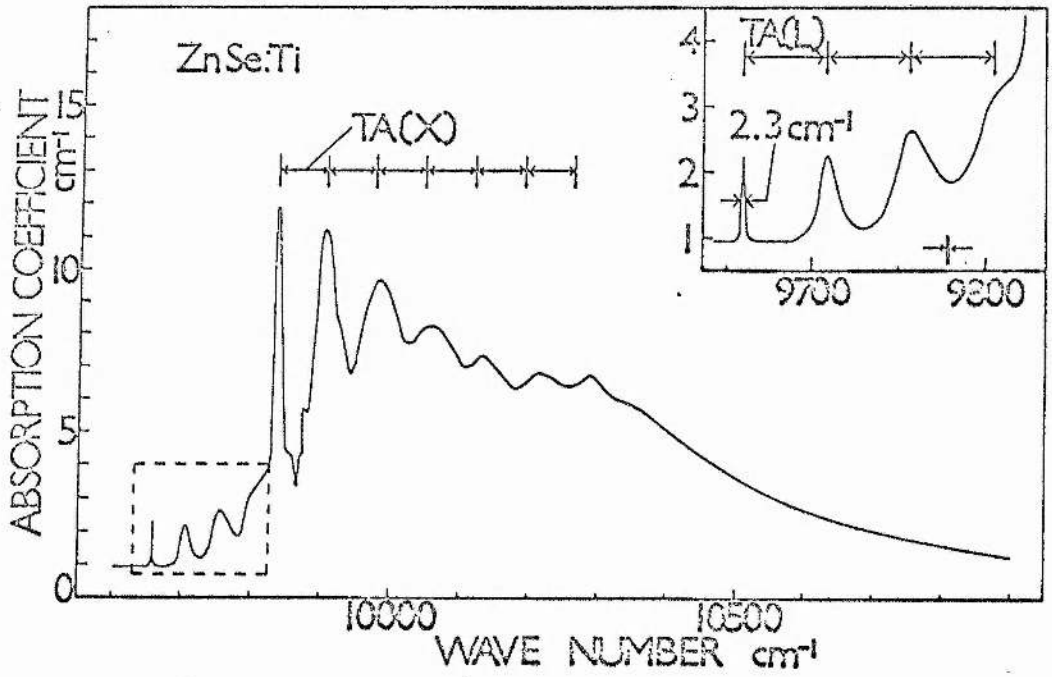

Figure 4(a)

$^3A_2 - {}^3T_1$ (^3P) band of ZnSe:Ti at 6°K

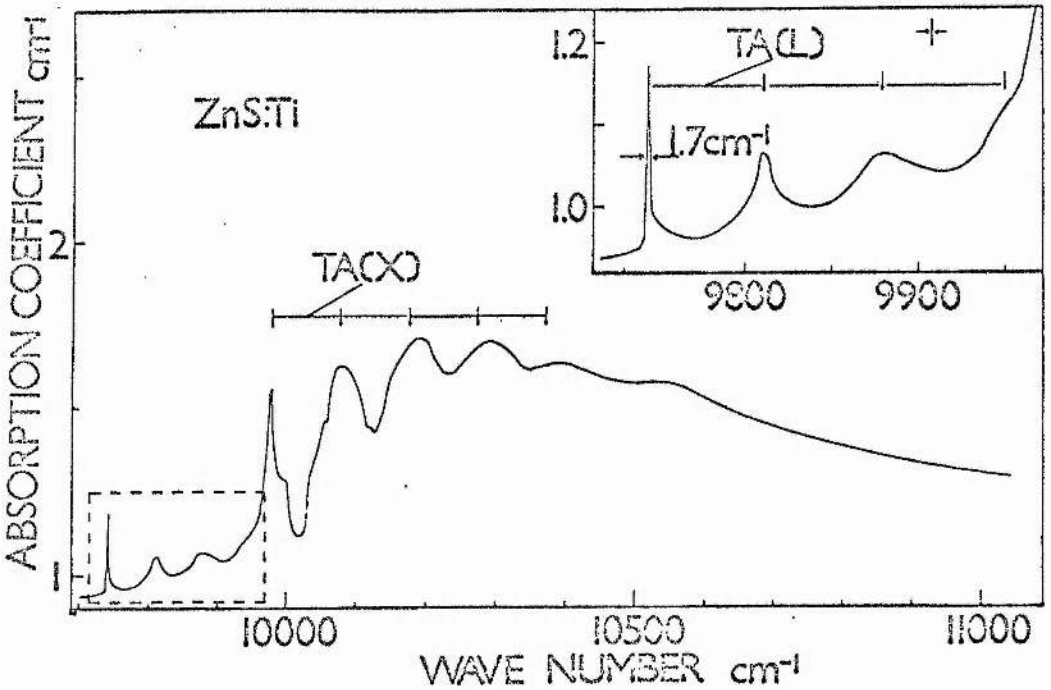

Figure 4(b)

$^3A_2 - {}^3T_1$ (^3P) band of ZnS:Ti at 6°K

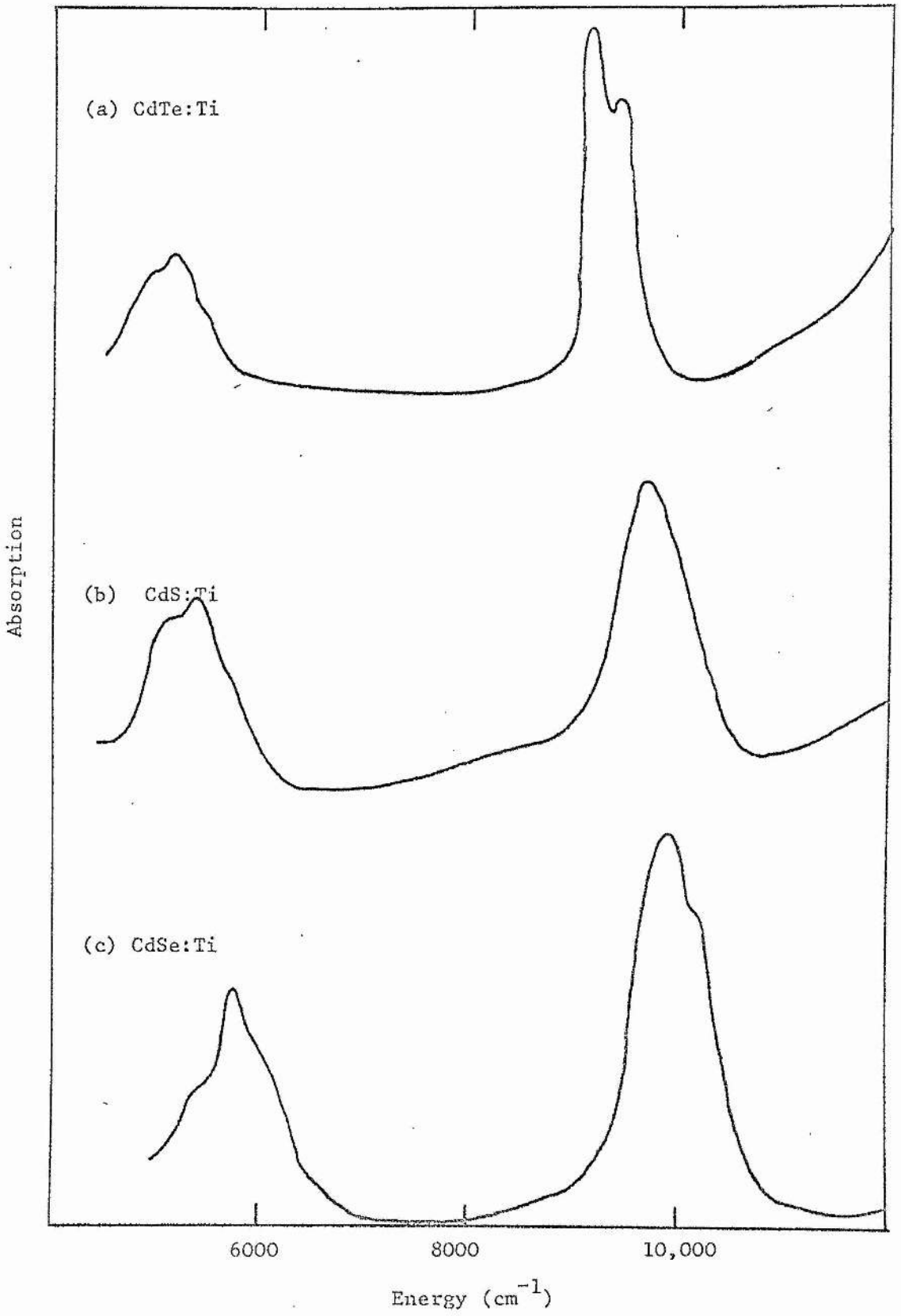

Figure 5

The internal d^2 absorption bands of some cadmium compounds doped with Ti, recorded at liquid helium temperature.

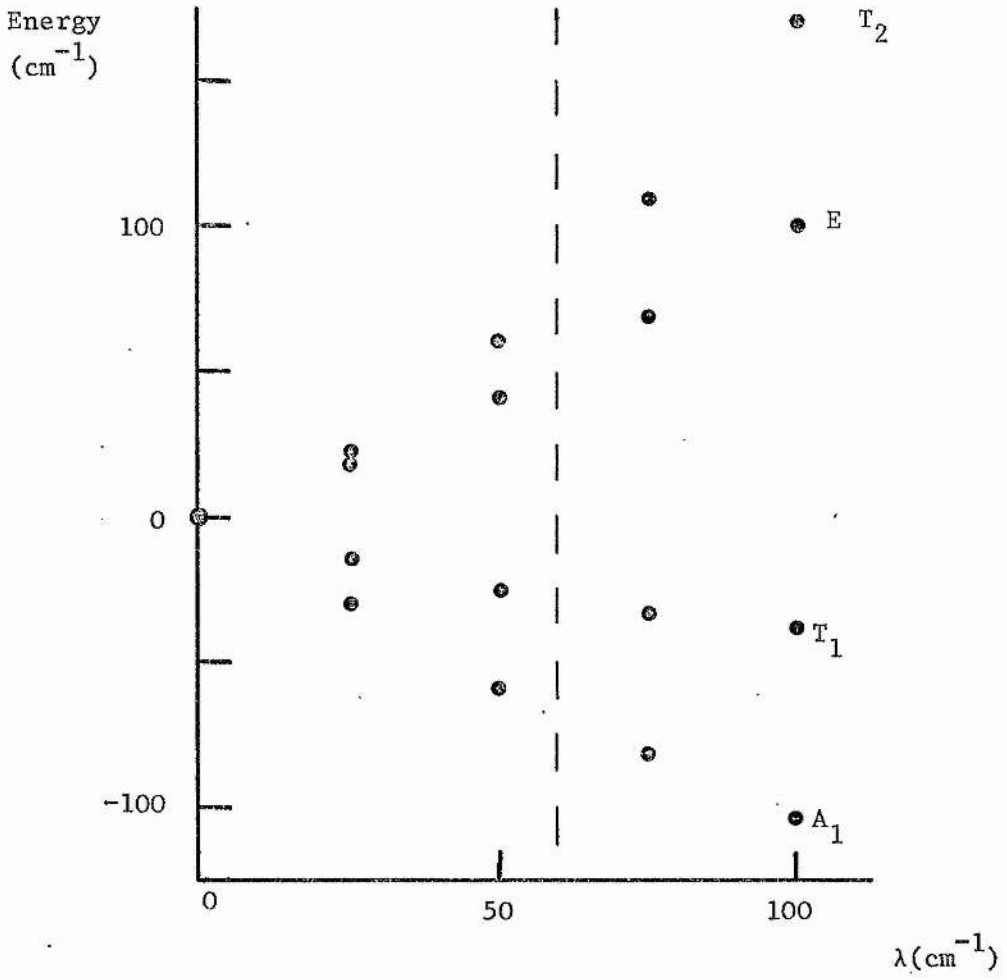

Figure 6

Spin-orbit splitting of the $^3T_1(^3P)$ state. The above figure was plotted for ZnSe:Ti, but the differences for ZnS:Ti are very slight. Crystal field parameters are taken from table 1, and C = 4.5B. The dashed line is at the free-ion value, λ = 60 cm^{-1} [7].

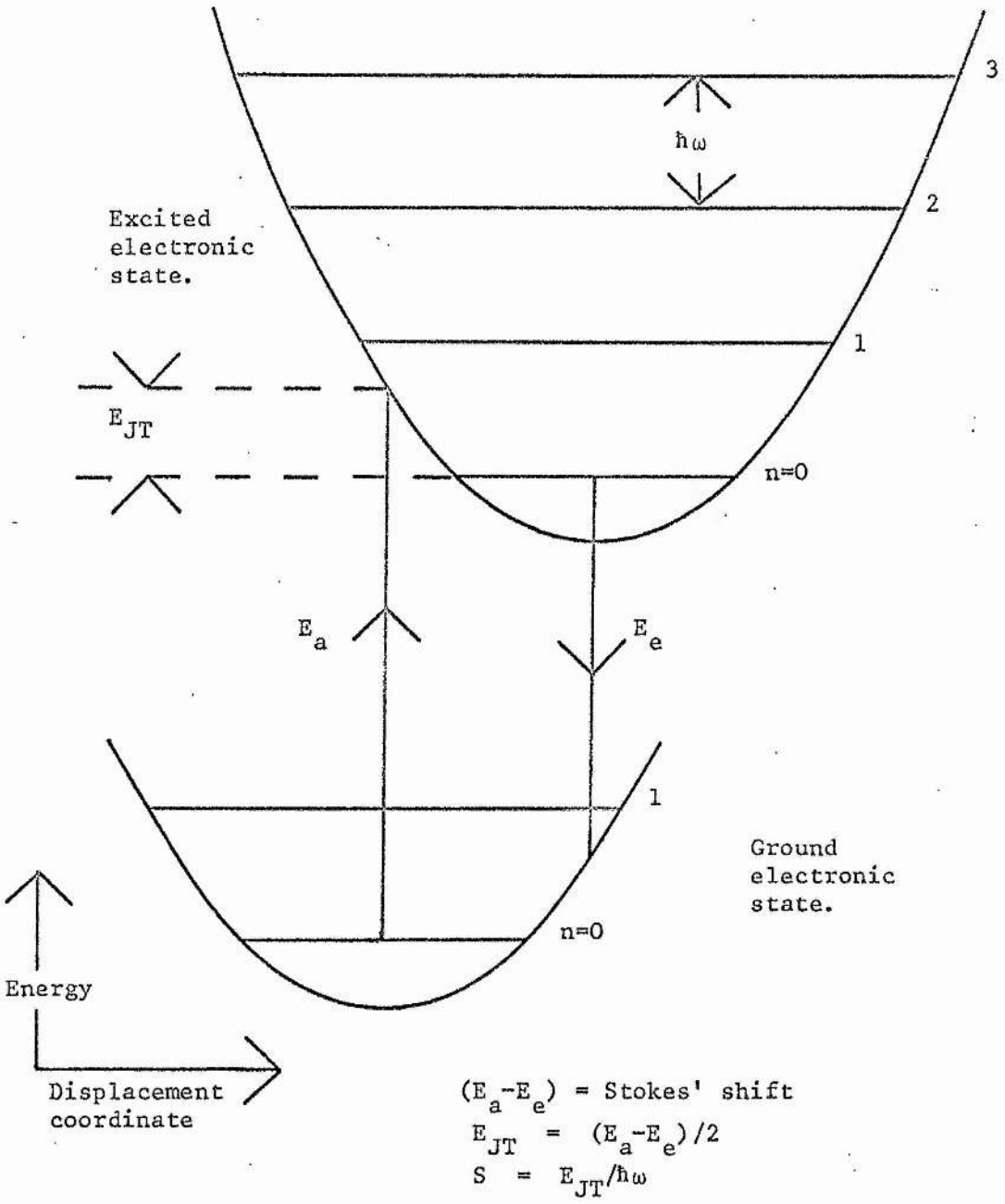

Figure 7

Single mode, configuration coordinate model diagram.

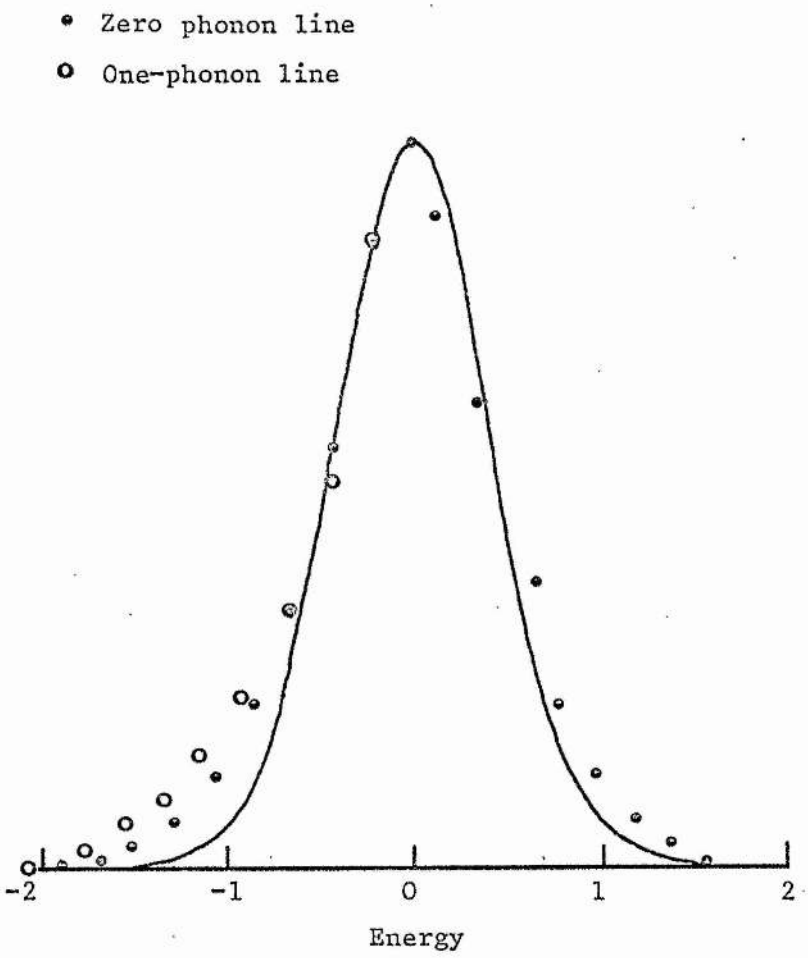

Figure 8

Comparison of phonon sidebands with gaussian behaviour. The energy scale is in units of F.W.H.M., with the parameters of table 6.

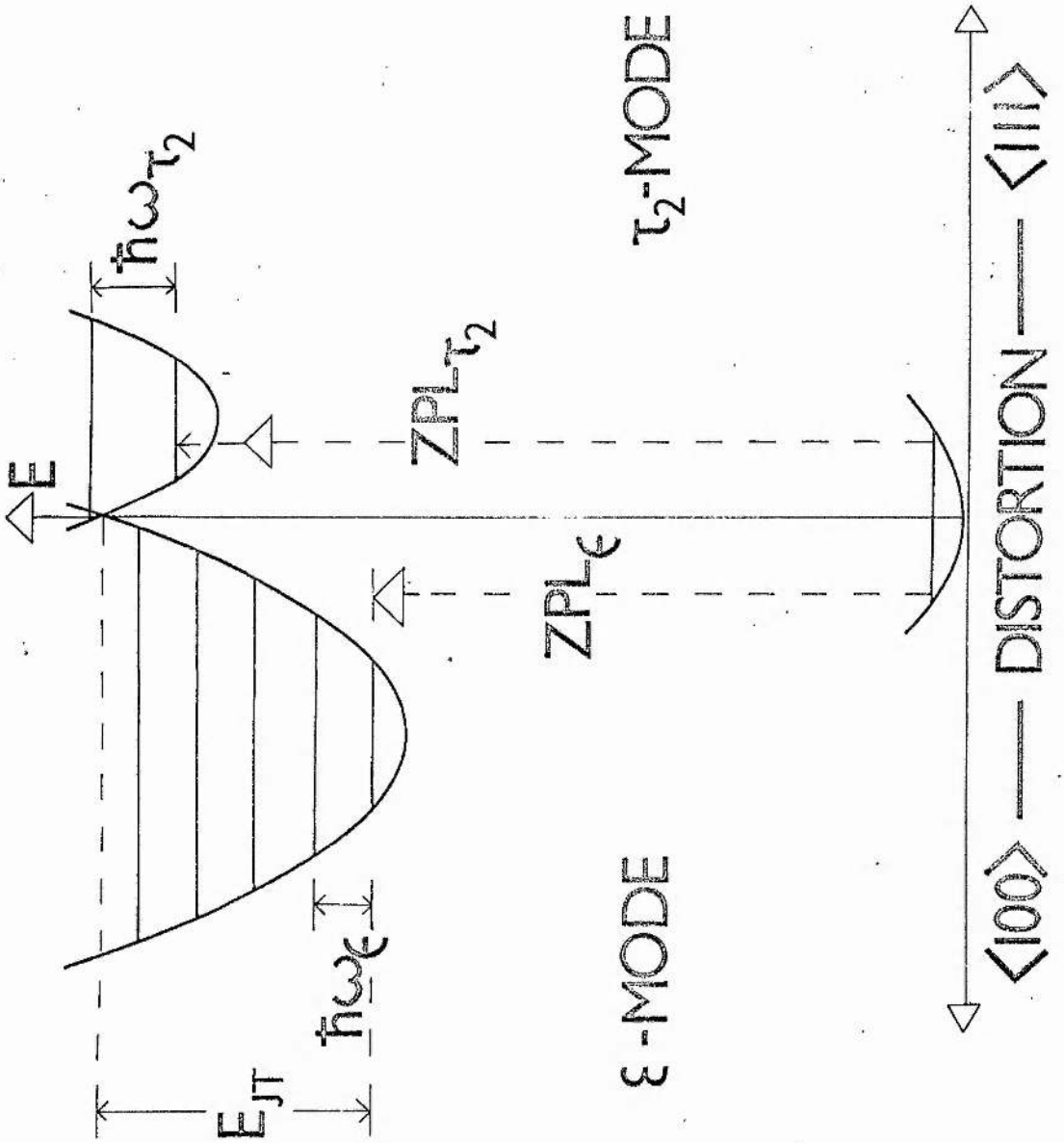

Figure 9

A possible model for the interaction with impurity states of two vibrational modes.
(The diagram shows the significance of E_{JT} for the tetragonal mode; the value for the trigonal mode is arrived at in a similar way).

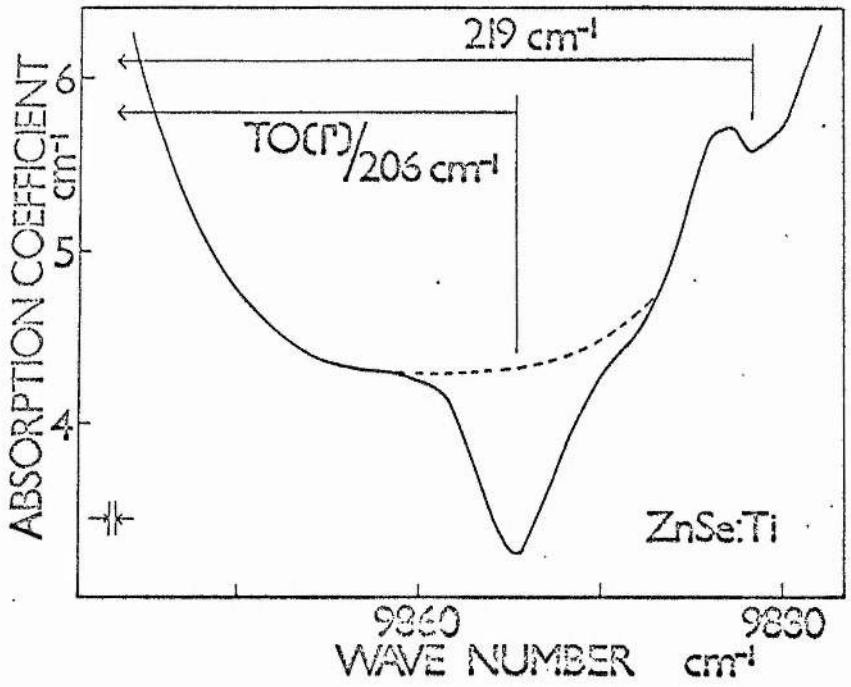

Figure 10

Details of antiresonance structure in the $^3A_2$ - $^3T_1(^3P)$ band of ZnSe:Ti

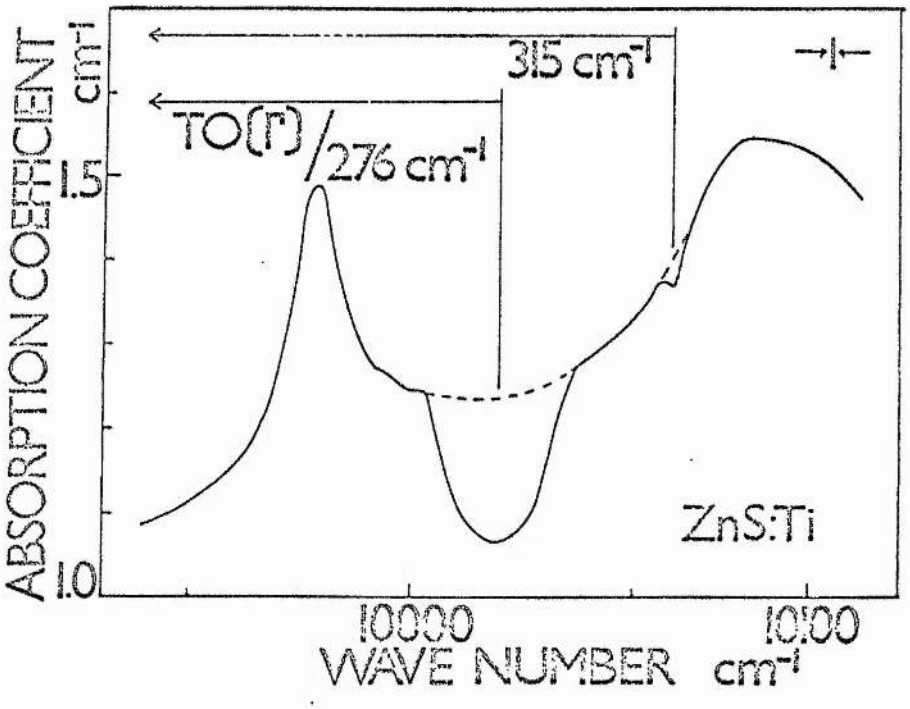

Figure 11

Details of antiresonance structure in the $^3A_2$ - $^3T_1(^3P)$ band of ZnS:Ti.

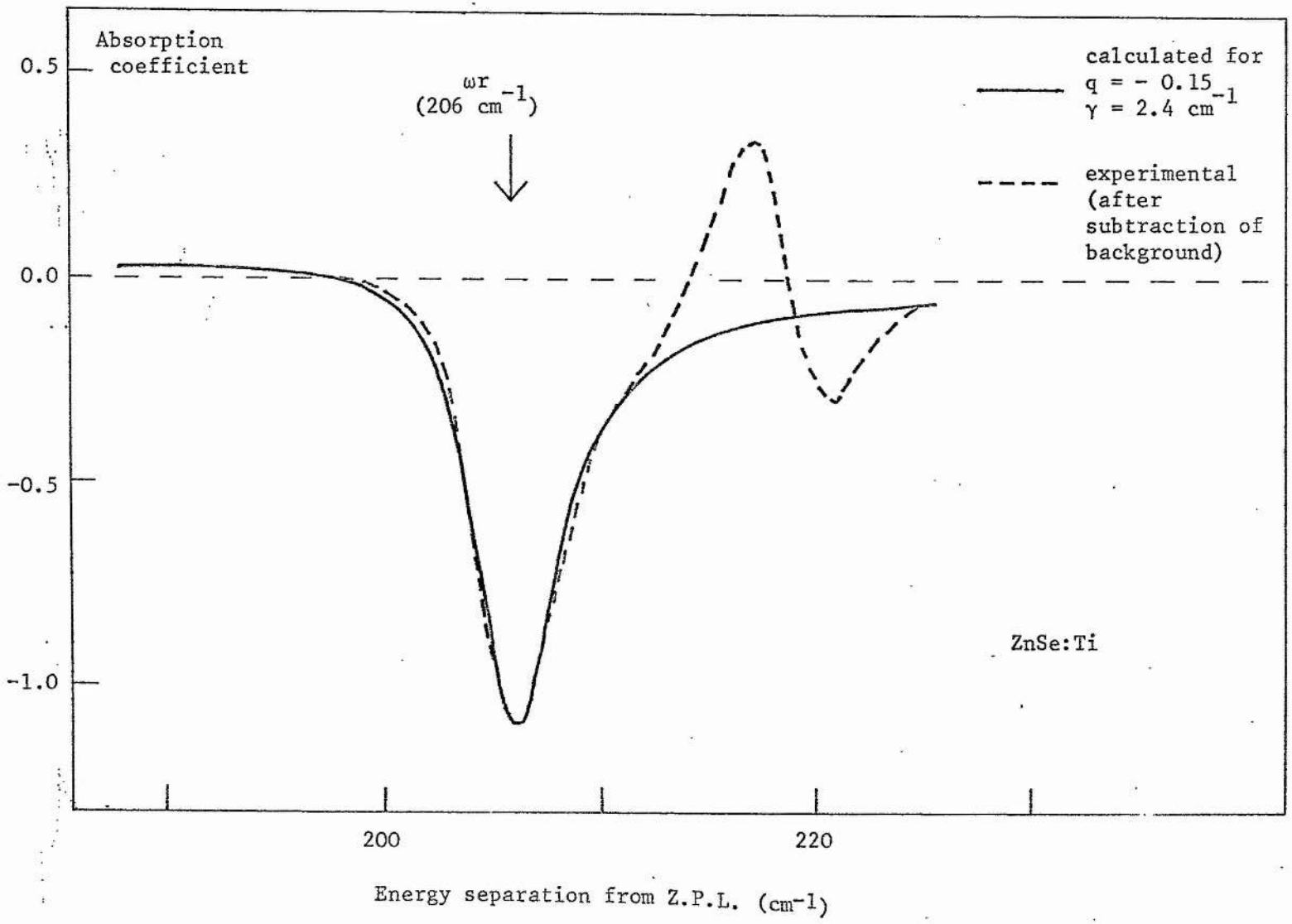

Figure 12

Main antiresonance in ZnSe:Ti

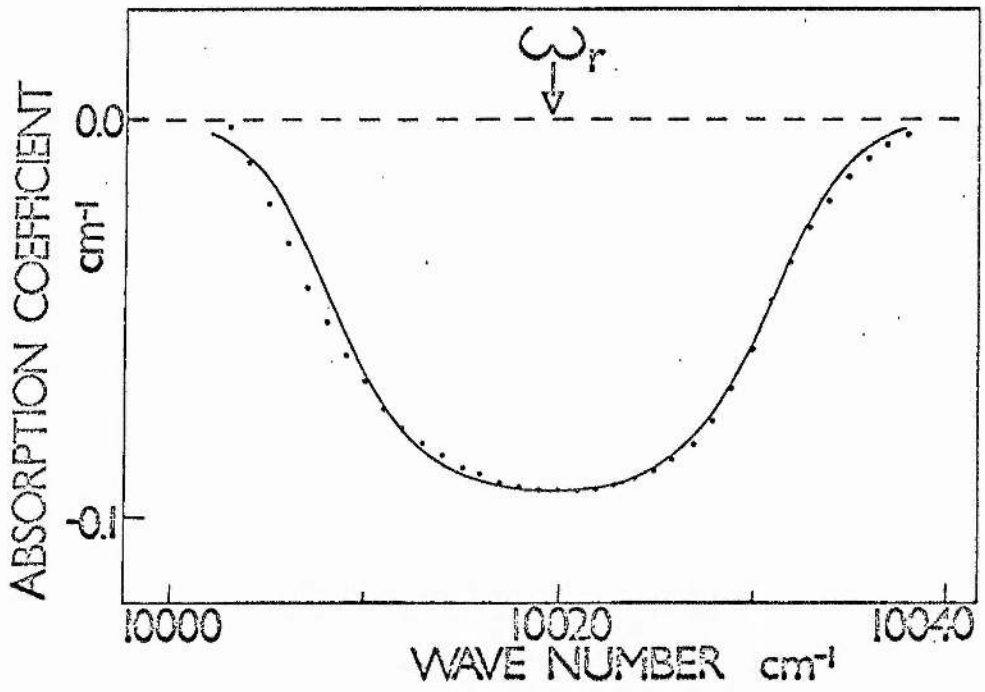

Figure 13

Main antiresonance in ZnS:Ti. The dots show experimental points. The solid line traces out $f(\omega)$, where

$$f(\omega)\alpha -(1 + \gamma^2(\omega-\omega_r)^2)^{-1}.$$

For values of parameters see text.

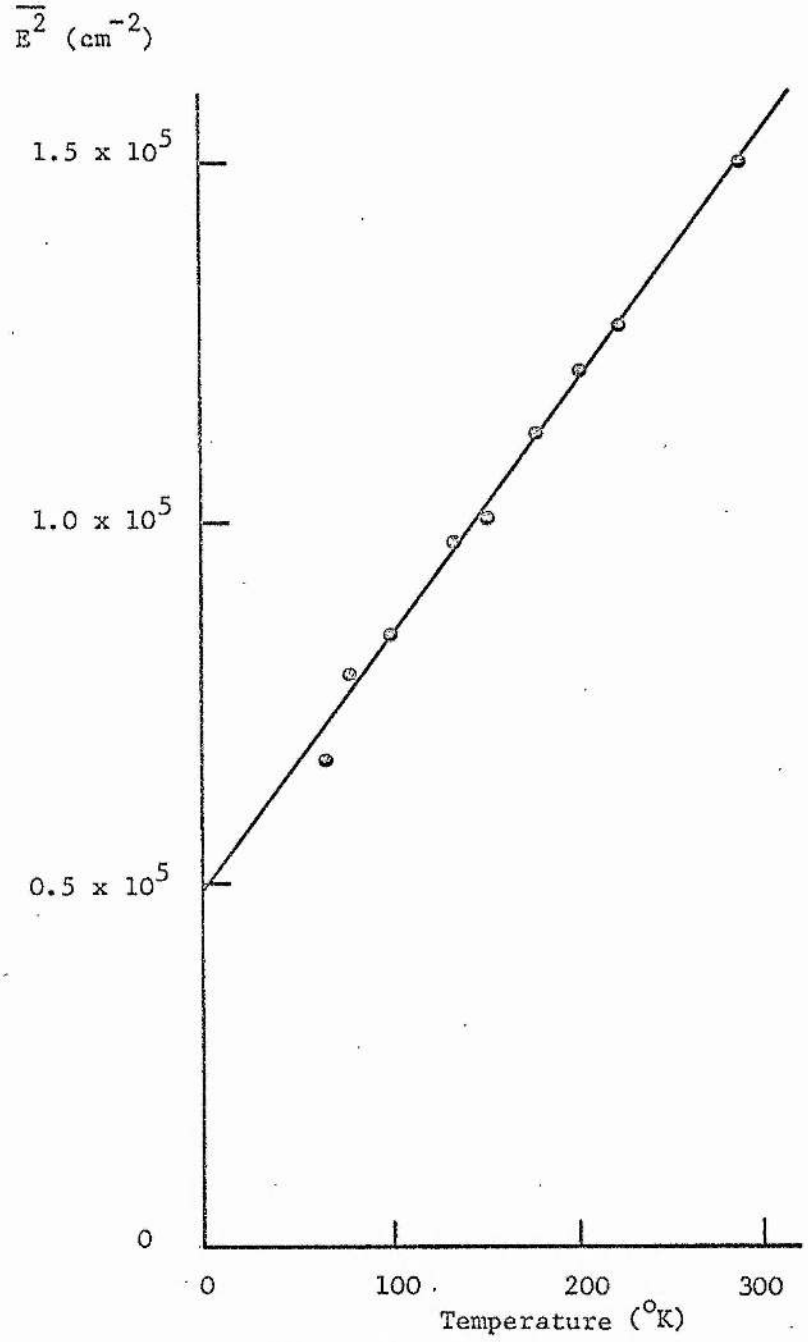

Figure 14

Variation with temperature of the second moment of the $^3A_2$ - $^3T_1$ (^3P) band of ZnSe:Ti.

TABLES FOR CHAPTER 6

Table 1

Empirical crystal field parameters for ZnSe:Ti and ZnS:Ti

	$\Delta(cm^{-1})$	$B(cm^{-1})$
ZnSe:Ti	3670	340
ZnS:Ti	3660	350

Table 2

Widths of zero phonon lines in $^3A_2$ - $^3T_1$ (^3P) absorption bands of ZnSe:Ti and ZnS:Ti

	F.W.H.M. $\Delta_1(cm^{-1})$	F.W.H.M. $\Delta_2(cm^{-1})$
ZnSe:Ti	2.4	8.2
ZnS:Ti	1.7	11.7

Table 3

Periodicity of structure of $^3A_2$ - $^3T_1$ (^3P) absorption bands of ZnSe:Ti and ZnS:Ti

	Spacing (cm^{-1})	
	Lower series	Upper series
ZnSe:Ti	48.5	71
ZnS:Ti	69	97

Table 4

Critical point phonons in ZnSe and ZnS.

	Phonon	Energy (cm^{-1})	J-T Active as (c)
ZnSe	TA(L)	49(a), 58(b)	ε
	TA(X)	70.5	ε, τ_2
ZnS	TA(L)	69	ε
	TA(X)	93	ε, τ_2

(a) Vallin et al [129] - impurity induced optical absorption.

(b) Irwin and La Combe [130] - Raman scattering.

(c) London [62].

Table 5

Theoretical values of relative intensities of phonon sidebands, with a simple model. For low values of n, the intensity of the n'th replica does not change greatly as S is varied.

			n = 0	n = 1	n = 2	n = 3
S = 4	$S^n/n!$	=	1 ,	4 ,	8 ,	11
S = 5	$S^n/n!$	=	1 ,	5 ,	13 ,	21

Table 6

Widths of zero and first phonon lines in the lower, ε-mode series of the $^3A_2$ - $^3T_1$ (^3P) bands of ZnSe:Ti and ZnS:Ti.

	F.W.H.M. (cm^{-1}) at 6^oK	
	zero phonon line	first phonon line
ZnSe:Ti	2.4	10.7
ZnS:Ti	1.7	20

Table 7

Jahn-Teller parameters for the upper, τ_2-mode series in ZnSe:Ti and ZnS:Ti, using

$$E_{JT}/\hbar\omega = S_{\tau_2}$$

	$E_{JT}(cm^{-1})$	$\hbar\omega(cm^{-1})$	S_{τ_2}
ZnSe:Ti	29	70.5	0.41
ZnS:Ti	41	93	0.42

Table 8

Expected relative intensities of phonon replicas in the τ_2-mode series, with a Huang-Rhys factor of 0.4

			n = 0	n = 1	n = 2	n = 3
S = 0.4	$S^n/n!$	=	1 ,	0.4 ,	0.08 ,	0.01

Table 9

Exact or near coincidence of optical and multi-acoustic modes in ZnSe and ZnS. The nature of the antiresonance between these modes in titanium-doped samples depends on the energy difference between such sidebands.

	Mode	Energy (cm^{-1})
ZnSe:Ti	TO(Γ)	209
	4 x TA(L)	194
ZnS:Ti	TO(Γ)	276
	4 x TA(L)	276

Table 10

Parameters of antiresonances in ZnSe:Ti and ZnS:Ti.

Material	Energy (cm^{-1})	Appearance	hν (cm^{-1})	Lifetime (secs)	q
ZnSe:Ti	206	Strong	2.4	2×10^{-12}	-0.15
ZnSe:Ti	219	Weak	1.6	3×10^{-12}	-1.4
ZnS:Ti	276	Strong	25	2×10^{-13}	0.0
ZnS:Ti	315	Weak	5	1×10^{-12}	0.0

Table 11

Lifetimes Δt_{ε} and Δt_{τ_2} of zero phonon states in ZnSe:Ti and ZnS:Ti, and interseries interaction time $\Delta t'$.

	Δt_{ε} (secs)	Δt_{τ_2} (secs)	$\Delta t'$ (secs)
ZnSe:Ti	2.1×10^{-12}	6.2×10^{-13}	8.8×10^{-13}
ZnS:Ti	2.9×10^{-12}	4.2×10^{-13}	4.9×10^{-13}

Table 12

Lifetimes of autoionizing states.

(a) Metallic solutions: data from Beaglehole [131]

	Lifetime (secs)
Cu Ni	5×10^{-15}
Au Ni	2.8×10^{-15}
Ag Pd	1.2×10^{-15}
Au Pd	1.7×10^{-15}

(b) Free atoms. Some instances are given below; see also reference [27].

Photoionization of the 3s3p ('P) state of Mg [132].

Final Level	Lifetime for ionization (secs)
$3p^2$ (^1S)	2.4×10^{-13}
3p 4p (^1S)	1.3×10^{-11}
3p 4p (^1D)	1.0×10^{-14}

Ca^+, electron scattering resonances [133].

Level	Lifetime (secs)
3d 5p (^1P)	6.6×10^{-14}
3d 4f (^1P)	-
3d 6p (^1P)	6.5×10^{-13}
4p 5s (^3P)	1.0×10^{-12}
4p 5s (^1P)	6.9×10^{-14}
3d 5f (^1P)	1.2×10^{-13}

Reported lifetimes of states in Xenon vary between 4.6×10^{-14} and 5.2×10^{-15} secs and in Argon between 5.6×10^{-14} and 9.1×10^{-14} secs [134].

Table 13

Results of Boyn and coworkers for anomalous band-broadening in CdS:Ti and CdSe:Ti. For definition of symbols and discussion see text.

	Absorption band	$\eta(\text{meV})^2$	t_I(secs)
CdS:Ti	$^3A_2 - {}^3T_1\ (^3F)$	2.2×10^3	1.3×10^{-14}
	$^3A_2 - {}^3T_1\ (^3P)$	2.3×10^3	1.3×10^{-14}
CdSe:Ti	$^3A_2 - {}^3T_1\ (^3F)$	1.1×10^3	1.9×10^{-14}
	$^3A_2 - {}^3T_1\ (^3P)$	1.7×10^3	1.5×10^{-14}

Table 14

Experimentally determined moments of the $^3A_2 - {}^3T_1\ (^3P)$ absorption band of ZnSe:Ti at various temperatures.

Temperature (^oK)	$\overline{E^0}$	$\overline{E^1}$ (cm^{-1})	$\overline{E^2}$ (cm^{-2})
59	0.43	10,142	0.665×10^5
76	0.45	10,141	0.785 "
100	0.44	10,116	0.841 "
135	0.44	10,111	0.972 "
153	0.41	10,084	1.005 "
176	0.42	10,081	1.116 "
205	0.39	10,058	1.208 "
225	0.36	10,041	1.275 "
290	0.34	10,025	1.500 "

Table 15

Separation of Gaussian sub-bands in absorption spectra of CdS:Ti and CdSe:Ti at liquid helium temperatures.

	Absorption band	Separation (cm^{-1})
CdS:Ti	$^3A_2 - {}^3T_1(^3F)$	600
	$^3A_2 - {}^3T_1(^3P)$	400
CdSe:Ti	$^3A_2 - {}^3T_1(^3F)$	600
	$^3A_2 - {}^3T_1(^3P)$	Not resolved.

Table 16

Vibrational coupling parameters for the transition $^3A_2 - {}^3T_1(^3P)$. Those relating to ZnS:Ti and ZnSe:Ti were found in the present work; the others were calculated from the results of Boyn and coworkers [2,33].

S_α, S_ε and S_{τ_2} are coupling parameters for modes of symmetry α, ε and τ_2 respectively.

	S_α	S_ε	$E_{vib\,(\varepsilon)}$* (cm^{-1})	S_{τ_2}	$E_{vib\,(\tau_2)}$*
CdS:Ti	3	0.05	-	5.2	557
CdSe:Ti	2.3	0.05	-	4.2	633
ZnSe:Ti	?	4.2	205	4.1	291
ZnS:Ti	?	4	276	4	388

* $E_{vib(x)} = S_x \times \hbar\omega_x$.

Table 17

Material	f_I (Philips ionicity)
ZnS	0.623
ZnSe	0.630
CdS	0.685
CdSe	0.699

Table 18

Crystal field parameters for titanium (d^2)

Material	B cm^{-1}	Δ cm^{-1}	Configuration Ascribed	Ref
CdTe	332	3120	d^2	[137]
	360	2890	d^2	[138]
CdS	340	3323	d^2	[2]
CdSe	365	3070	d^2	[57]
ZnSe	340	3670	d^2	This work
ZnS	350	3660	d^2	This work

Table 19

Crystal field parameters for ZnSe:Ti, if the metal is present as $Ti^+(d^3)$

Pos^n of band cm^{-1}	Ascription	Δ cm^{-1}	B cm^{-1}	β*
	(a)			
10140	$^4T_1(^4F)-^4A_2(^4F)$	5200	88	.10
6000	$^4T_1(^4F)-^4T_1(^4F)$			
	(b)			
10140	$^4T_1(^4F)-^4T_1(^4P)$	3240	524	.62
6000	$^4T_1(^4F)-^4A_2(^4F)$			

*β is the ratio of B given above to that of the free ion, which is extimated by extrapolation of the data given by Griffith, page 437 [8] and is taken to be 840 cm^{-1}.

Chapter Seven
Nickel in ZnSe and ZnS

Chapter Seven
Introduction

This chapter presents the results of experimental studies of nickel centres in ZnSe and ZnS. Discussion of the data falls naturally into two distinct sections.

The first deals with transitions between the internal levels of these impurities, whereby the charge state, or more precisely, the number of d-shell electrons of the absorbing centre does not change. Many of the absorptions bands clearly show fine structure due to vibrational effects. It is shown that Jahn-Teller coupling is involved, and the consequences of this for ZnSe:Ni and ZnS:Ni are compared with those for other systems, especially those studied in the previous chapter. There is also evidence of vibronic antiresonance.

The second section comprises a study of photoionization and related effects. Here optical absorption does result in changes of the occupancy of the impurity d-shell. In contrast to the discussion of vibrational effects on the internal transition bands, most interest lies in the electronic nature of the ionizing process. This is because information about photoionization enables the positions of energy levels to be found with respect to energy bands of the host, not merely relative to each other. From this point of view the associated phonon coupling is, on the whole, just an interesting complication. Values of energy thresholds for ionization are found by fitting to a simple model.

Main Features of Absorption Spectra

Atomic nickel has the electronic structure

(Ar) $3d^8\ 4s^2$, and therefore would be expected to appear in the configuration d^8 when present as an impurity in II-VI compounds. This is substantiated by published spectra of CdSe:Ni [57], ZnSe:Ni [5] and

Weakliem's study of CdS:Ni, ZnS:Ni and ZnO:Ni [58]. In all these cases absorption bands seen are due to transitions between crystal-field levels of Ni(d^8), and suitable parameters have been found to fit the observed spectra.

The relevant values for ZnSe:Ni and ZnS:Ni are given in table 1. This also contains the calculated level spacings found using these values, for all the crystal-field levels. Not all of these have been observed, but the table will be useful later.

In addition to absorption bands due to such transitions most of the compounds mentioned above show intense absorption at energies less than those of the band-gaps of the pure materials. This absorption may be observed as a band or, if very strong, it may appear that the band-gap has shifted. It has been shown for some of the materials listed above that illumination of samples by light in the wavelength region of this intense absorption may produce differently charged nickel centres. Measurements of electron spin resonance have shown the existence of Ni^+ (d^9) and Ni^{3+}(d^7)[57,60]. These effects are associated with photoionization of nickel centres and will be discussed in section B.

Section A : Internal Transitions
Fine Structure at Low Temperatures

Figures 1a, b, c show the absorption spectra of nickel in three materials at room temperature and liquid nitrogen temperature. These are taken from reference [58]. There are clearly similarities between the different spectra, particularly as regards the relative intensities and shape of the various bands.

This comparison can be extended to the spectrum of ZnSe:Ni obtained in the present work. Figure 2 shows this spectrum, which resembles those of figure 1, although there is much more fine structure

visible, since it was obtained at liquid helium temperature.

Since the d-shell configuration of nickel in ZnSe is d^8, the various absorption bands may be assigned to electronic transitions (figure 2). Two of the strongest arise from

$$^3T_1\ (^3F) \ - \ ^3T_2\ (^3F)$$

and $$^3T_1\ (^3F) \ - \ ^3T_1\ (^3P).$$

In these bands the spacing between fine structure components is rather irregular and not easily ascribed to either phonon replicas or spin-orbit effects. Since the electronic states are orbitally degenerate Jahn-Teller coupling may be present. This has been demonstrated for the corresponding transitions in ZnS:Ni and ZnO:Ni [61,35]. In the following pages an approach similar to that discussed in these references is applied to ZnSe:Ni, and the results compared.

$^3T_1$ - $^3T_2$ Absorption Band

The appearance of this band in ZnSe:Ni is shown in detail in figure 3. The temperature was 6^oK. There are several features which might be due to phonon repeats of the strongest line, as shown in table 2. The modes of vibration that could split the excited electronic state are found from

$$[T_2^2] = A_1 \oplus E \oplus T_2 \qquad (1)$$

Thus there could be a Jahn-Teller interaction in the excited state due to trigonal or tetragonal modes. The Stokes' shift may be deduced from the difference between the energy of the zero phonon line and the position of the band maximum. Since it is of the order of 200 cm^{-1} the Jahn-Teller coupling cannot be very strong.

By analogy with the bands of titanium impurities in ZnS and ZnSe, it might be suggested that the component some 50 cm^{-1} above the zero phonon line be due to interaction with the TA(L) phonon. The following

arguments show that this cannot be so.

The presence of a defect in a crystal reduces the symmetry to that of the point group. Thus the TA(L) phonon may be expressed as the sum $T_1 \oplus T_2 \oplus E$, in terms of the local distortion it introduces around the impurity [62]. Thus it may be ε or τ_2 active.

(1) If it couples to an ε-mode distortion, then a regularly spaced series of levels is expected [24]. The first phonon replica is strong compared with the zero phonon line, so the second repeat at least should also be seen. No such line is seen.

(2) If there is $T_2 \otimes \tau_2$ coupling, then the energy of the first line above the zero phonon line is less than that of the active mode, unless the coupling strength is very weak [13]. (This may be seen from figure 4, which gives the calculated energy levels as a function of interaction strength).

If the structure were due to weak coupling of this type, the strength of the first vibrational replica is unexpectedly large in the measured band. Again, the series of levels should be regular, so a second phonon repeat would be seen.

Thus the absence of a uniformly spaced series of lines with the periodicity of the TA(L) phonon rules out the hypothesis of coupling to this mode.

A more reasonable model involves coupling to the TA(X) mode, or to transverse acoustic modes from the part of the Brillouin zone close to the X point. Loudon shows that this mode could be τ_2-active [62]. The energy of the lattice mode is 70.5 cm^{-1}, but comparison with figure 4 shows that the separation between the zero phonon line and the nearest higher energy level would be in the measured range, with a value for k, the ordinate of this figure, of 0.7. The physical meaning of k is that the vibrational energy by which the Jahn-Teller interaction reduces

the energy of the zero phonon transition is given by

$$E_{JT} = \frac{2}{3} k^2 \hbar\omega \qquad (2),$$

where $\hbar\omega$ is the energy of the interaction mode. In figure 5 the calculated and actual spectra are compared; the fit is fair but not very convincing.

The corresponding band in ZnO:Ni contains sharp lines, due apparently to different spin-orbit levels. Kaufmann et al account for the separations of these lines fairly well by a model of coupling to a high energy optical mode, whose symmetry is not certain [61]. The band in ZnS:Ni is more like that in ZnSe:Ni: Kaufmann et al identify the structure with various critical point phonons, but the model developed here for ZnSe:Ni could apply, with a similar value of k (see figure 6).

$^3T_1 - {}^3T_1$ Absorption Band

Figure 7 shows this band in ZnSe:Ni at 6^oK. The spectrum is very complicated, with more than one sharp line present. If these are due to transitions into purely electronic states separated by spin-orbit coupling, then the separations are certainly less than those calculated from crystal field theory. This is shown in table 3, and suggests the Ham effect may be involved.

Figure 8 shows the corresponding band in ZnS:Ni. Kaufmann and Koidl have pointed out that most of the structure can be correlated with critical point phonon replicas of the only sharp line seen [35]. The only phonon sideband not seen is the TA(L) replica; using a model similar to the one proposed in the last section, they suggest that coupling to this mode, which has an energy of 70 cm^{-1}, produces the otherwise unidentified band some 50 cm^{-1} above the zero phonon line. An analogous argument is advanced for the case of ZnO:Ni. A defect of this explanation is that most of the intensity of the band in each material is due to states showing interaction with modes other than TA(L).

In the case of ZnSe:Ni, it is not possible to correlate the observed structure with the phonon spectrum. It is not clear why this should be so, and contrasts with the similarities in vibrational coupling in ZnS:Ti and ZnSe:Ti.

Jahn-Teller Coupling in the $^3T_1$ Ground State

In the above discussion no account has been taken explicitly of the effects of vibrational effects in the ground state of nickel. It is, however, in no way obvious that there should not be Jahn-Teller coupling in the orbitally triply-degenerate ground state, of comparable strength to that found in the excited states.

If spin-orbit coupling in the ground state is considered then the lowest level has symmetry A_1 [61]. In this way spin-orbit interaction can stabilize a level against vibrational splitting [19], but table 1 shows that the spin-orbit splitting of the ground state is of the same order as in excited states, so that comparable coupling to vibrations would be expected. For example, the Jahn-Teller energies of different cobalt levels in ZnS:Co and MgO:Co are given in table 4: the coupling is less for the ground and low energy states, but is not negligible in either case.

The structure seen in the absorption spectra is due to the energy levels of the excited electronic configurations, and the separations of these levels are not affected by ground state interactions. However any coupling to vibrations in the ground level would certainly influence the intensities of the measured fine structure.

$^3T_1 - {}^1T_2$ (^1G) Absorption Band

Figures 9 and 10 show in detail the absorption bands arising from

the $^3T_1$ - $^1T_2(^1G)$ transition in both ZnSe:Ni and ZnS:Ni. The samples' temperature was 6^oK.

Although this transition is spin-forbidden it is made quite strong through interaction with the nearby $^3T_1$ level. This level is split by spin-orbit coupling:

$$T_1 \otimes T_1 = A_1 \oplus E \oplus T_1 \oplus T_2 \qquad (3)$$

since the spin-orbit interaction operator transforms as T_1. The T_2 component then mixes with the $^1T_2$ state, leading to a spin-forbidden band with one per cent of the intensity of the spin-allowed transition.

The resolution used to record these spectra was about 3 cm^{-1}. However the fine structure in the spectrum of ZnS:Ni is less sharp than that of ZnSe:Ni. Table 5 shows that this broadening is evident even in the half-widths of the sharpest lines.

In ZnSe:Ni this line is followed by several components at fairly low energy separation. These are listed in table 6. Although they seem to form a sequence of replicas of the sharp line at uniform spacing there are neither critical point phonons nor maxima in the phonon density of states in this energy region. Nor can the structure be due to spin-orbit coupling, since the $^1T_2$ state is a spin-singlet.

Instead the structure is interpreted as the result of coupling to TA(X) modes, which are τ_2-active. By comparison with figure 4 it is found that excellent agreement with the positions of the first few measured levels is reached with k equal to 1.4.

Although less structure can be seen in the band of ZnSe:Ni, a similar ascription is made. The calculated and measured level spacings are given in table 6, for both materials, together with the parameters concerned.

The calculated levels are shown on figures 9 and 10. The lines

shown are not a complete set except for the lowest levels; the multiplicity of states increases more rapidly at higher energies than is indicated. Since modes from the region of the Brillouin zone close to the X point, but with slightly different energy may be involved in the coupling, the high energy states will closely approximate a continuum. The fine structure on this continuum (in both materials) is discussed in the next section.

With no Jahn-Teller coupling the ground vibronic state of $^1T_2$ is a triplet. At high coupling strengths the system becomes four-fold degenerate, corresponding to distortions along <111> and equivalent directions. The four states are nor orthogonal, but at high coupling the interaction between them is quenched. However in the intermediate case the level splits into a ground triplet and a higher A_1 state [50]. (If the distortions are static, this splitting is due to tunnelling between wells). Similar considerations apply to higher levels. Thus the lowest level most closely resembles a zero vibrational state, while the character of higher levels depends on the relative strengths of the Jahn-Teller coupling and the "tunnelling splitting" of distorted configurations. This illustrates the vibronic or mixed electronic-vibrational nature of Jahn-Teller coupled states.

Vibronic Antiresonance

In both ZnSe:Ni and ZnS:Ni the absorption band due to the $^3T_1$- $^1T_2$ transition contains absorption dips. These are visible in figures 9 and 10, and are shown in greater detail in figures 11 and 12, after the background absorption has been removed. By anology with ZnSe:Ti and ZnS:Ti these are identified with antiresonances. Parameters derived from fitting the lineshape formula of Fano (see chapter four, equation eleven) are given in table 7. Another resonance is seen in the

$^3T_1 - {}^3T_1$ band ofZnS:Ni. This is shown in figure 13 and the parameters are also contained in table 7.

The continuum background in all these cases is due to a complex superposition of Jahn-Teller coupled states, of much more intricacy than in the titanium-doped materials.

Table 8 summarizes the information obtained about the energies of the antiresonances seen in the four different materials, and relates them to various phonons in these substances. It is often doubtful whether the phonon energies are accurate, and so identification of the resonances is not always possible. A further possibility, mentioned in the last chapter, is that the antiresonances do not necessarily involve lattice modes of special symmetry, from critical points, but that they are related to peaks in the phonon density of states. Calculations of this also differ, as shown in the appendix. Thus no firm conclusions can be drawn on this point.

Section B : Photoionization

Introduction

One of the most direct ways of telling whether a crystal contains impurities is to look at its colour. This may be altered quite markedly by the extra absorption associated with the presence of imperfections. For example, while pure ZnSe is yellow, doping with titanium, chromium or manganese results in green, red and orange crystals respectively.

In sufficient concentration, nickel added to ZnSe or ZnS makes these materials green. This colour change is related to the strong absorption bands which occur in each doped material from energies of roughly one electron volt below the band-gap, and upwards. It is with these bands that this section will deal.

Different Charge States

Electron spin resonance measurements have shown that nickel impurities in ZnSe and ZnS may have the configuration d^7, d^8 or d^9. The relative numbers of these different charge states are affected by illumination of the samples by light with energy below that of the intrinsic band-gap [59,60]. The resolutions used to control the spread of energy in the illuminating beams do not seem to have been very high, so no precise data about the ionization energies were obtained by these experiments.

It was suggested that the most important absorption process produced nickel (d^7) directly:

$$d^8 + h\nu \rightarrow d^7 + (\text{conduction band } e^-) \qquad (4),$$

and that nickel (d^9) resulted from a d^8 centre capturing an electron. However the evidence for these processes was not unambiguous.

Photoionization Spectra

Samples of ZnSe:Ni and ZnS:Ni with strong d^8 absorption bands may be made by evaporation of the metal onto slices of crystal, which are subsequently heated in vacuo for several days [chapter 5]. Such specimens also exhibit strong photoionization absorption bands. The appearance of these at low temperature is shown in figures 14 and 15.

At energies below those shown in the figures the spectra are quite flat, except where there are internal d^8 absorption bands. When a certain value of energy is reached the absorption begins to increase quite rapidly, and at higher energies than shown, the absorption is so strong that, with the experimental method used, the transmitted light can not be distinguished from the non-monochromatic light scattered inside the spectrometer. This restricts the range over which the shape of these bands may be determined. No further transmitted light is

detectable up to the band-gap energy of the crystal host. Close to the low energy part of the band, in each material a sharp line is seen in the absorption spectrum. This is followed by broader replicas at higher energy, superimposed on the main absorption curve.

This fine structure has been observed previously in these materials by Kazanskii and Ryskin [63], and the nature of the sharp lines and of the broad absorption band have been studied by them using a variety of methods [64,65,66]. Similar effects have been reported in CdS:Ni [67,68].

Some of the conclusions of these papers are summarized in table 9. Not all of these are in agreement with the results of the present work. However it is agreed

(1) that the intense absorption band is due to the transition

$$d^8 + h\nu \rightarrow d^9 + \text{(valence band hole)} \qquad (5)$$

in contrast to equation (4) and

(2) the fine structure is due to a bound hole at the nickel site.

Rather than review these papers in detail now, the points of interest will be discussed in conjunction with the results of the present work.

Ionization Threshold Energies

In a simple model, the absorption coefficient, A, due to the photoionization transition of a deep level in a semiconductor is given by

$$A = 0 \qquad E < E_I \qquad (6a),$$

$$A \propto (E - E_I)^{3/2} \qquad E \geq E_I \qquad (6b).$$

E_I is the value of the threshold energy at which ionization becomes possible [69]. Thus at energies above the ionization threshold,

$$(A)^{2/3} \propto (E - E_I) \qquad (7).$$

Where this theory applies, it is clear that the threshold energy may readily be obtained from experimental data. Figures 16 and 17 show the results of plotting the two-thirds power of the absorption data for the ionization bands of ZnSe:Ni and ZnS:Ni, against energy. In each case a straight line may be fitted to the data, with good agreement except at small values of absorption near the threshold energy. Allen has pointed out that phonon participation may have to be considered in this region [69]. The threshold energies, obtained in each case by extrapolation of the straight line, are given in table 10.

Temperature Effects

The absorption band of ZnSe:Ni has been recorded over a range of temperatures, from liquid helium to room temperature. It is found that equation (7) can be fitted to the data at all temperatures, but some changes in behaviour are noticeable. Figure 18 shows some of the results.

There are two main trends in the shape of the absorption band as the temperature is varied.

(1) The value of E_I is not constant. This is shown in figure 19. Above $100^{\circ}K$ and up to room temperature the threshold energy steadily decreases. Over this range the change is 480 cm^{-1}, which is about half of the decrease in the band-gap of ZnSe, 800 cm^{-1}, with the same temperature variation. Below $100^{\circ}K$ the variation is more complicated, and it is found that the ionization energy increases by 50 cm^{-1} between $6^{\circ}K$ and $8^{\circ}K$. This value is close to the change in the value of average thermal energy, kT. It is also approximately equal to the energy of the TA(L) phonon in ZnSe, 49 cm^{-1}. Although this behaviour is not fully understood, it is possible that the variation in threshold energy below $100^{\circ}K$ is due to vibrational coupling in the final, ionized state of the nickel centre, such that the most probable populated state is not the ground vibrational state, but one in which a localized mode is excited. The TA(L) mode can

be ε or τ_2 active, and so could couple to the ground electronic state of either nickel (d^7) or (d^9).

(2) There is an energy region near threshold, where deviation of the experimental points from the behaviour of equation (7) is significant. The width of this region does not vary greatly with temperature.

The presence of absorption below threshold, and the departure from the simple power law just above it seem to be due to phonon-assisted transitions. There have been only a few papers dealing with these effects [70, 71 and references therein]. The model described in the latter paper agrees with the experimental findings that, sufficiently far above threshold, the influence of phonons is not significant. However the critical test comes in the region near and below threshold where it is predicted that the absorption should vary much faster than a simple exponential function of energy, merging smoothly into the power law at higher energies. Where the agreement with this theory is compared, it is apparent that there is not complete agreement in the threshold region [71, figure 2; 72, figure 4].

In contrast, experimental work in GaAs:Cr [69] and CdTe: Cr [73] shows that the absorption A, below the threshold of ionization is given by

$$A \alpha \exp [E/E_o] \qquad (8)$$

where $E < E_I$

and E_o is a constant, for a given temperature.

The models mentioned above would predict

$$A \alpha \exp(-[E-E_I]^2/\text{const}) \qquad (9)$$

In ZnSe:Ni the region below E_I where the absorption is measurably large was, with the samples available, only some 200 cm^{-1} in width. This made testing the behaviour rather difficult. However the data are consistent with equation (8), with a value for E_o of 93 ± 17 cm^{-1}. There

are large uncertainties in this value due to experimental conditions; it is clear from figure 20 that no conclusions are possible about the variation of E_o with temperature.

From the above comments (1) and (2) it is apparent that vibrational effects are playing a part in the ionization process, but that phonon coupling is not very strong. Thus the interaction of the centre with the lattice is not changed much by the alteration of charge state.

Fine Structure

Comparison of the recorded spectra with the data of table 1 shows that the sharp lines and complicated structure seen near the ionization thresholds of the two materials are not attributable to transitions between states of nickel (d^8). They are therefore ascribed to the existence of bound states lying just below the ionization limit.

Table 11 gives the energies by which the sharp, no-phonon lines lie beneath the ionization thresholds. These correspond to the binding energies of a charged particle in a shallow level about the nickel centre, trapped by the Coloumb potential of the ionized impurity. It is not yet clear, from the evidence presented so far, whether the particle is a hole, trapped just above the valence band, or a weakly bound electron.

Table 12 gives the calculated energies of holes and electrons trapped in the electric potential of singly charged centres in ZnSe and ZnS. The acceptor levels were calculated by Baldereschi and Lipari for an impurity in a cubic environment [74]. They do not take account of central-cell corrections, or of any interaction between the hole and the magnetic moment of the transition metal [75].

The donor levels are calculated using a hydrogenic model, whereby

the binding energy in the n'th shell is given by

$$E_n = - \frac{13.6}{n^2} (m^*/m_o)/k^2 \text{ eV} \qquad (10),$$

where m^* = the effective electronic mass

and k^2 = dielectric constant.

Woodbury and Aven found this approach gave good agreement with the measured binding energies of shallow donors in several II-VI compounds [76].

The binding energies of table 11 lie in the same region as the lowest donor states, and the higher acceptor states. It might be argued that a transition from a d-shell will be more probable with a p-type final state than an s-state. Thus the zero phonon line might result from a transition to a 2-p acceptor state. However, considering that the transition is much weaker than the allowed transitions within the d^8 configuration, it may not be reliable to base an identification of the process on arguments involving parity.

Vibrational Coupling

At higher energies than the zero phonon lines in ZnSe:Ni and ZnS:Ni there is considerable fine structure. As shown in figures 14 and 15 it is possible to detect regular patterns in this structure. The energies at which the structure recurs differ by amounts that correspond to lattice phonons, as shown in table 13. The agreement is most striking for optical modes, whereas the acoustic bands are wide, with less well resolved structure. These bands are shown in detail in figures 21 and 22.

In ZnS:Ni a second sharp line is seen, some 200 cm^{-1} above the zero phonon line. This separation is much less than the valence band spin-orbit splitting at the Γ point, some 560 cm^{-1} [77]. It is possible that this peak is due to a local mode, with an energy in the gap of phonon density of states [78]. In ZnSe there is no such gap, so that a mass-defect mode could be broadened by resonance with other modes. Also,

selenium being heavier than zinc, or nickel, a localised oscillation on a zinc site is more likely to have an energy associated with optical modes [12].

Both multiple acoustic and multiple optic sidebands are seen in the spectra, and combination bands are also visible. Table 14 gives the relative intensities of the first few components, and the values of coupling strength found by fitting to a Poisson distribution, modified to take account of the different intensities of the acoustic and optical one-phonon sidebands that are convoluted together to provide the combination bands [14]. Although the structure is visible up to the fourth replica, only the first few bands are used in the fitting because of the widening of the higher order replicas and the strong background absorption.

Hopfield has shown that the Huang-Rhys factor S for an impurity electron with large orbital radius is given by

$$S = \frac{e^2}{\sqrt{2\pi}\, a\, \hbar\, \omega} \left(\frac{1}{4\pi\varepsilon_\infty} - \frac{1}{4\pi\varepsilon_o} \right) \qquad (11)$$

where $\hbar\omega$ is the characteristic phonon energy, ε_∞ and ε_o are the optical and static dielectric constants, and a is the half-width of the spatial distribution of the localised electron or hole [79].

It is assumed that the charge distribution is Gaussian, but the formula may be used for hydrogenic orbits where a is taken to be half of the mean radius of the orbit [79]. The electron-phonon coupling is modelled on the Frohlich interaction [80]. S is to be found by comparing the relative intensities of the phonon replicas, although some authors use the relative peak heights [79, 81].

Table 12 shows the expected coupling constants for hole and electron 1s states in ZnSe and ZnS. Values for levels above this ground state are progressively less, by a factor of two for 2p states.

Comparison with table 14 shows that the measured coupling strengths

are more in agreement with those calculated for acceptor states. The agreement is not convincing. It is perhaps not surprising that this approach does not permit the final state to be identified definitely since the coupling factor S must involve the charge distribution not only of the bound particle but also of the impurity centre, if this is changed by the absorption of a photon. Although little is known about this aspect, it is clear that the angular distribution of d-shell electrons will be altered by the removal of a hole or electron and possibly the radial spread also [82].

Identification of Ionization Process

The evidence presented still does not discriminate between the ionization processes represented by equations (4) and (5).

The corresponding process in CdS:Ni has been identified as (5) using an argument based on measurements of capacitive photovoltage [68]. This model is complicated by concentration effects which lead to different ionization energies, seemingly involving different crystal bands at high and low doping levels.

Kazanskii and Ryskin have measured the g-factor of the state corresponding to the zero phonon line below the intense band in ZnS:Ni [66]. They show that the experimental value agrees with a value calculated for a hole localised in a fully symmetric orbit about a d^9 nickel centre.

However the strongest evidence has been provided by measurements of photocapacitance [83].

Complementary Ionization

When the nickel centre d^8 in ZnSe or ZnS absorbs a photon whose energy lies in the intense absorption region, the ionized centre that results has a long lifetime at low temperatures [65,84]. In these

references it is shown that it is possible to measure the induced absorption associated with these ionized centres.

Szawelska and Allen have constructed Schottky diodes of ZnSe:Ni and have measured the change in capacitance resulting from illumination in the energy range of the induced absorption band [83] . This shows that the process results in the creation of a free electron. The threshold E_1 for the production of this photoelectron is found to be 8,470 cm^{-1} at 77°K. The threshold E_2 for the intense band seen in ZnSe:Ni (d^8) at this temperature is 14,960 cm^{-1}. The two values E_1 and E_2 add up closely to the band-gap energy:

$$E_1 + E_2 = 23{,}430 \text{ cm}^{-1} \qquad (12)$$

$$E_g = 22{,}660 \text{ cm}^{-1} \qquad (13)$$

Thus the process seen in absorption by ZnSe:Ni (d^8) is identified as

$$d^8 + h\nu \rightarrow d^9 + \text{hole} \qquad (14)$$

and in photocapacitance as

$$d^9 + h\nu^1 \rightarrow d^8 + \text{electron} \qquad (15)$$

The small value of relaxation energy evident from a comparison of (12) and (13) is consistent with the weak vibronic coupling seen in the photoionization. Kazanskii and Ryskin have also pointed out the near equalities of E_g and $E_1 + E_2$ in ZnSe:Ni, although they used less accurate values of threshold energy [65] . From figure 2, reference 74 it seems that the same equality would be found in ZnS:Ni.

The complementary ionization has also been seen by absorption in conducting, n-type ZnSe:Ni. Figure 23 shows the absorption spectrum. The specimen was prepared by heating ZnSe in a bath of zinc and nickel (see chapter 5). Material prepared in this way luminesces under ultra-violet excitation, while heavily nickel-doped material, prepared by diffusion, does not. The nickel centre responsible for the absorption band

shown in figure 23 could not have been produced by photo-excitation of nickel (d^8) since the incident light was filtered by silicon. The cut-off due to this filter is evident on the figure. The nickel (d^9) thus resulted from the high Fermi-level in the conducting crystal. No absorption characteristic of nickel (d^8) was seen with this material, showing that all the centres were acting as filled acceptors. The similarity of the induced absorption seen by Kazanskii and Ryskin, and the absorption in this material clearly shows that (d^9) is responsible for both. Thus the process represented by equation (4) may be firmly ruled out as an explanation of the experimental data.

It is interesting that the absorption shown in figure 23 is also describable by equation (6). Figure 24 shows a plot of the two-thirds power of the absorption, leading to a value of 8000 cm^{-1} for the threshold energy at $6^{o}K$. Langer has suggested that different power laws should apply to transitions to the s-like conduction band and to the p-like valence band [85] . In the systems studied here this is clearly not the case, and may reflect the lack of definite parity and covalent mixing present in impurity d-states.

Summary

Accurate measurements have been made of absorption arising from photoionization and associated processes. In conjunction with photo-capacitance measurements the scheme shown in figure 25 is advanced as a model. Thus the position of the levels of nickel d^9 in ZnSe and ZnS are known with respect to the energy bands of the bulk medium.

There are several aspects that require further study; in particular the effects of phonon interactions with the different charge states of the impurity, and with the localised charge carriers bound in shallow states above the valence band.

Figures for Chapter Seven

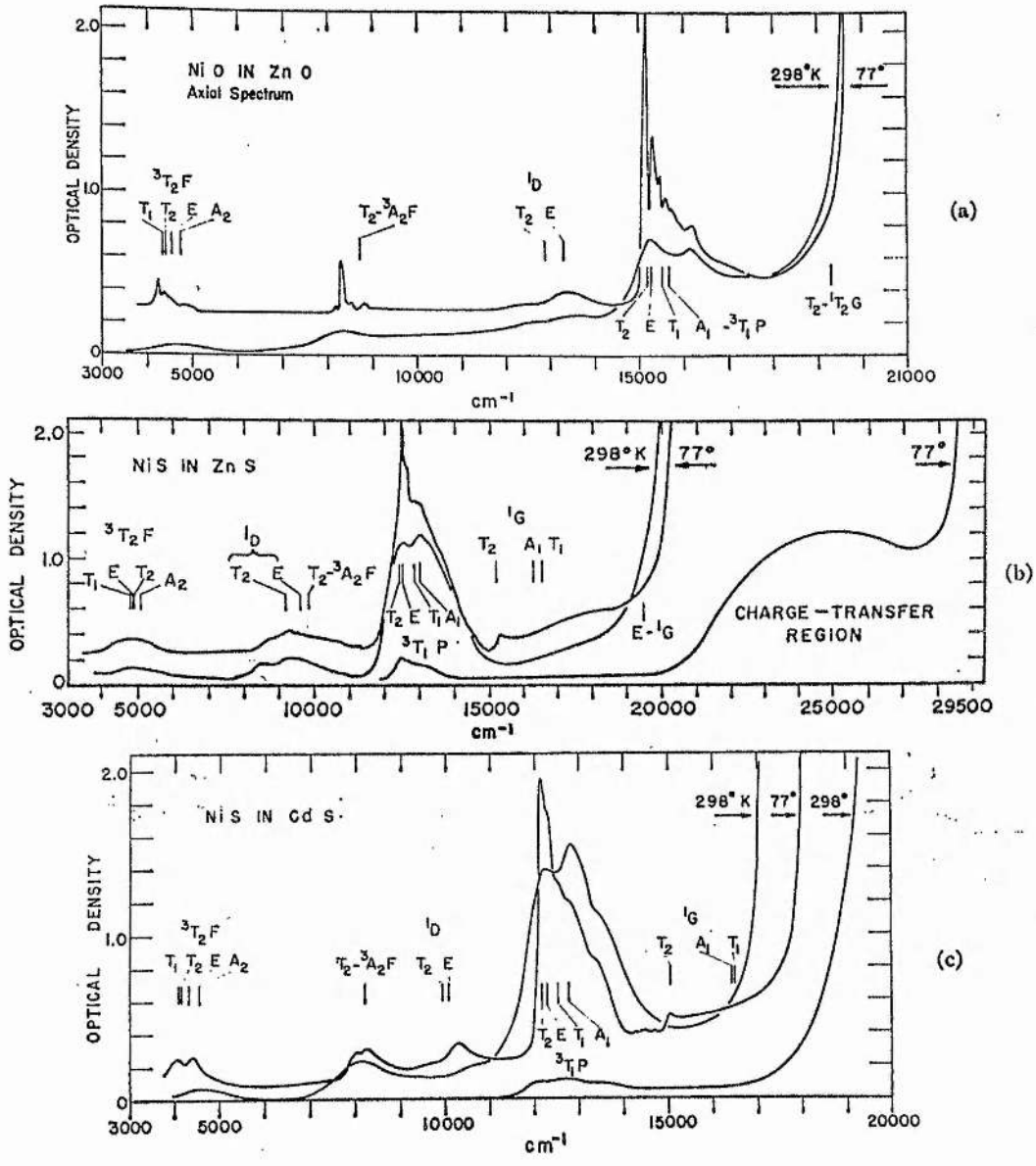

Figure 1

These spectra, taken from reference [58], should be compared with that of ZnSe:Ni (figure 2).

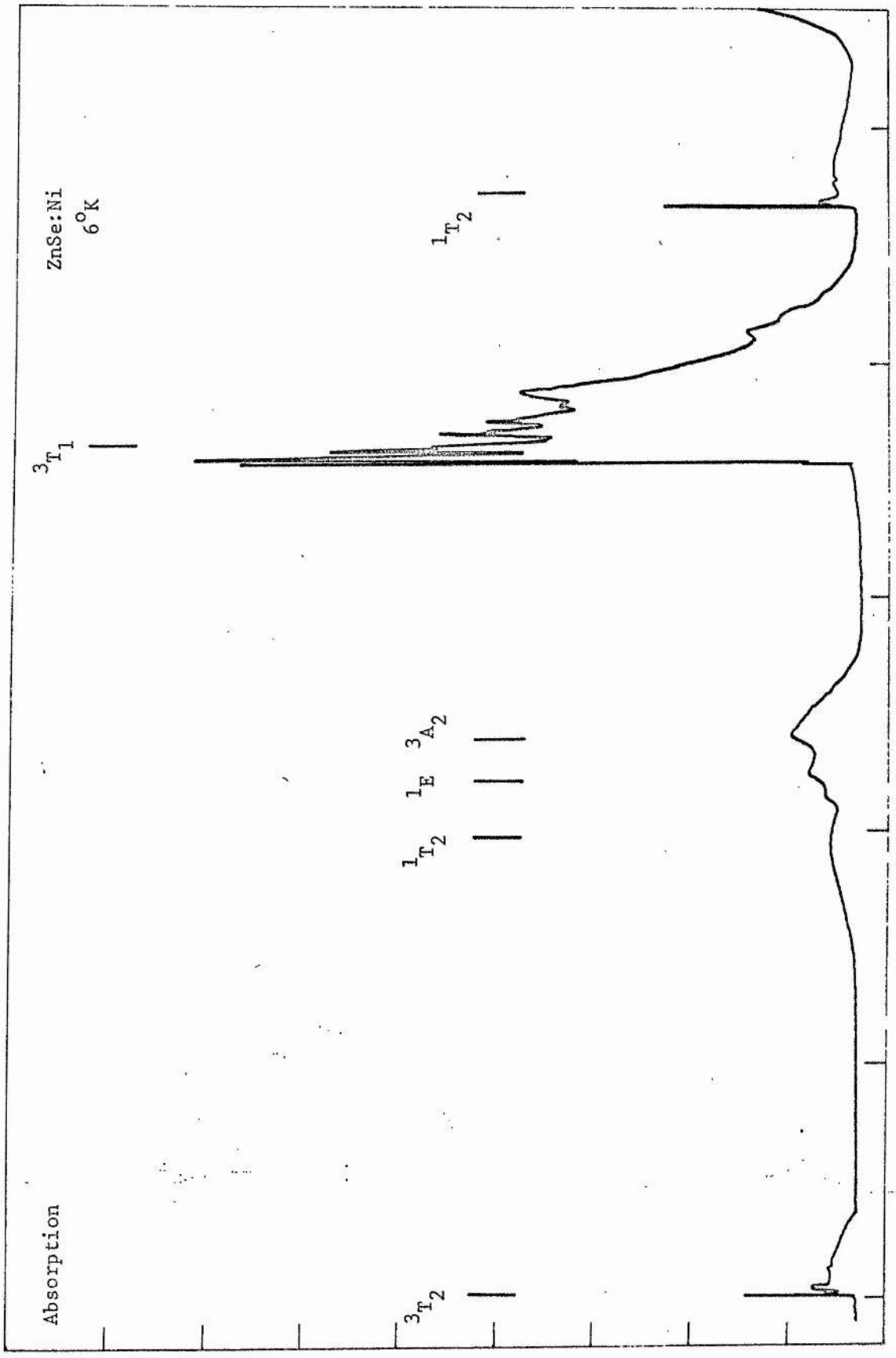

Figure 2
Absorption spectrum of ZnSe:Ni. The internal d-shell transitions originate in the $^3T_1(^3F)$ ground state of $Ni(d^8)$ and terminate in the excited states indicated.

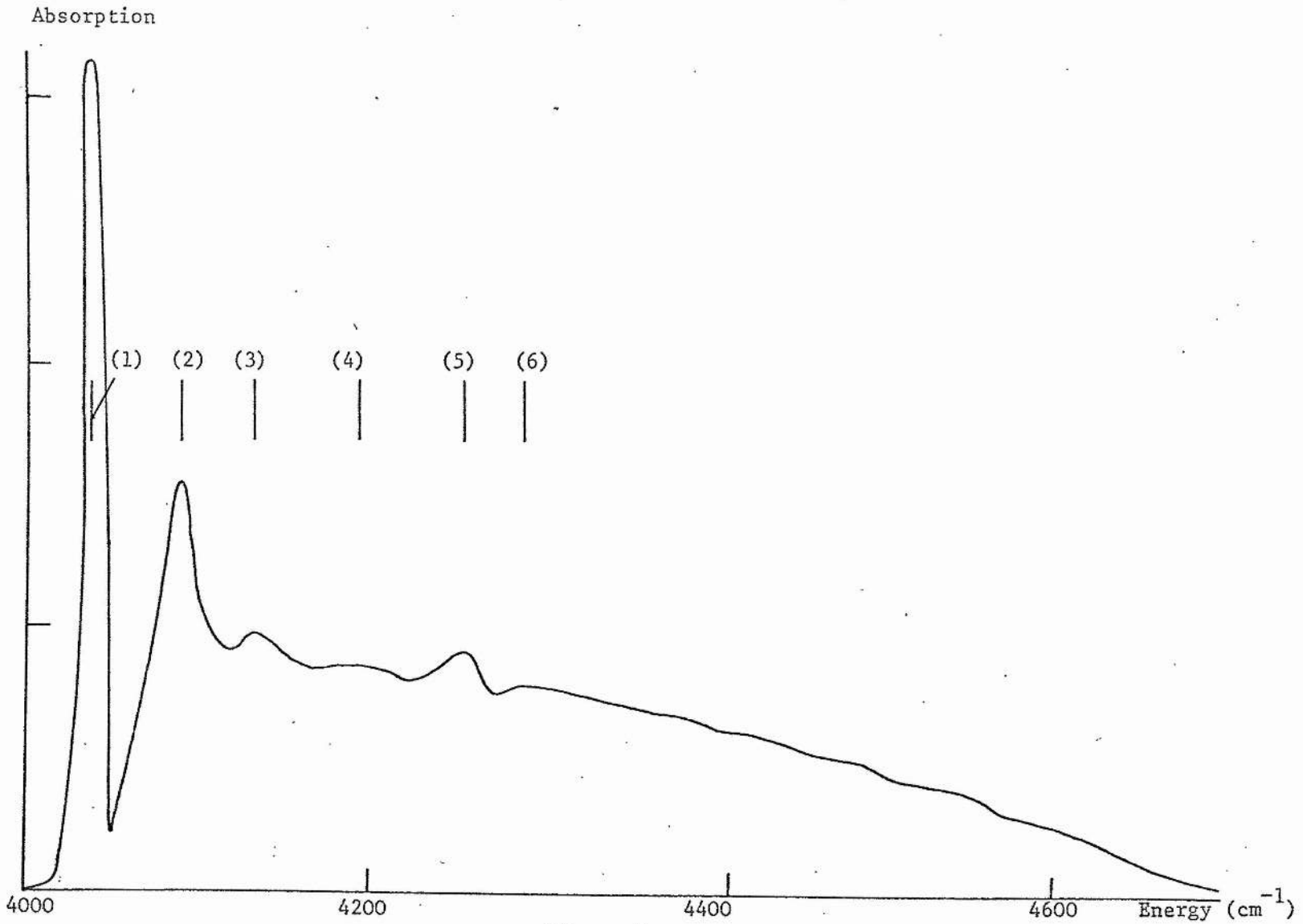

Figure 3
$^3T_1 - {}^3T_2$ band of ZnSe:Ni at 6°K.

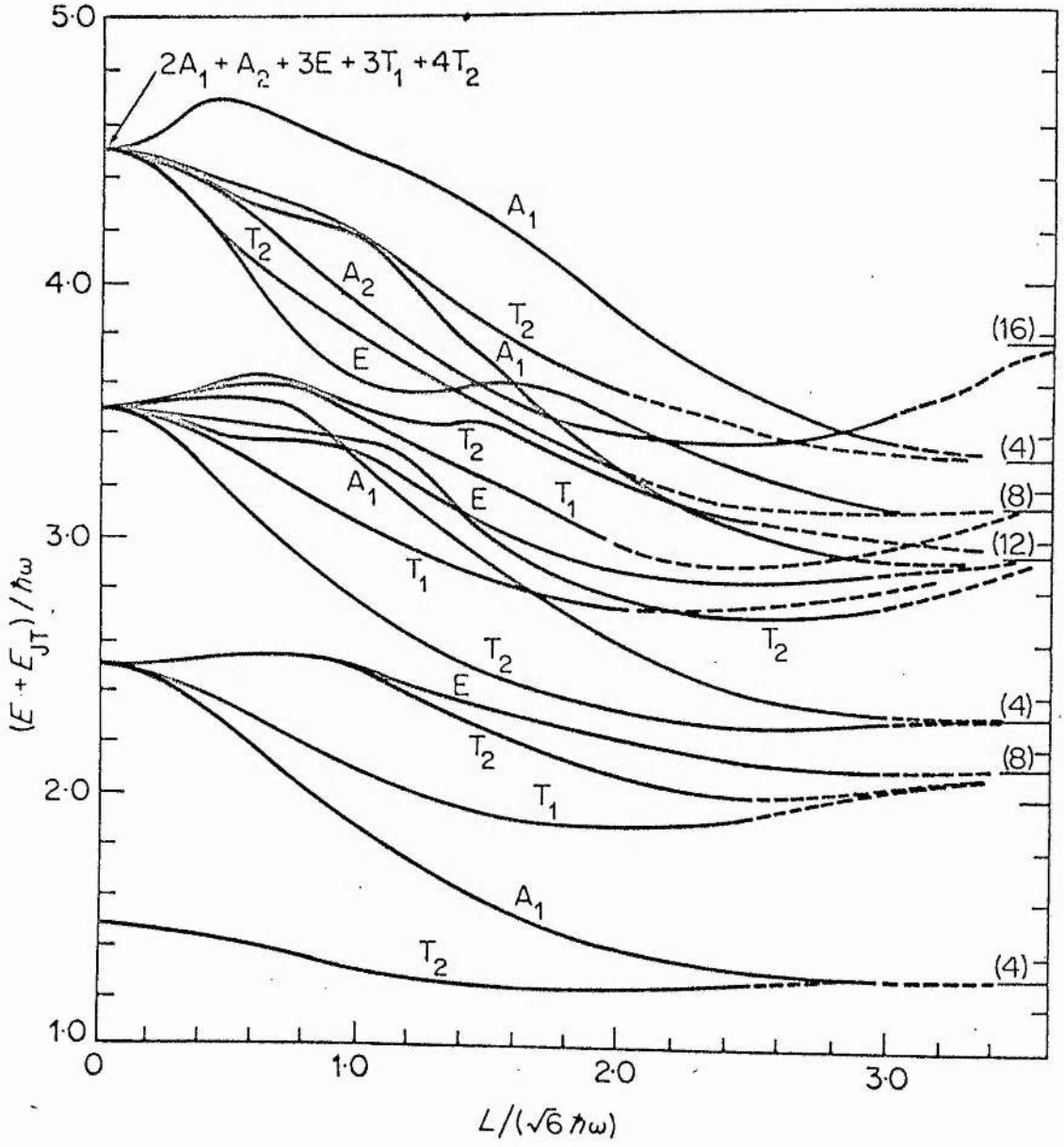

Figure 4

Vibronic levels produced by $T_2 \otimes \tau_2$ coupling (taken from [13]).
Notation: in this thesis, $L/(\sqrt{6}\,\hbar\omega) \equiv k$.

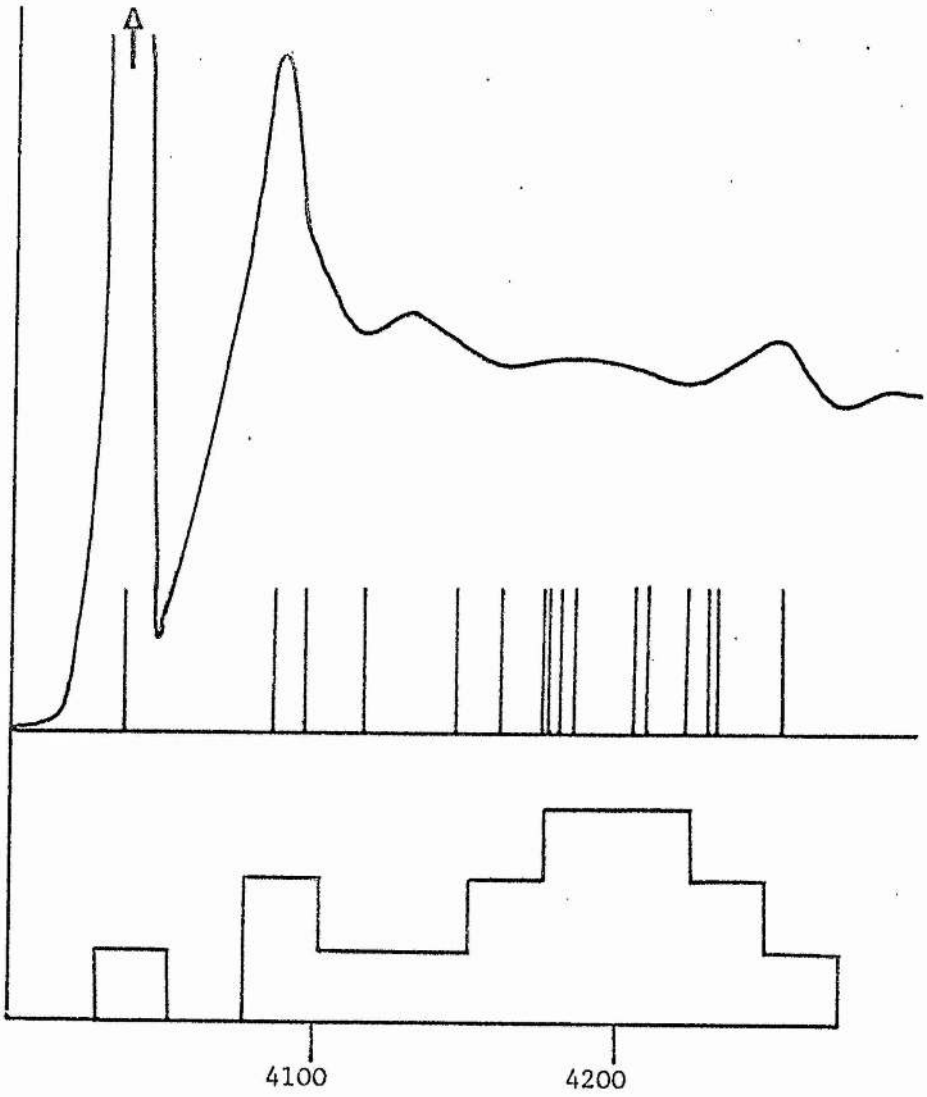

Figure 5

$^3T_1 - {}^3T_2$ absorption band of ZnSe:Ni.
The vertical lines indicate the calculated positions of vibronic levels with $k = 0.7$, $\hbar\omega = 70.5\ cm^{-1}$.
The histogram gives a rough indication of the density of states in the band.

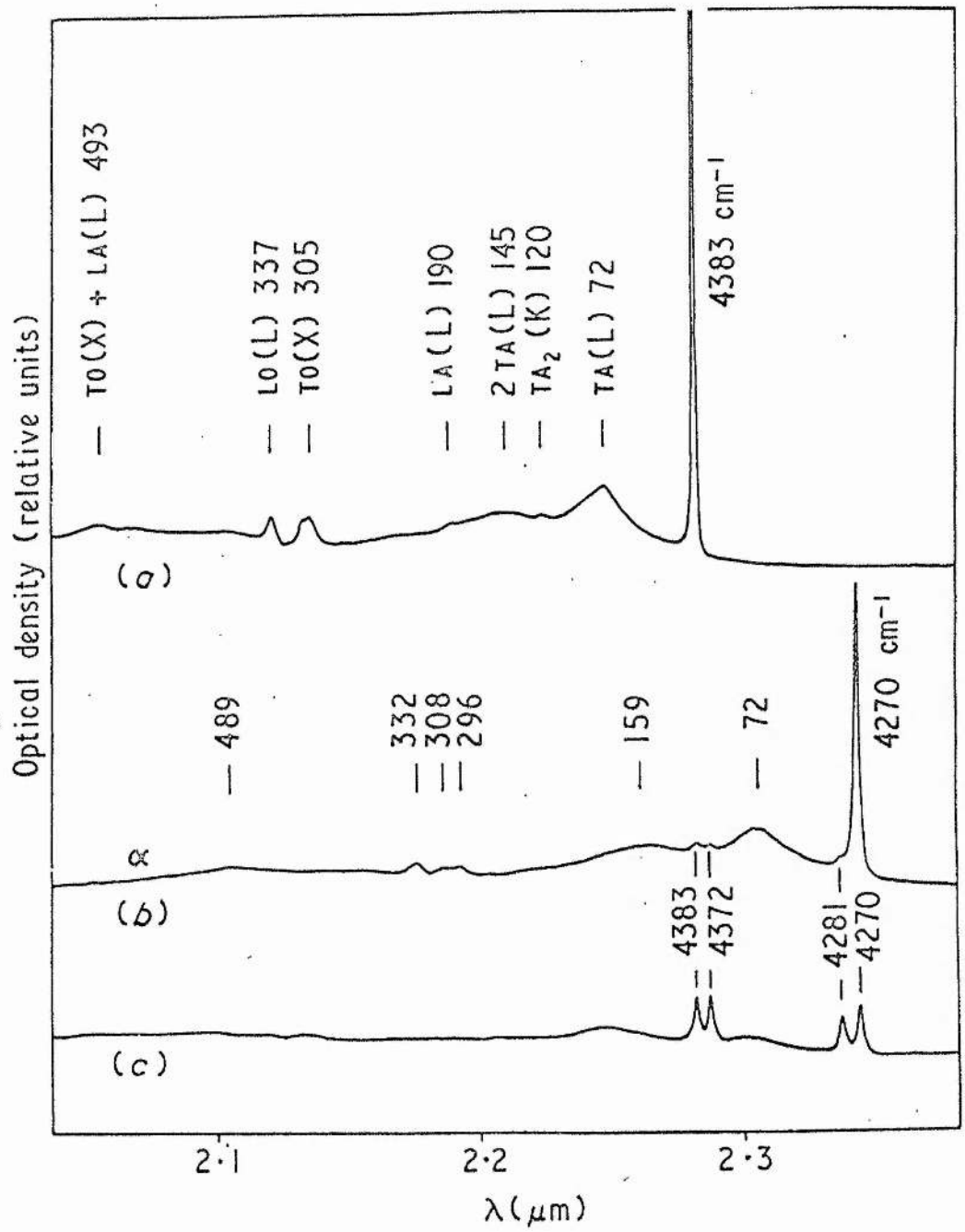

Figure 6

The $^3T_1 - {}^3T_2$ absorption band of ZnS:Ni, recorded at 6°K. This figure is taken from reference [61].

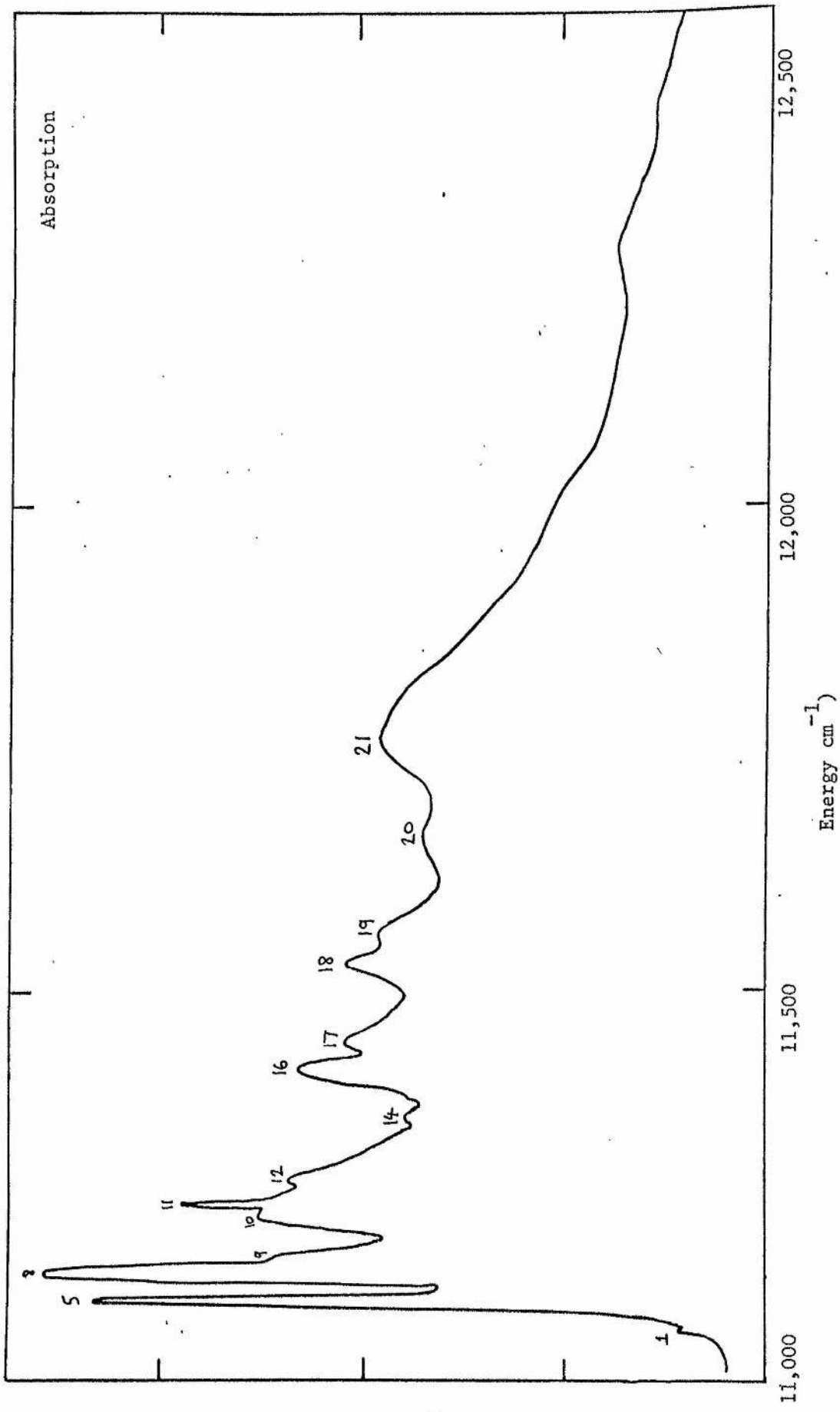

Figure 7
The $^3T_1 - {}^3T_1$ absorption band of ZnSe:Ni at 6°K.

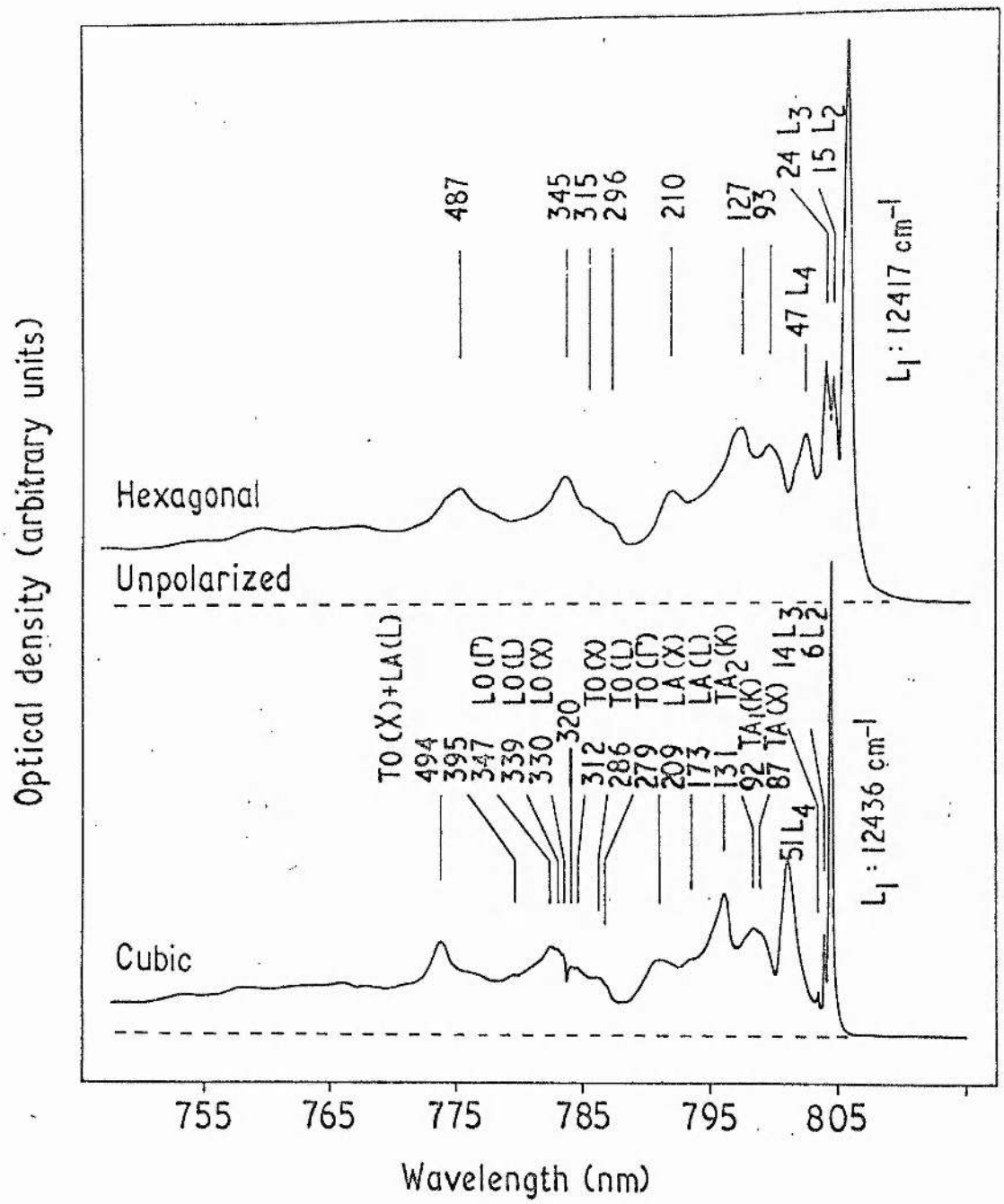

Figure 8

The $^3T_1 - {}^3T_1$ absorption band of ZnS:Ni, taken from reference [35].

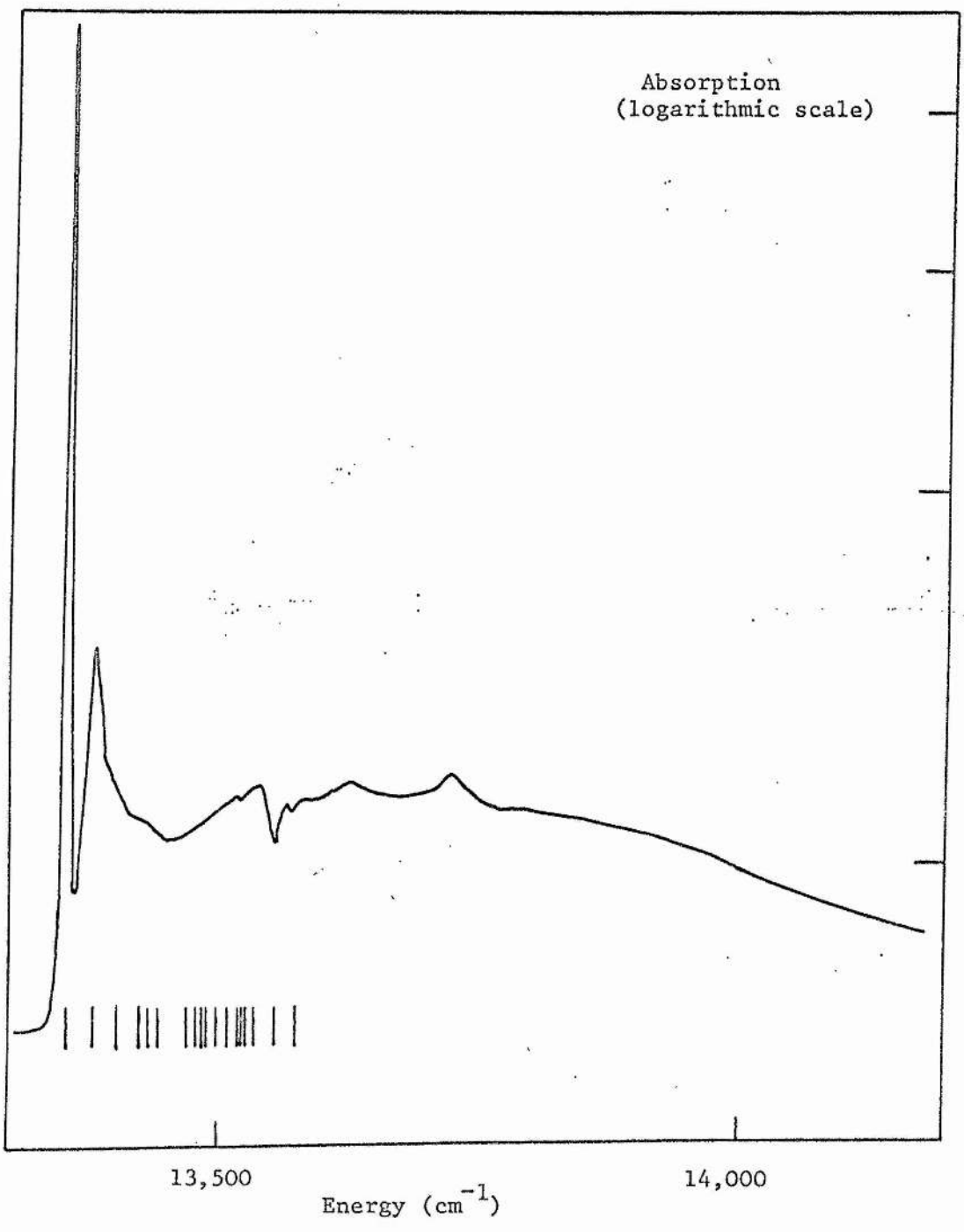

Figure 9

The $^3T_1$-$^1T_2$ absorption band of ZnSe:Ni. Calculated levels for $T_2 \otimes \tau_2$ coupling are shown (see text and table 6).

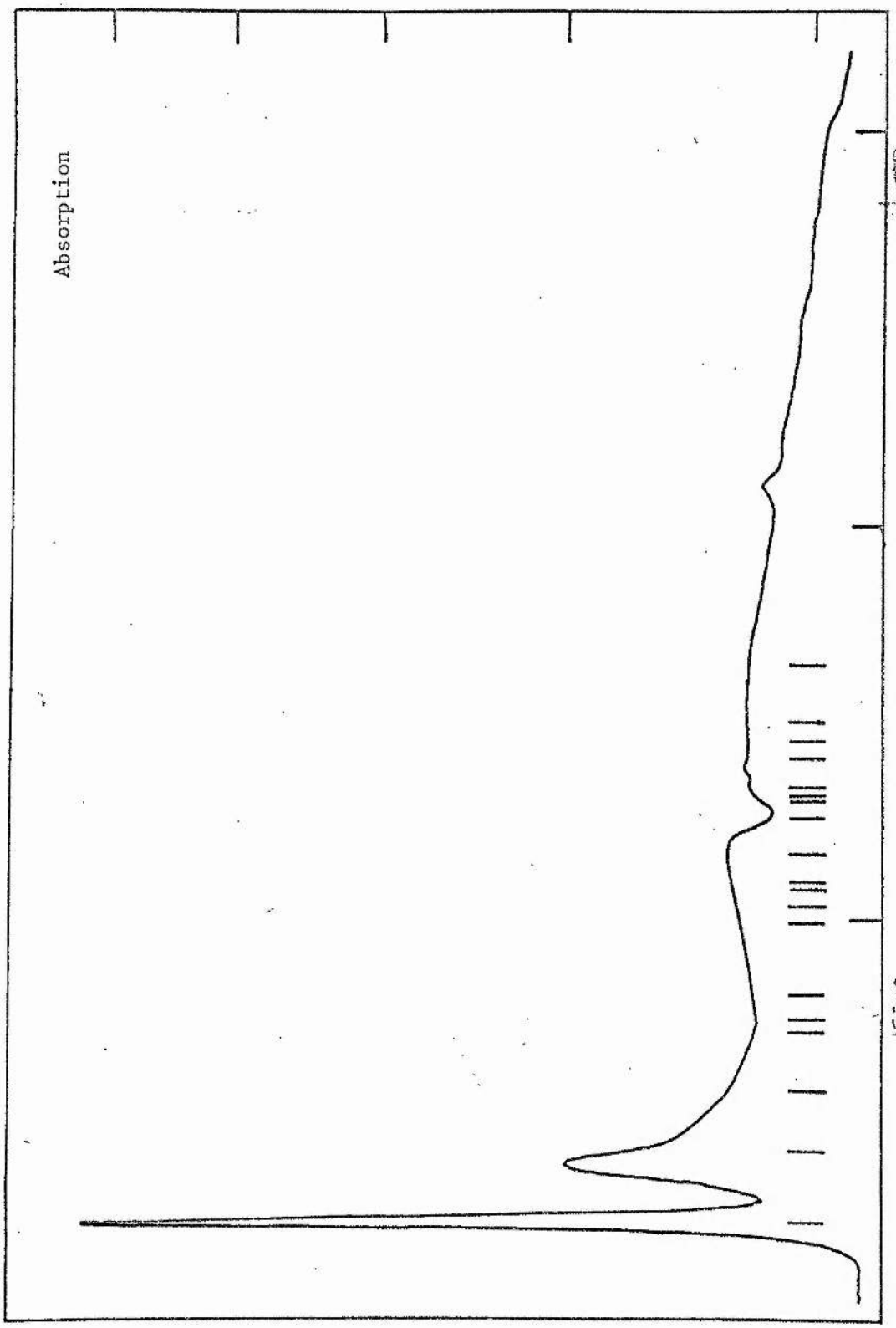

Figure 10
The $^3T_1$-$^1T_2$ absorption band of ZnS:Ni. Calculated levels for $T_2 \otimes \tau_2$ coupling are shown (see text and table 6).

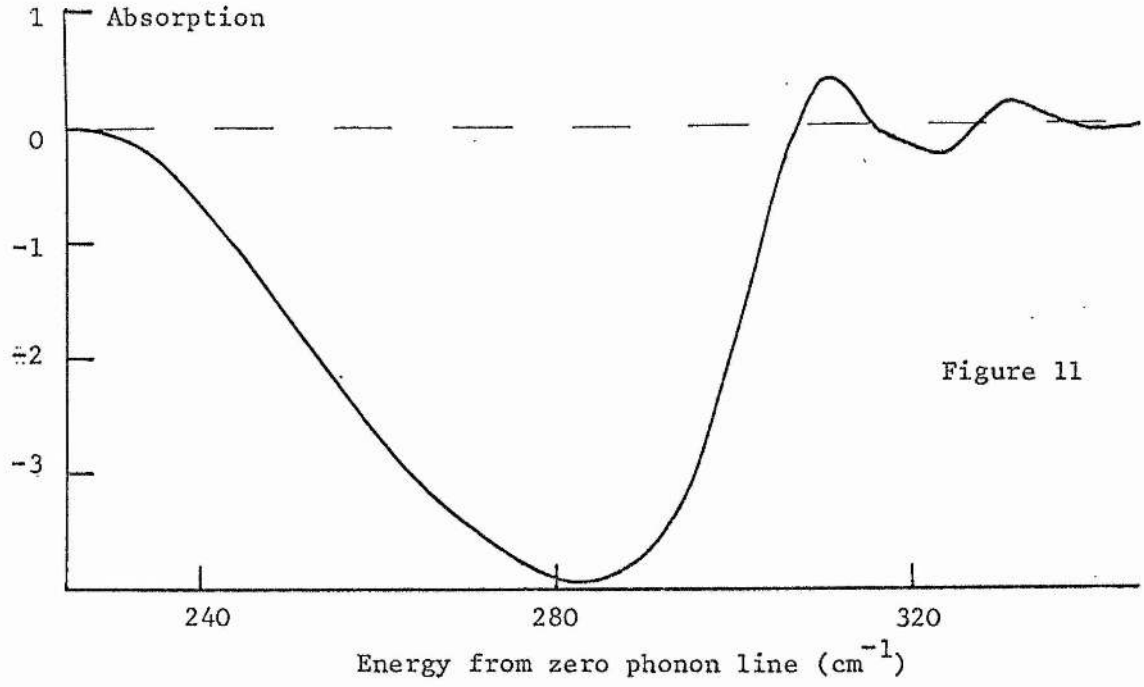

Figure 11

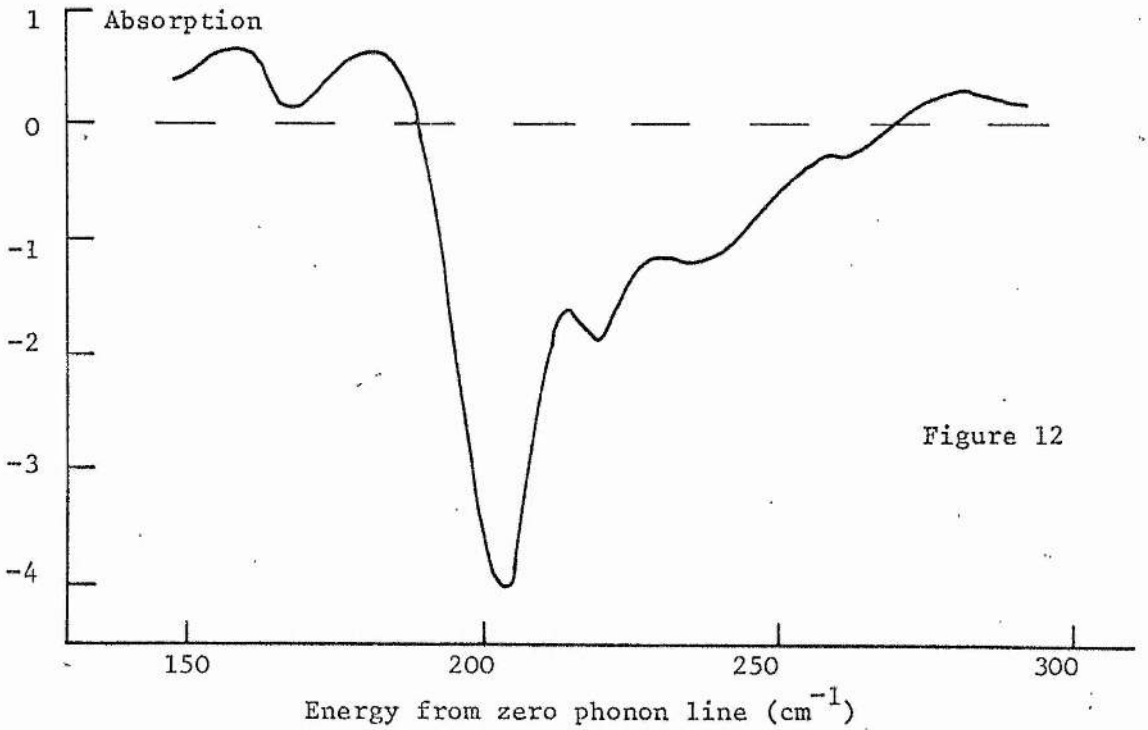

Figure 12

Figure 11: Antiresonances in $^3T_1$-$^1T_2$ band of ZnS:Ni.

Figure 12: Antiresonances in $^3T_1$-$^1T_2$ band of ZnSe:Ni.

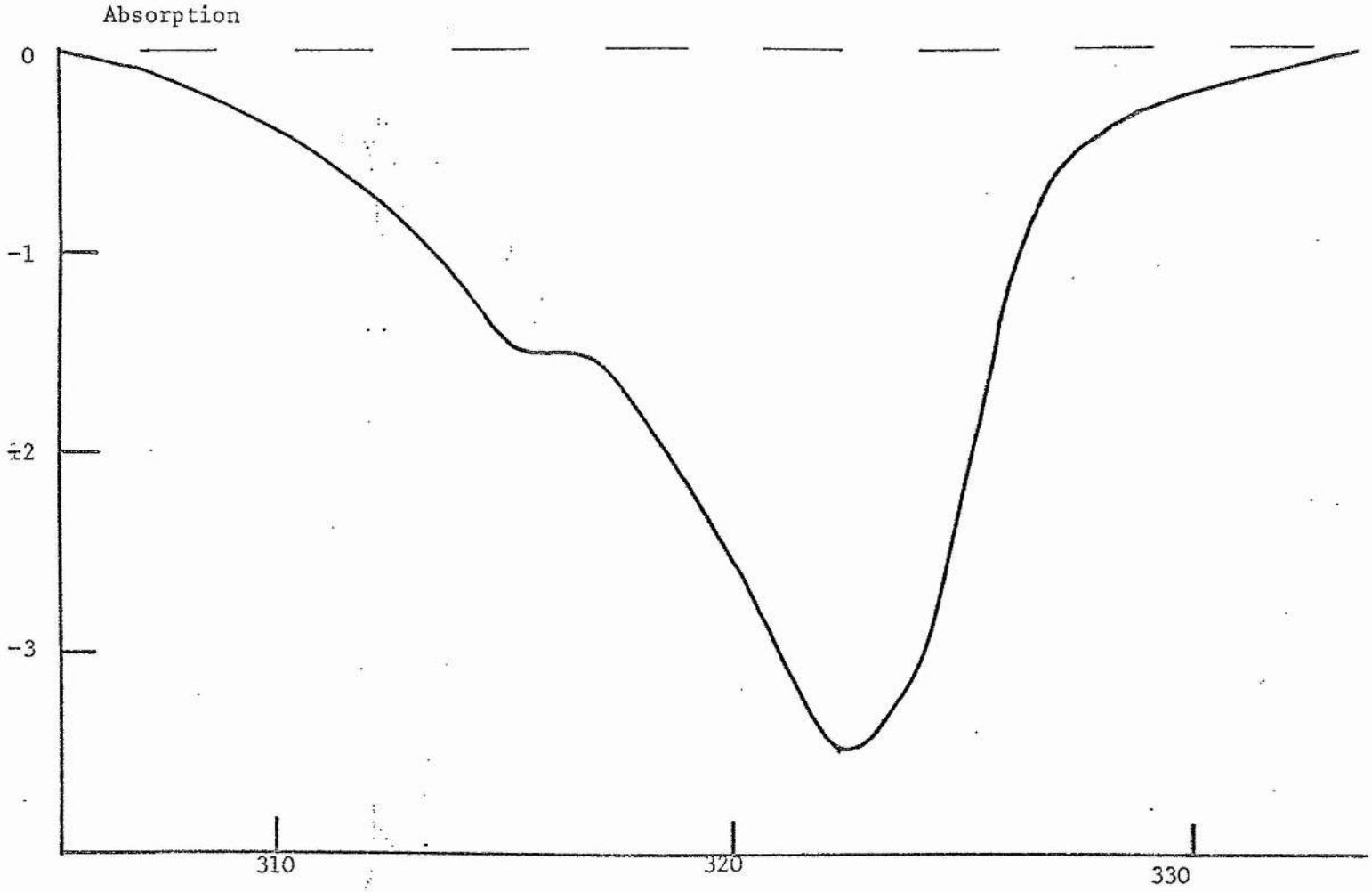

Figure 13
Antiresonances in $^3T_1 - ^3T_1$ band of ZnS:Ni.

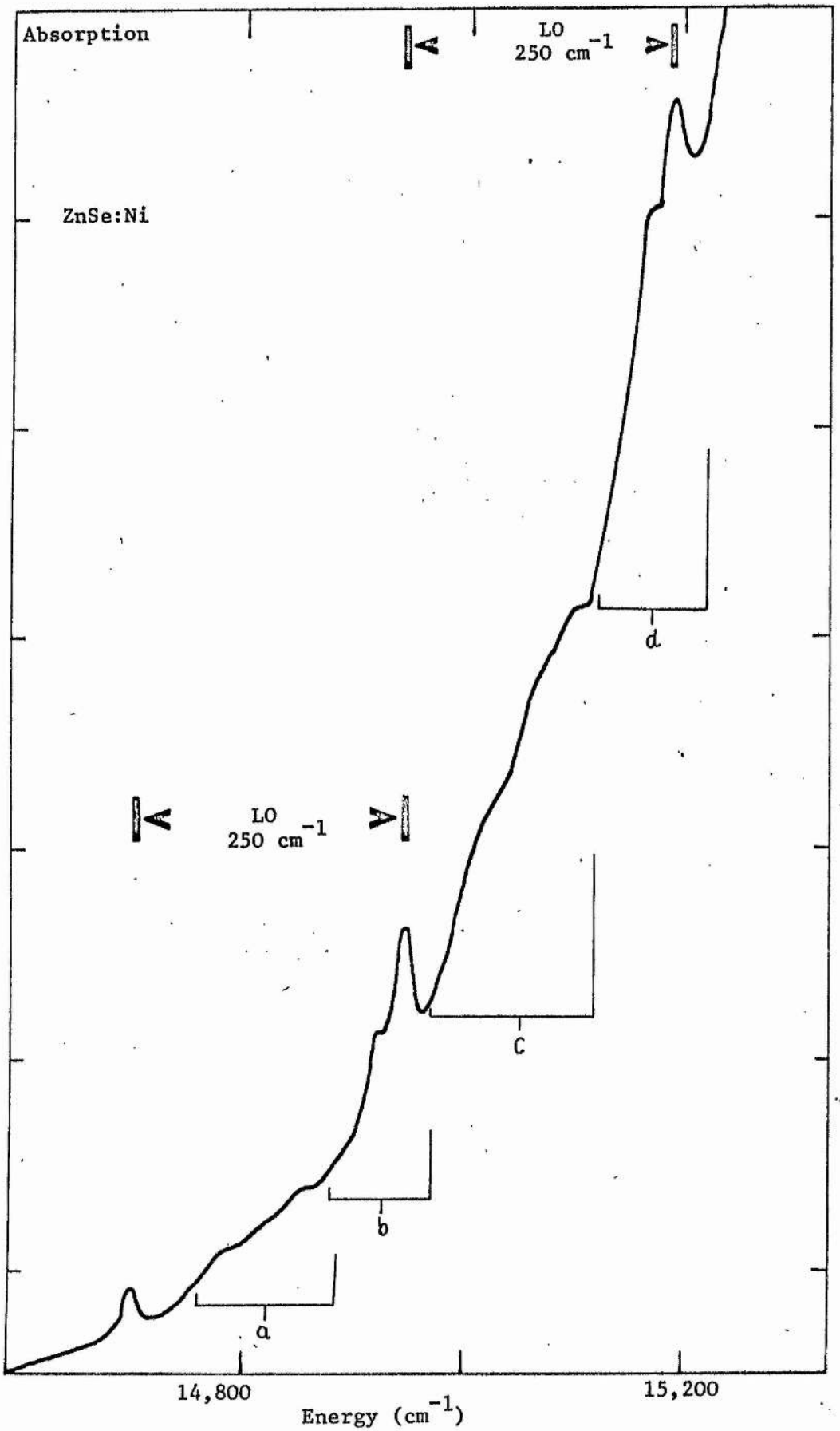

Figure 14
Photoionization edge of ZnSe:Ni
at 6°K

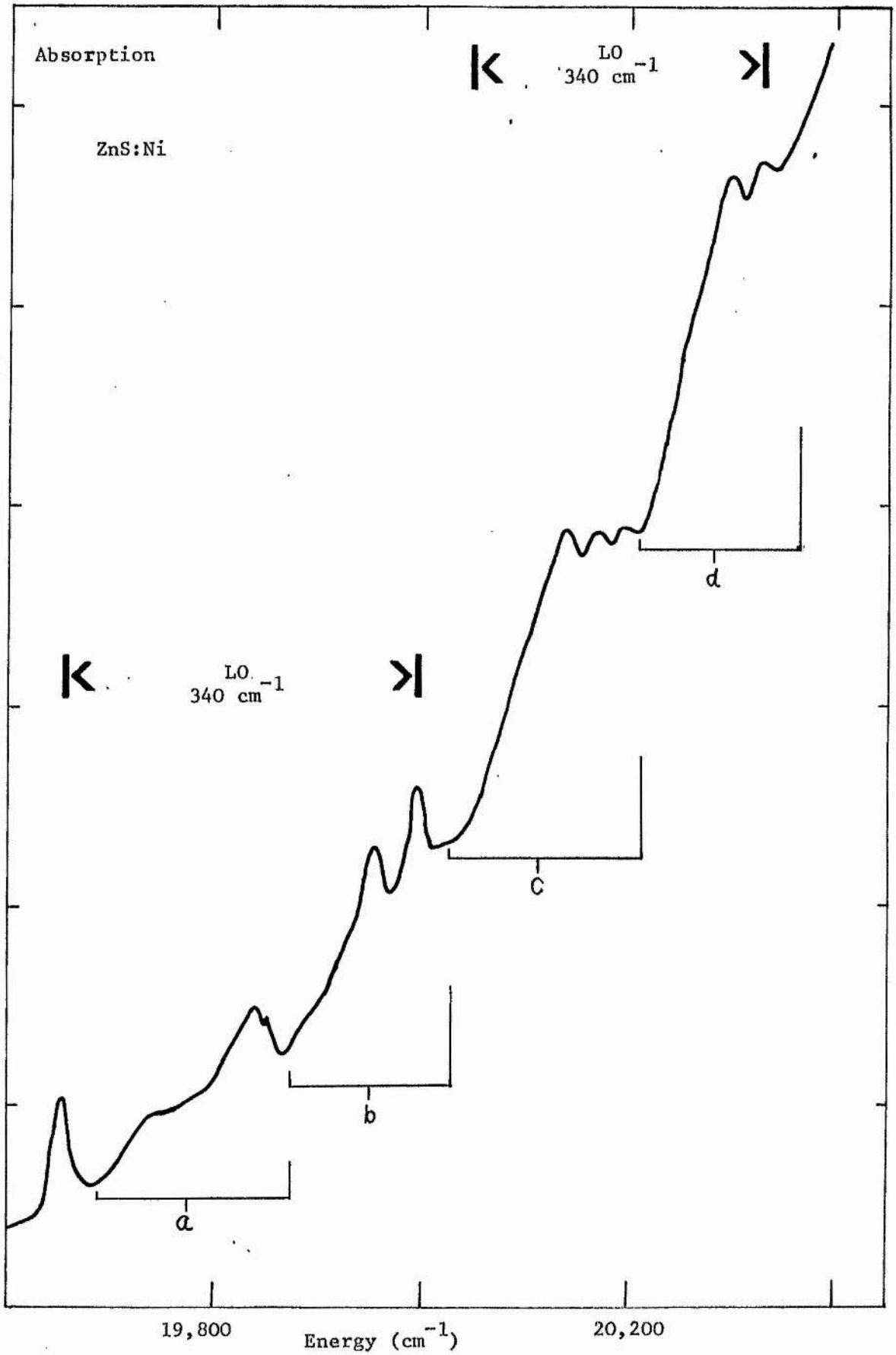

Figure 15
Photoionization edge of ZnS:Ni at 6°K.

Figure 16, ZnSe:Ni

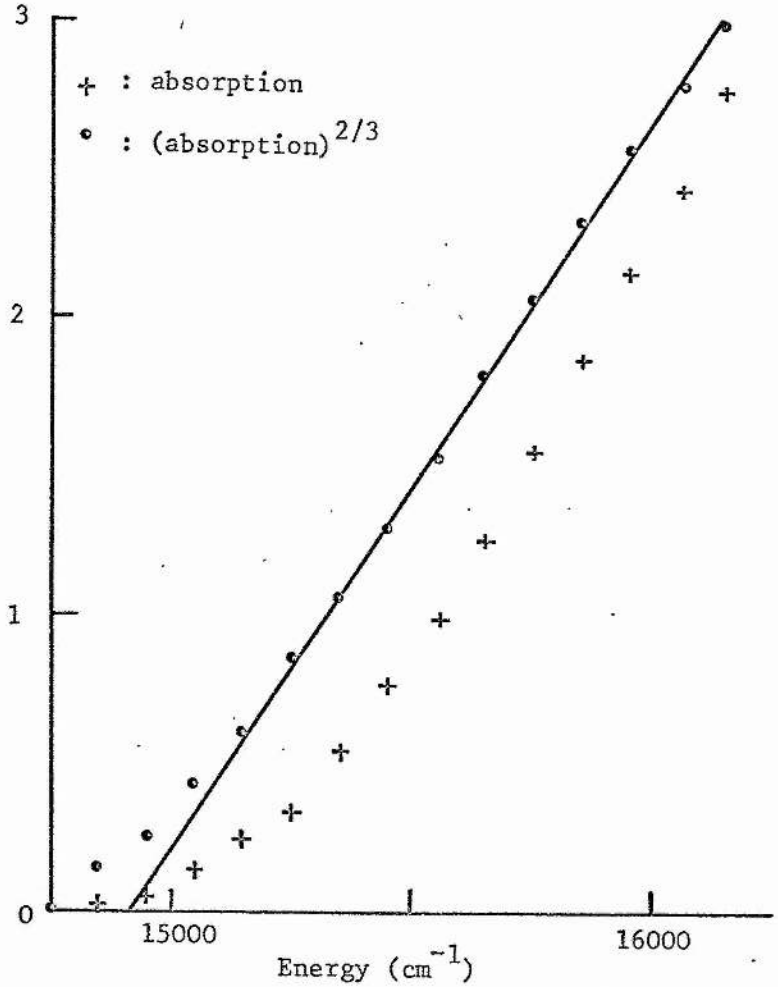

Figure 17, ZnS:Ni

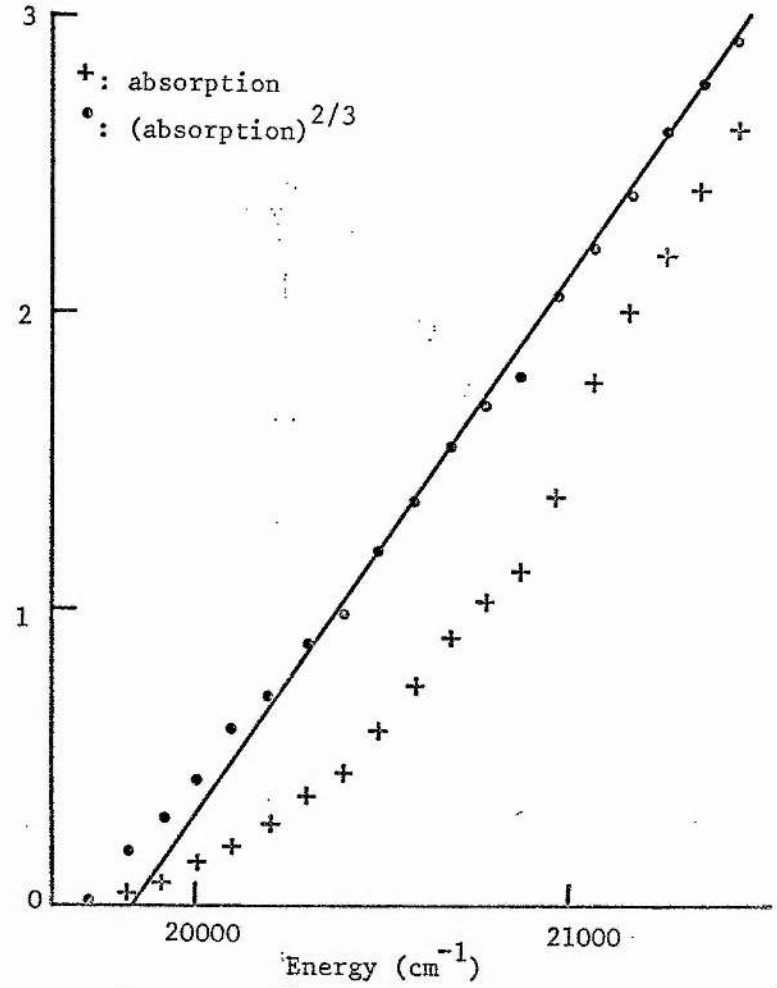

Absorption bands at 6°K, showing behaviour near threshold.
The vertical scale is linear, with arbitrary units.

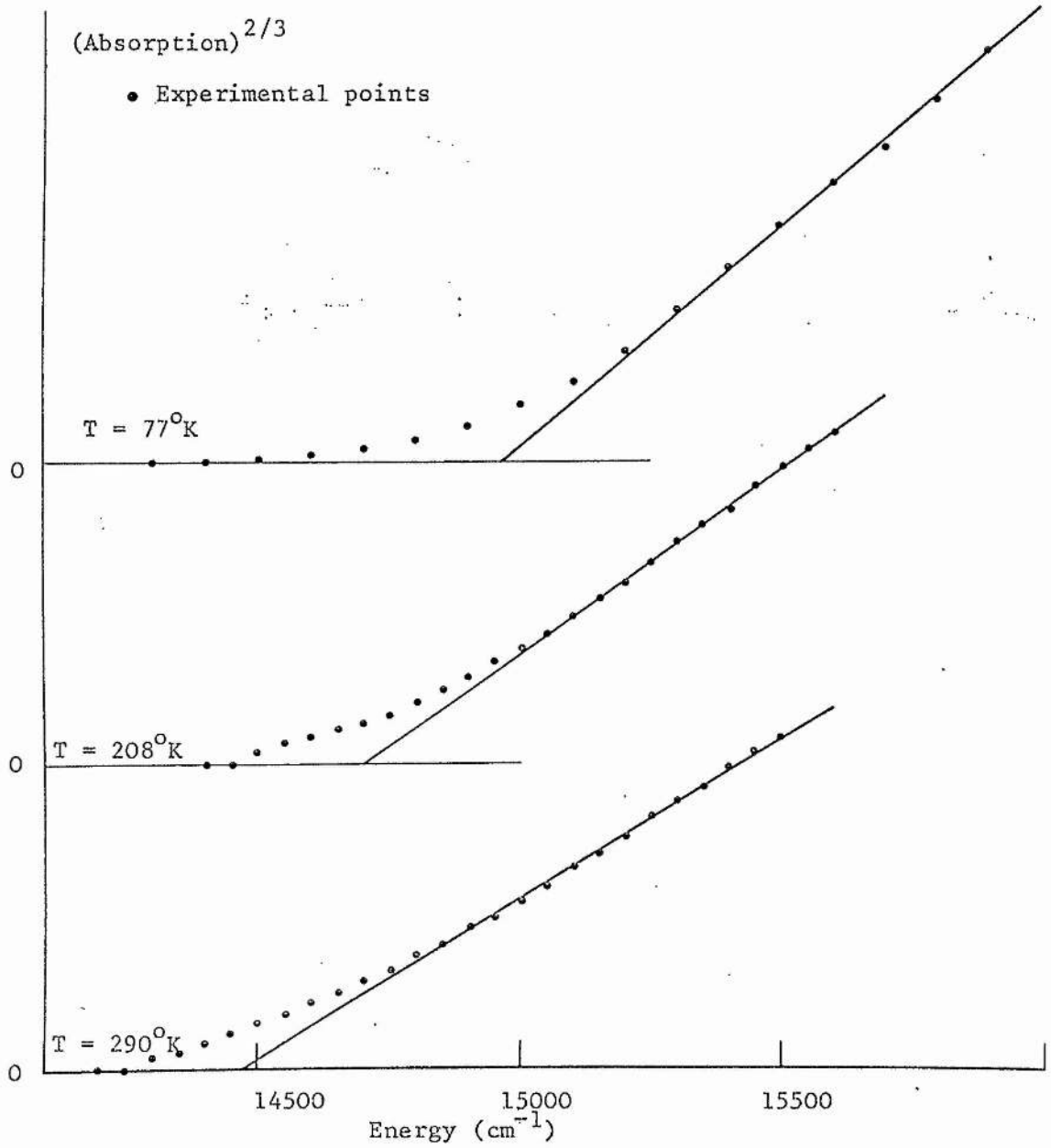

Figure 18

Behaviour of absorption in ZnSe:Ni near photoionization energy, at various temperatures.

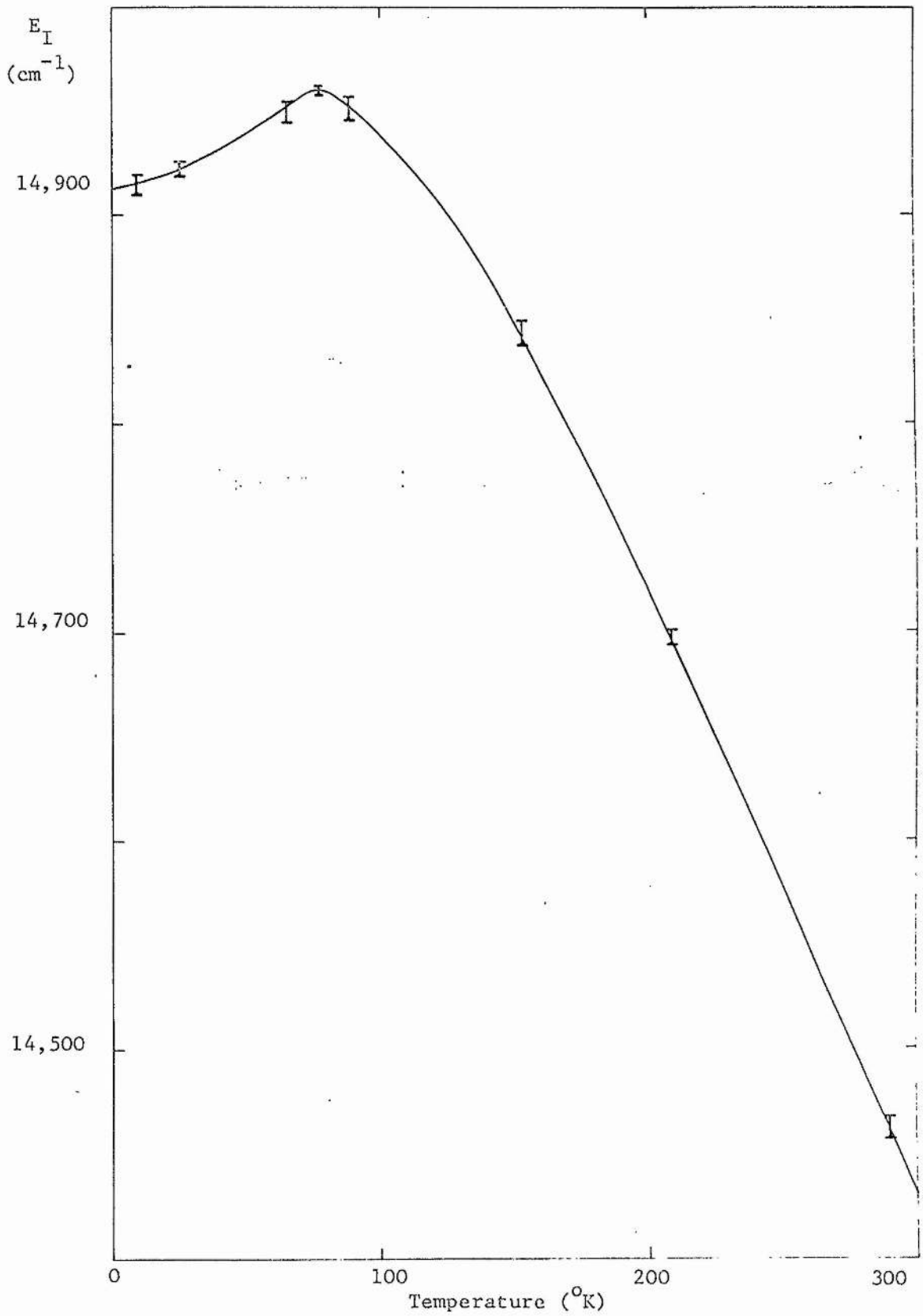

Figure 19
Variation of ionization threshold energy of ZnSe:Ni.

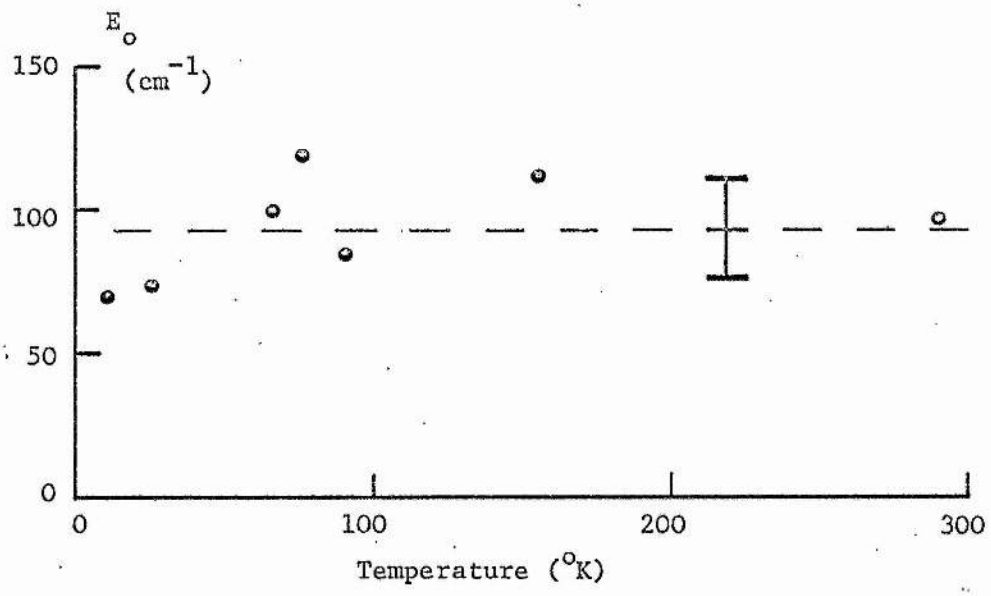

Figure 20

Behaviour of below-threshold absorption in ZnSe:Ni at different temperatures.

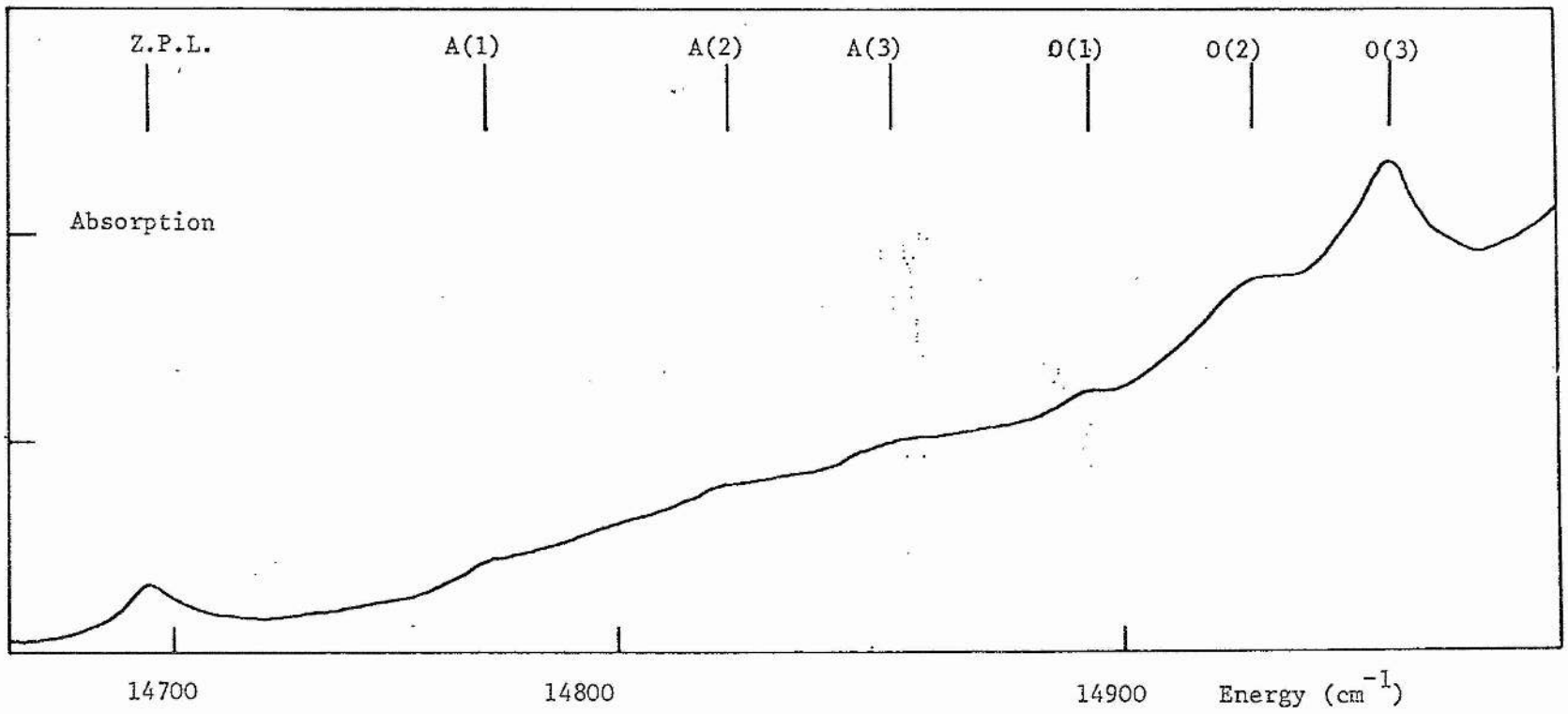

Figure 21

Vibrational sidebands near the ionization threshold energy of ZnSe:Ni. The peaks are labelled according to the notation of table 13.

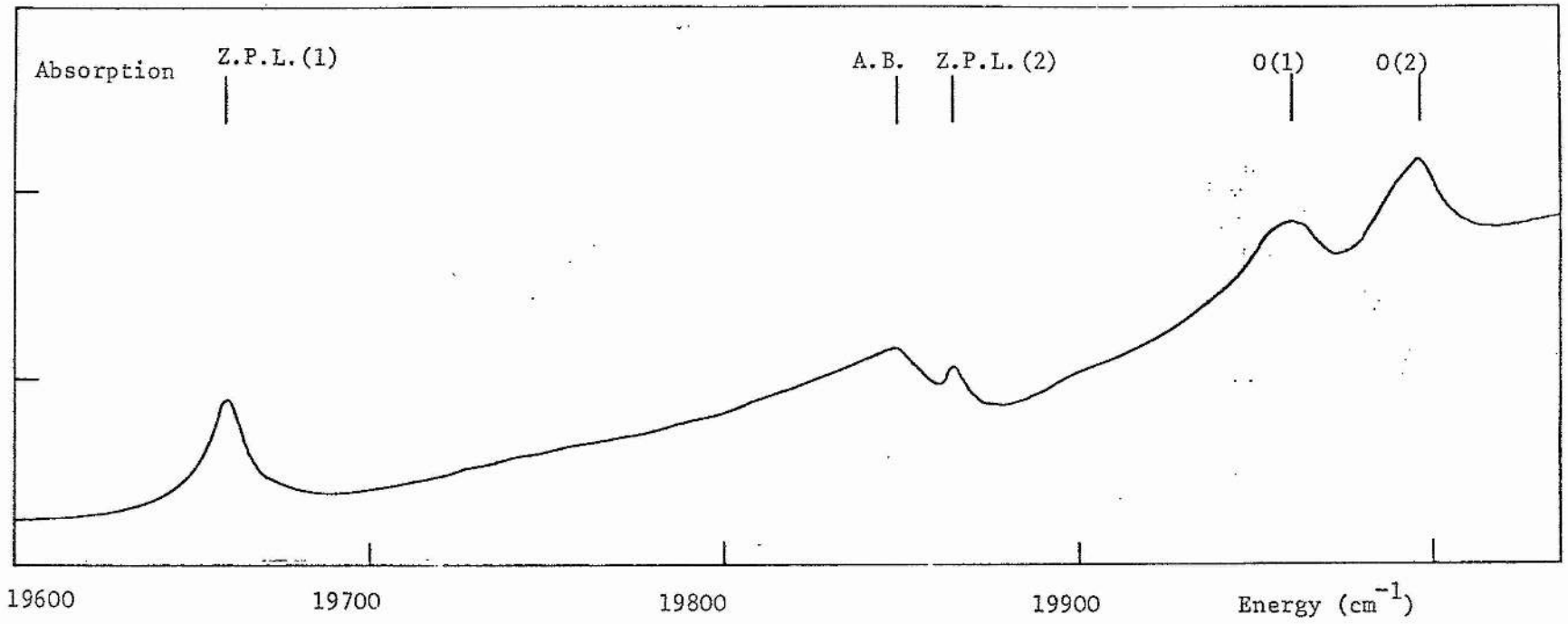

Figure 22

Vibrational sidebands near the ionization threshold energy of ZnS:Ni.
The peaks are labelled according to the notation of table 13.

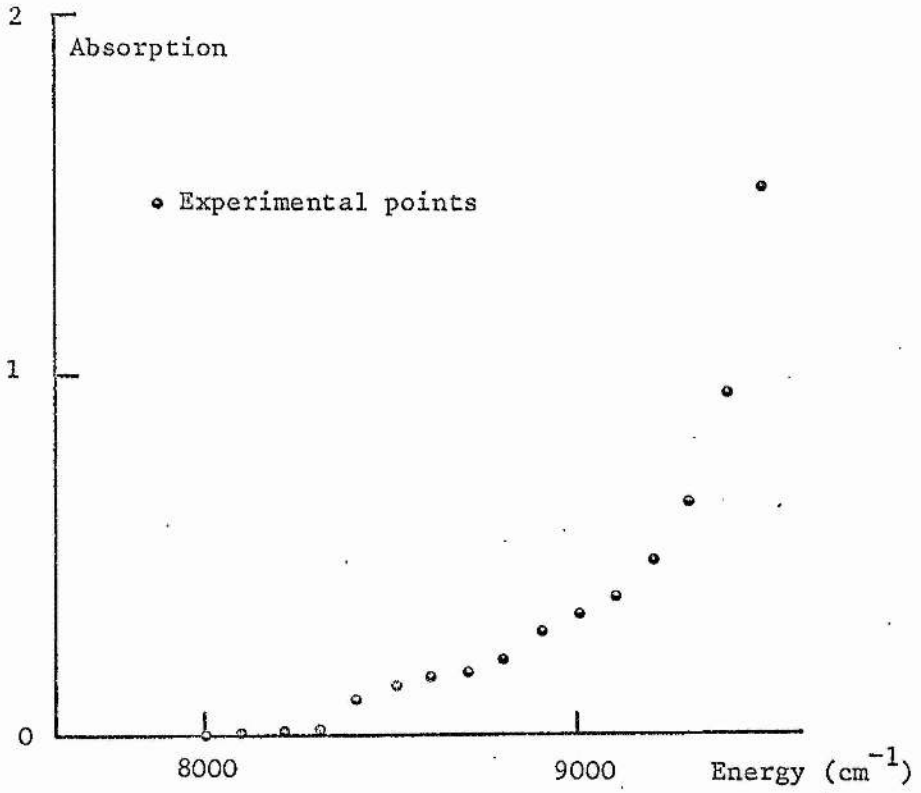

Figure 23

Complementary ionization in ZnSe:Ni, at 6°K.

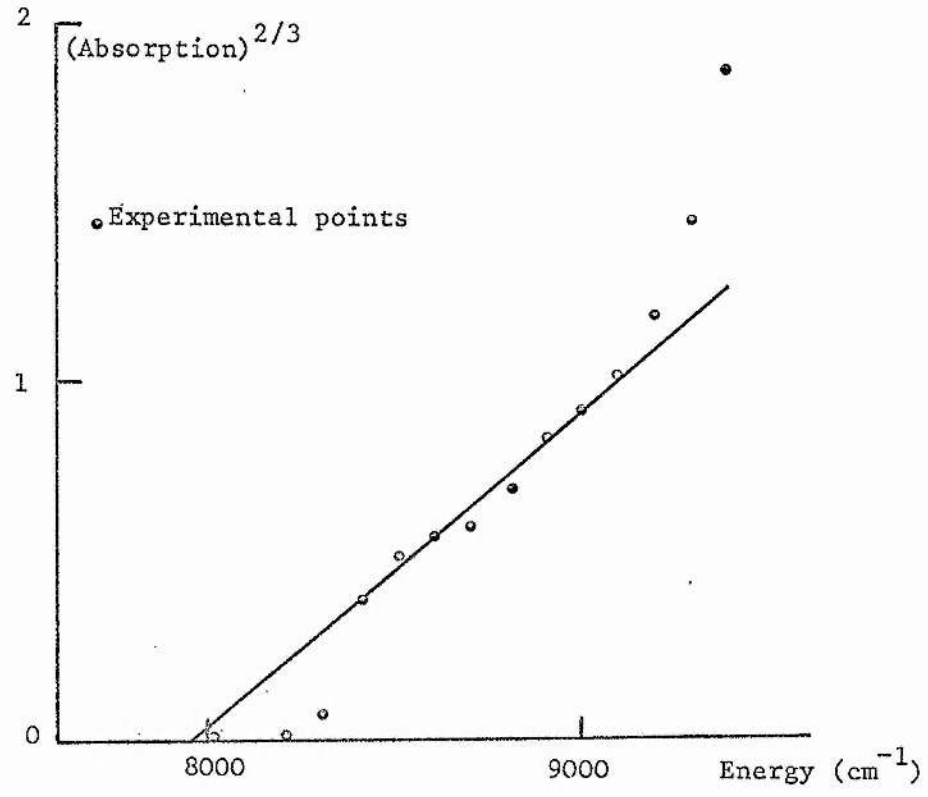

Figure 24

Comparison of absorption near low energy ionization threshold of ZnSe:Ni with theory.

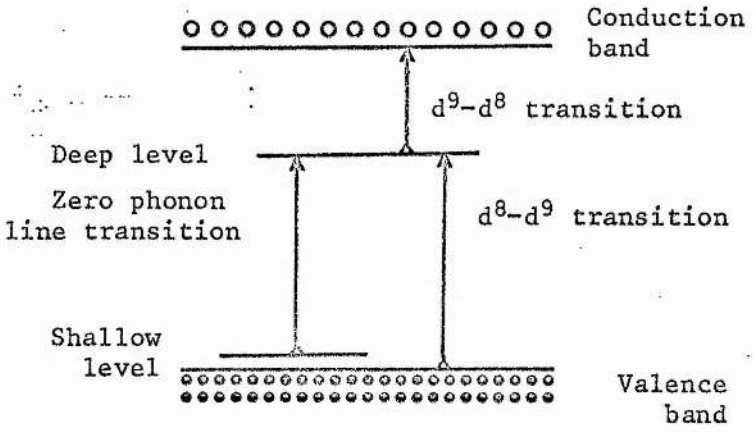

Figure 25

Absorption processes seen in ZnSe:Ni and ZnS:Ni.

TABLES FOR CHAPTER 7

Table 1

Eigenvalues of d^8 energy matrices by numerical diagonalisation. The matrices were found theoretically by Liehr and Ballhausen [9].

(a) ZnS:Ni

$\Delta = 4260\ cm^{-1}$
$B = 587\ cm^{-1}$
$C = 2170\ cm^{-1}$
$\lambda = -250\ cm^{-1}$

$C \div B = 3.7$

These values are due to Kaufmann and Koidl [35,61].

Eigenvalue (cm^{-1})	Symmetry type
32,808	$^1A_1$
18,248	^1E
15,804	$^1T_1$
15,595	$^1A_2$
14,421	$^1T_2$
12,986	$^3T_1$
12,842	$^3T_1$
12,485	$^3T_1$
12,435	$^3T_1$
9,174	^1E
9,118	$^1T_2$
8,495	$^3A_2$
4,652	$^3T_2$
4,438	$^3T_2$
4,380	$^3T_2$
4,329	$^3T_2$
1,014	$^3T_1$
867	$^3T_1$
311	$^3T_1$
0	$^3T_1$

(b) ZnSe:Ni $\Delta = 4400\,cm^{-1}$: Wray and Allen [5].

$B = 530\,cm^{-1}$ " "

$\lambda = -250\,cm^{-1}$: Weakleim [58] finds this value of λ suitable for ZnS:Ni, CdS:Ni and ZnO:Ni.

Eigenvalue (cm^{-1}) with $C \div B = 3.7$	Eigenvalue (cm^{-1}) with $C \div B = 4$	Symmetry type
30,388	31,449	$^1A_1$
17,557	17,876	^1E
14,843	15,164	$^1T_1$
14,484	14,858	$^1A_2$
13,537	13,848	$^1T_2$
12,260	12,271	$^3T_1$
12,134	12,134	$^3T_1$
11,775	11,790	$^3T_1$
11,718	11,733	$^3T_1$
9,099	9,134	$^1T_2$
8,354	8,658	^1E
8,056	8,325	$^3A_2$
4,795	4,795	$^3T_2$
4,570	4,571	$^3T_2$
4,499	4,508	$^3T_2$
4,470	4,469	$^3T_2$
1,008	1,009	$^3T_1$
867	868	$^3T_1$
313	312	$^3T_1$
0	0	$^3T_1$

Table 2

$^3T_1 - {}^3T_2$ absorption band of ZnSe:Ni; comparison of phonon energies with separation of sidebands from lowest sharp line in band. The sidebands are numbered as in figure 3.

Sideband	Energy (cm^{-1})	Energy above z.p.l. (cm^{-1})	Phonons* (cm^{-1})
(1) ≡ Z.P.L.	4,040	0	-
(2)	4,090	50	TA(L):49,57
(3)	4,133	93	?
(4)	4,190	150	(3) + TA(L), P.D.S.**
(5)	4,255	215	TO(X), LO(X) , TO(Γ)
(6)	4,290	250	LO(Γ)

* see appendix.

** P.D.S. stands for "Peak in one-phonon Density of States".

Table 3

Structure of $^3T_1 - {}^3T_1$ band of ZnSe:Ni. Components are numbered according to figure 7.

(a) Sharpest lines.

Line	Energy* (cm^{-1})
1	0
4	16
5	29
6	34
11	132

(b) Strongest lines

Line	Energy* (cm^{-1})
5	0
8	32
11	103
16	240

(c) Calculated spin-orbit levels (see table 1)

Line**	Energy* (cm^{-1})
T_2	0
E	57
T_1	416
A_1	542

* relative to first line in each set

** labelled according to reference [35].

Table 4

Jahn-Teller energies of cobalt impurity states in different materials.

(a) MgO:Co(d^7) [123],

State	Jahn-Teller energy (cm^{-1})
$^4T_2$ (excited level)	450
$^4T_1$ (ground level)	100

(b) ZnS:Co(d^7) [122],

State	Jahn-Teller energy (cm^{-1})
$^4T_1$ (higher energy excited state).	110 - 420
$^4T_2$ (lower lying excited state).	40 - 130

Table 5

Widths of zero phonon lines of $^3T_1 - {}^1T_2$ absorption bands of ZnSe:Ni and ZnS:Ni, at 6°K.

	Width (cm^{-1})
ZnSe:Ni	3.5
ZnS:Ni	14

Table 6

Measured and calculated positions of the first few vibronic levels of the $^1T_2$ state of nickel in ZnS and ZnSe, assuming coupling to a trigonal mode.

(a) ZnSe:Ni Active mode is TA(X) = 70.5 cm^{-1}

K = 1.4; E_{JT} = 92 cm^{-1}

Measured energy (cm^{-1})	Calculated energy (cm^{-1})
0 (Z.P.L.)	0
27	27
45	49
75	74

(b) ZnS:Ni Active mode is (TA(X) = 93 cm^{-1}

K = 1.4; E_{JT} = 122 cm^{-1}

Measured energy (cm^{-1})	Calculated energy (cm^{-1})
0	0
35	36

Table 7

Parameters of antiresonances in ZnS:Ni and ZnSe:Ni.

Material	Energy (cm^{-1})	Appearance	$h\nu$ (cm^{-1})	Lifetime (secs)	q
ZnSe:Ni	164	Weak (a)	5	1×10^{-12}	-0.8
ZnSe:Ni	200	Strong (a)	8	6×10^{-13}	-0.4
ZnSe:Ni	215	Weak (a)	4.5	1×10^{-12}	-1.5
ZnS:Ni	296	Strong (b)	20	3×10^{-13}	0.4
ZnS:Ni	324	Weak (b)	4	1×10^{-12}	1.0
ZnS:Ni	314	Weak (c)	1.4	3×10^{-12}	0.0
ZnS:Ni	322	Strong (c)	3.3	1.4×10^{-12}	-0.1

(a) $^3T_1 - {}^1T_2$ band

(b) $^3T_1 - {}^1T_2$ band

(c) $^3T_1 - {}^3T_1$ band

Table 8

Correlation of antiresonances and lattice modes in ZnSe and ZnS.

(a) ZnSe

Material	Band	Energy (cm^{-1})	Ascription*
ZnSe:Ni	$^3T_1-^1T_2$	164	P.D.S. **
ZnSe:Ni	$^3T_1-^1T_2$	200	TO
ZnSe:Ti	$^3A_2-^3T_1$	206	TO(Γ)
ZnSe:Ni	$^3T_1-^1T_2$	215	TO,LO(X),P.D.S.
ZnSe:Ti	$^3A_2-^3T_1$	219	TO,LO(X),P.D.S.

(b) ZnS

Material	Band	Energy (cm^{-1})	Ascription*
ZnS:Ti	$^3A_2-^3T_1$	276	TO(Γ)
ZnS:Ni	$^3T_1-^1T_2$	296	TO(L)
ZnS:Ni	$^3T_1-^3T_1$	314	TO(X)
ZnS:Ti	$^3A_2-^3T_1$	315	TO(X)
ZnS:Ni	$^3T_1-^3T_1$	322	TO(X),P.D.S.
ZnS:Ni	$^3T_1-^1T_2$	324	TO(X),P.D.S.

* see appendix.

** P.D.S. stands for "Peak in one-phonon Density of States".

Table 9

Summary of published work on CdS:Ni, and ZnSe:Ni.

(a) Photoionization band of CdS:Ni [67,68].

With low concentration of Ni, abs^{n} coeff. $\alpha(E-E_I)^{3/2}$,

where E_I = 17,960 cm^{-1} at 77°K.

E_I varies with temperature, and photovoltage measurements show mainly free electrons are produced in the ionization process.

With concentrations of Ni greater than 0.1%,

abs^{n} coeff. $\alpha(E-E_I)^{3/2}$, where 18,225 cm^{-1} <E<18,870 cm^{-1}

and $\alpha(E-E_I^1)^{1/2}$, E > 18,870 cm^{-1}

E_I^1 = 18,815 cm^{-1}

Photovoltage measurements show that current carriers are mainly holes. It is suggested that E_I^1 is the threshold for transitions involving valence band states. A zero phonon line is seen at 17,669 cm^{-1}: this is explained as being due to a valence band hole binding to an impurity, with a binding energy of 1146 cm^{-1} i.e. 0.14 eV.

Phonon replicas are seen; the main repeat interval corresponds to a band edge LO phonon. The Huang-Rhys factor is 8.5.

(b) ZnS:Ni [63,64,84,66]

The photoionization band near 20,000 cm^{-1} is seen. A zero phonon line is seen at 19,663 cm^{-1}, followed by sidebands due mainly to optical phonons of the lattice.

It is suggested that the zero phonon line is due to a valence band hole localised near a nickel (d^8)impurity. This is supported by measurements of magnetocircular dichroism which show that in the ground state of the complex

$0.1 \lesssim g \lesssim 0.3$

(continued/)

Table 9 continued

Another experiment which measures the luminescence of crystals containing nickel and copper shows that the copper, normally present as d^{10} may be ionized by hole capture when light of greater energy than 20,833 cm^{-1} is shone on the crystal. It is suggested that the holes are originally created by the process

$$h\nu + Ni(d^8) \rightarrow Ni(d^9) + \text{hole},$$

and then migrate to the copper sites. If this process has an ionization threshold of 20,833 cm^{-1}, then the binding energy of the impurity-hole complex is 0.17 eV or 1170 cm^{-1}.

However it is clear that intense absorption in nickel-doped samples, seemingly due to photoionization, is detected at lower energies than this "threshold".

(c) ZnSe:Ni [63,65]

A zero phonon line is seen at 14705 cm^{-1}, followed by optical phonon replicas.

The photoionization band is attributed to

$$h\nu + Ni(d^8) \rightarrow Ni(d^9) + \text{hole},$$

with an ionization threshold of 15×10^3 cm^{-1}. Induced absorption may then be detected, with a threshold at 9×10^3 cm^{-1}. This is ascribed to the process

$$h\nu + Ni(d^9) \rightarrow Ni(d^8) + \text{electron}.$$

After this second absorption, anti-Stokes' luminescence is seen.

The thresholds for the two processes are not found precisely, but it is noted that they add up to little more than the band-gap energy of ZnSe.

Table 10

Thresholds of photoionization bands of ZnS:Ni and ZnSe:Ni at 6°K.

	E_I (cm^{-1})
ZnSe:Ni	14916
ZnS:Ni	19820

Table 11

Positions of near-photoionization threshold zero phonon lines in ZnS:Ni and ZnSe:Ni, and binding energies.

	$E_{Z.P.L.}$ (cm^{-1})	E_B(cm^{-1}) $= (E_I - E_{Z.P.L})$	E_B (meV)
ZnSe:Ni	14695	221	27.4
ZnS:Ni	19654	166	20.6

Table 12

(a)Binding energies of shallow acceptors [74]

State	Energy (cm^{-1})	
	ZnS	ZnSe
$^1S_{3/2}$	1,416	889
$^2P_{3/2}$	626	404
$^2S_{3/2}$	419	266
$^2P_{5/2}(\Gamma_8^-)$	400	254
$^2P_{5/2}(\Gamma_7^-)$	287	183
$^2P_{1/2}$	94	49

(b)Binding energies of shallow donors.

Hydrogenic state	ZnS	ZnSe
n = 1	494	237
n = 2	124	59

(c)Huang-Rhys factors for hydrogenic acceptors and donors.

State	ZnSe	ZnS
Donor n = 1	0.74	1.40
n = 2	0.37	0.70
Acceptor n = 1	5.79	7.93
n = 2	2.89	3.97

Table 13

Vibronic sidebands seen in the near-threshold spectral regions of ZnSe:Ni and ZnS:Ni.

(a) ZnSe:Ni

Energy (cm^{-1})	Ascription
14,695	Z.P.L.
14,775	Z.P.L. + A(1)
14,819	Z.P.L. + A(2)
14,848	Z.P.L. + A(3)
14,888	Z.P.L. + O(1)
14,918	Z.P.L. + O(2)
14,948	Z.P.L. + O(3)
15,020	Z.P.L. + O(3) + A(1)
15,069	Z.P.L. + O(3) + A(2)
15,097	Z.P.L. + O(3) + A(3)
15,142	Z.P.L. + O(3) + O(1)
15,175	Z.P.L. + O(3) + O(2)
15,198	Z.P.L. + 2(O(3))

A(1) = 73 $\pm$ 5 cm^{-1}*
A(2) = 119 $\pm$ 5 cm^{-1}
A(3) = 150 $\pm$ 3 cm^{-1}
O(1) = 193 $\pm$ 2 cm^{-1}
O(2) = 225 $\pm$ 2 cm^{-1}
O(3) = 250 $\pm$ 3 cm^{-1}

Only the O(2) and O(3) replicas are strong, but the structure can be traced over three multiples of O(3). All two or more-phonon sidebands involve O(3).

* The uncertainties in energy quoted refer to the difficulties in determining the peaks of the sidebands: the widths of these are all much greater than these values.

(continued/)

Table 13 continued

(b) ZnS:Ni

Energy (cm^{-1})	Ascription
19,654	Z.P.L. (1)
19,843	Z.P.L. (1) + A.B.
19,859	Z.P.L. (2)
19,955	Z.P.L. (1) + O(1)
19,991	Z.P.L. (1) + O(2)
20,027	Z.P.L. (1) + 2(A.B.)
20,137	Z.P.L. (1) + A.B. + O(1)
20,178	Z.P.L. (1) + A.B. + O(2)
20,203	Z.P.L. (2) + O(2)
20,302	Z.P.L. (1) + O(1) + O(2)
20,335	Z.P.L. (1) + 2(O(2))

A.B. ≡ Acoustic band, peak at 189 $\pm$ 3 cm^{-1}.

O(1) ≡ Optical band, peak at 305 $\pm$ 3 cm^{-1}.

O(2) ≡ Optical band, peak at 340 $\pm$ 2 cm^{-1}.

Five repeats of O(2) are visible in good spectra.

Z.P.L.(2) is 205 cm^{-1} higher in energy than Z.P.L.(1), and might be due to a localised vibrational mode (see text).

Table 14

Intensities of phonon sidebands of near-threshold zero phonon lines in ZnSe:Ni and ZnS:Ni.

(a) ZnSe:Ni

Band*	Measured Intensity	Theoretical Intensity	Fitting Parameters
Z.P.L.	1.0	1.0	1.0
a : First acoustic	2.8	Sac.	2.8
b : First optical	5.2	Sop.	4.9
c : First combined optical and acoustic	6.9	Sac.x Sop./2	6.9
d : Second optical	11.7	$S_{op.}^2/2$	12.0

* : labelled according to figure 14.

(b) ZnS:Ni

Band*	Measured Intensity	Theoretical Intensity	Fitting Parameters
Z.P.L.(1)**	1.0	1.0	1.0
a : First acoustic	3.0	Sac.	3.0
b : First optical	3.9	Sop.	3.5
c : First combined optical and acoustic	5.0	Sac.x Sop./2	5.3
d : Second optical	5.1	$S_{op.}^2/2$	6.1

* : labelled according to figure 15.

** : the contribution to the strength of the sidebands due to Z.P.L.(2), and its replicas, is assumed to be negligible.

CHAPTER 8

DISCUSSION

Razumikhin: "I like people to talk rot. It's man's only privilege over the rest of creation. By talking rot, you eventually get to the truth. I'm a man because I talk rot. Not a single truth has ever been discovered without people first talking utter rot a hundred times or perhaps a hundred thousand times..."

F.Dostoyevsky, "Crime and Punishment". (trans. D.Margarshack).

Chapter Eight
Introduction

The work reported in the preceding chapters can be classified into three categories:

(1) Fine structure in absorption bands.

(2) Vibronic and electronic antiresonance in solids.

(3) Photoionization of impurities, and associated effects.

It is the aim of this final chapter to show what the present research has added to the understanding of these topics, and to consider whether any of the implications merit further investigation.

1) Fine Structure

It has been clear for a long time that the positions of absorption and emission bands of transition metal impurities can be understood in terms of crystal field theory. When experiments carried out at low temperatures revealed that these bands frequently contain many sharp lines, it was thought at first that the fine structure was due to spin-orbit coupling. This view was endorsed by calculations made by Tanabe, Sugano and Kamimura in 1958, showing that the inclusion of spin-orbit effects in the theory of impurity spectra successfully explained some experimental results [86,87] . More exact treatments followed; an example is the "complete theory" of Liehr and Ballhausen [9] . It seemed then that all important interactions were included in this type of formulation. In fact a review dating from this period suggests that theory and experiment would be brought into complete accord by the use of molecular orbital calculations to allow for the effects of covalency [7] . This approach to the interpretation of experimental data is exemplified by a paper of Weakliem [58] who was able to ascribe fine structure in the spectra of several materials to spin-orbit splitting. The fitting of theory and data used parameters derived from the experiments. It was quite plausible that differences between these parameters and the known values for free ions were due solely to covalency.

An inkling of unsuspected complications was first induced by measurements of fine structure which could not be explained totally in such terms; Anderson found that phonon replicas of electronic transitions occurred in the spectra of ZnO:Ni and ZnO:Co, and noted that this might be due to Jahn-Teller coupling [88]. This is the earliest example of recorded spectra being considered in such terms.

It is now clear thatthe fine structure in spectra is due in general to a combination of spin-orbit coupling and Jahn-Teller coupling. There are other perturbations, usually of lesser importance. When the two main interactions couple to the same transition the spectral band may be very complicated, and interpreting the significance of the many sharp lines or wider bands which may appear becomes difficult. The reasons for the strong interplay of these effects were given first by Ham, who showed that matrix elements of interactions between different electronic states may be greatly affected by Jahn-Teller coupling [24]. Consequently many physical properties are altered.

An early paper explaining spectral details on the basis of this model is by Ham and coworkers [89]. Many more recent references are given in a publication by Koidl [90]. In many cases considerable agreement with experiment is reached, but it is frequently the case that calculations are feasible only after extensive approximations and simplifications have been made. Thus although one may require to know accurately the strength of coupling to different modes of vibration or the energies of the interaction modes, it may not be clear how much significance attaches to parameters derived in this way.

For example, it is much simpler mathematically to use a cluster model in which only the motion of the impurity and its nearest neighbours is considered to be important, than it is to take into account all the localised and un-localised modes that actually exist. However Halperin

has shown recently that such a model is realistic only in the limit of strong coupling [91]. Thus weak coupling is hard to handle. In contrast the static distortions which accompany strong coupling are usually not considered explicitly in the formulation of a problem, since they are caused by high order interactions. Although they constitute one of the most characteristic features of Jahn-Teller coupling, they are introduced rather qualitatively after a model of dynamic distortion has been elaborated.

In the course of the present work it was found that at low temperatures the absorption spectra of ZnSe:Ti and ZnS:Ti contain bands which consist of two regular series of peaks. Various arguments led to the suggestion that this structure was due to simultaneous linear and non-linear Jahn-Teller coupling to both trigonal and tetragonal vibrational modes in an excited electronic level. The coupling is strong enough to suppress any observable effects of spin-orbit splitting.

This circumstance of coupling to both ε and τ_2 modes is quite common, but the resulting spectra are hard to interpret not least because of mathematical difficulties [13,92]. In addition the fine structure due to different vibronic levels is often found to be broadened out so that the energies of the interaction modes have to be found by deconvolution of the wide band. This is not the case with the systems studied here, where the energies of the modes may be found by inspection. They appear to be closely related to phonons from critical points of the Brillouin zone, so that both symmetry and energy of each interaction mode can be established. Furthermore the interaction strengths can be judged from the intensities of the various phonon sidebands. This might make accurate calculations feasible.

The detection of similar spectra in both ZnSe:Ti and ZnS:Ti shows that the effects being studied are not peculiar to just one system.

Furthermore the presence of the anomalous contribution to the second moment, unexplained by the theory of linear vibronic coupling, is shown not to be due to autoionization of the excited centres. Thus it is expected that the spectra of the cadmium compounds have an underlying structure of a similar nature, although it is broadened so that no fine structure may be seen.

It is therefore likely that a model to explain the structure of the bands detailed in this work would be important and could be applicable to many other systems, where perhaps only wide, featureless bands are seen, or because the spectra are very complex, only the first few vibronic levels have been fitted to the theory.

The difficulties in deducing basic information about Jahn-Teller coupling are typified by those met in a study of ZnSe:Ni and ZnS:Ni. In these materials the bands cannot be easily described although it is clear that much of the structure is vibronic in origin. In these materials the Ham effect is less strong so that spin-orbit splittings are large enough to produce well resolved fine structure. The T_2 bands show τ_2 coupling, stronger in the higher energy band, leading to rather similar band-shapes. There are many features which seem due to vibronic coupling but cannot be ascribed to critical point modes. They involve local modes or phonons from wide regions of the Brillouin zone. The presence of wide side-bands and coupling to many lattice modes is

consistent with the strength of coupling, which is less for these nickel-doped specimens than for material containing titanium. A more refined theory is evidently required for the proper interpretation of these spectra.

Clarification of the effects of Jahn-Teller coupling is not just of academic interest, but would be useful for the understanding of many impurity properties (see section three, this chapter).

Summary

The main points in this section were:

1) The detailed explanation of features seen in the various spectra.
2) The detection of some interesting anomalies.
3) The fact that some of the systems studied might repay theoretical investigation.

2) Antiresonance

Introduction

There are two usages of the term "antiresonance". The first is concerned with the interaction between a continuum of states and a discrete state whose energy is degenerate with the continuum. This meaning reflects the theoretical viewpoint. The second describes the actual dip or window measured experimentally, which is the form in which the practical physicist recognises the phenomenon.

In many instances it has not been found possible to link experimental data with a rigorous model, so that when "antiresonances" are detected, the subsequent analysis tends to be qualitative. This is possibly because these effects are seen rather as curiosities, or because the present theory is not adequate to encompass these rather high-order processes.

In this section previously published examples of antiresonances in solids will be given, and it will be seen that a rather superficial treatment is proffered in many cases. It is interesting to compare these approaches with the techniques of atomic physics [27].

It is recorded in passing that a formulation applying "a diagram method for group theoretic coupling calculations to the analysis of Feynman diagrams arising in the line shape problem" has been established by Stedman [93]. It is suggested that this technique may be potentially very useful.

Antiresonances in Solids

Antiresonances are most frequently recognised when the spectrum of a crystal contains a wide band, due to transitions to vibronically coupled states, which overlaps the position of a sharp line due to an electronic transition only weakly coupled to phonons. Thus Arkhangelskaya et al. [94] and Taylor [95] saw antiresonances due to sharp transitions in rare-earth ions in crystals. These crystals also contained vacancies which were colour centres with broad absorption bands in the same energy region as the sharp lines. When the two types of defect were close together in the crystal coupling between them produced interference effects in the absorption spectra. Similar features were recorded by van der Ziel for $Eu_3Ga_5O_{12}$:Pt [96], where the broad band of transitions due to Pt contains several antiresonances due to electronic lines of Eu. A discussion of the necessary conditions for experimental observation of such events is given by Iida [97]. He finds that it is necessary that a parameter Δ be large, where

$$\Delta = V_{int}/E_o \qquad (1)$$

V_{int} is the interaction matrix element between discrete and continuum states, E_o is the width of the broad band if coupling is to acoustic phonons,

but is the phonon energy if optical modes are involved.

Similar effects have been seen in materials containing transition metal impurities, when a sharp energy level of an impurity atom is degenerate with the vibronic band of another energy level of the same atom. Sturge has found that interaction between such states produces resonances with Fano line-shapes [41], although some of the parameters have a complicated energy dependence.

Transitions of shallow acceptors or donors in silicon occur at energies near those of optical phonons. It has been found that interference between the two types of excitation leads to asymmetry in the phonon spectrum seen in Raman scattering: the asymmetry lies to the high or low side of the peak depending on whether the material is n-type or p-type [98,99] (Cerdeira also saw similar effects in p-type silicon, doped with boron, involving localised vibrations of the impurity atoms [100].) Balkanski showed that the Raman scattering cross-section σ is given by

$$\sigma = \sigma_o \frac{(q + \varepsilon)^2}{(1 + \varepsilon)^2} \qquad (2)$$

and that q is negative for n-type material, positive for p-type [101]. Chandrasekhar et al investigated this effect in silicon doped with gallium acceptors, using uniaxial stress to shift the resonance energy [102]. Friedman and Hochstrasser show generally that interference effects may be expected frequently in resonance Raman spectroscopy [103], and some instances of this are quoted by Ohta and Ito [104a].

Vibronic Antiresonance

In this work several cases were found of coherent interference between impurity states resulting from coupling to different vibrational modes. They reveal themselves by dips or antiresonances in the optical absorption spectra, caused by a cancellation of the transition probabilities into the interacting vibronic states compared with those involving non-

coupled states. It is suggested that the forces responsible for the interaction are anharmonic, which would tend to be strong in the systems studied because of Jahn-Teller coupling.

No previous records of similar cases exist. In other types of system, however, the importance of phonon-phonon interaction has been known for a long time. An instance is the temperature dependent expansion of solids and the shifts in phonon energies which are explained only as signs of phonon interaction, for example with a model of a lattice with anharmonic forces [105]. A more directly comparable situation, in a pure material, was reported by Barker after he recorded phonon spectra by infra-red absorption and Raman scattering [42]. He found that the asymmetric shape of a TO(Γ) sideband was due to coupling to a two-phonon mode composed of one TA(X) and one LA(X) phonon.

A theoretical paper by Martin deals with the situation where a defect of different mass and charge from the host atoms is present in a crystal [106]. He shows that there are conditions when "the dipole moment of the crystal changes sign" and the absorption due to impurity-induced vibrational transitions is exactly zero. Experimentally this might be interpreted as a local mode in resonance with the host phonon continuum. Henry et al have reported that in emission from bound excitons, structure due to both localised and free optical modes may be seen [107]. The two species are coupled by a process involving virtual ionization of the centre.

In the systems studied in this thesis the interpretation is largely empirical. In the cases of ZnSe:Ti and ZnS:Ti there is especially strong interaction between the TO(Γ) phonon and a sum of four TA(L) modes, suggesting some form of selection rule applies to the coupling of phonons of different symmetry and wave number. The nature of the modes involved

is not clear; they may be local modes or if the Jahn-Teller coupling involves many frequencies of vibration, as suggested by the increasing width of phonon replicas with energy, the antiresonances may be interpreted as the decay of virtual states involving quasi-localized phonons. It is also shown that the parameters obtained by fitting to Fano's formula cannot be interpreted simply, but depend on the form of the continuum, which is often unknown.

Impurities with internal degrees of freedom can affect the thermal conductivity of the host very strongly. The internal modes might be localised vibrational excitations. This is discussed at length in the review by Narayanamurti [31]. A well known example is ZnS:Fe [108]. In this system, however, it is spin-orbit splitting of the iron ground state that leads to resonant scattering of acoustic phonons. Jahn-Teller splitting may produce similar effects.

The optical modes which produce antiresonances in the measured spectra are not expected to interact strongly with impurities. However the impurity-induced resonant coupling with acoustic modes means that scattering of optical phonons could become possible. This could lead to changes in thermal conductivity. Optical phonon scattering might also be important in determining relaxation times for reorientation between different distorted configurations, since the energy of one optical phonon may be as large as several acoustic quanta. Thus although in thermal equilibrium there will be fewer optical phonons excited, it may be more likely for a one optical phonon induced transition between wells to occur than a multi-phonon acoustic scattering process.

It would be interesting to know if these processes do exist, and if they have significant roles in any materials.

Electronic Antiresonance

Only a brief mention will be made of this topic, since the results reported in this work are wholly negative.

In many substances there are sharp lines at low temperatures due to transitions which do not, to first order, involve the creation of phonons. If the final state of such a transition is degenerate with the conduction band, then antiresonance could be possible. Since this process would lead to ionization of the centre, it is also called autoionization.

An example of a system where this has been seen is $Kr:C_6H_{12}$ [109]. Here a weak, sharp transition between localised electronic states of the benzene molecule is degenerate with ionizing transitions between the benzene ground state and the krypton conduction band. Antiresonances are detected whose width indicates that autoionization of the excited states of benzene occurs within 1.7×10^{-14} seconds of the initial absorption.

It is also known from a wide range of materials that resonance states exist when donors or acceptors have levels associated with different bands, so that levels below one band extremum may be degenerate with another [110]. The discrete states are not core-like, but may have energies in agreement with an effective mass model [111]. In this last reference, Onton finds the half-width of a 2p state in the gap of GaP to be 0.6 meV, so that τ is about 1.1×10^{-12} seconds, where

$$\tau = \hbar \; / \; [\text{half-width}] \qquad (3)$$

A 2p state lying in the conduction band has a width of 20 meV, and a lifetime of 3×10^{-14} seconds.

Another system showing particularly strong interference effects is GaP:N [112]. In this case the antiresonances arise from the degeneracy of the conduction band with phonon-coupled states of an exciton bound at a nitrogen state. Altarelli has studied such systems theoretically, and shows that the typical Fano shape is to be expected [113].

Resonant coupling involving excitons has also been seen in SiC, and shows up as "transparency lines" [114].

The lifetimes of states in ZnSe:Ti and ZnS:Ti known to lie in the conduction bands are not less than 2×10^{-12} seconds.

Since a large part of any broadening of zero phonon lines is due to strains produced by crystal inhomogeneity, the lifetime for autoionization is certainly much too great to give any measurable effect in the absorption spectra of these materials. Other evidence presented in chapter six seems to refute earlier findings of autoionization with a short lifetime in these and other systems.

The reasons why autoionization is not more apparent are not known. Shibatani et al have studied the possibility of autoionization in such systems, but reach only general conclusions [115].

There are similarities between the existence of an excited transition metal impurity state in a conduction band, and the virtual bound states in alloys, described by Friedel [29]. These are discussed in chapter four. A recent review points out that Friedel's approach is in some ways equivalent to a particular formulation of the Anderson Hamiltonian [116]. This latter method is applied by Haldane and Anderson [82] and Fleurov and Kikoin [112] to the problem of deep levels of transition metal impurities. It is shown that there is considerable mixing between crystal states and the d-levels of these centres.

The interaction producing autoionization should link the d-levels to the orbitals of atoms in the crystal further away than nearest neighbours. It should be greater for materials where the crystal field is strong, so that transition metals in III-V or group IV materials may be more likely to shown signs of autoionization. However it may be that the vibronic interactions which produce distorted configurations, and which also may result in extremely large reductions in matrix elements of interactions between different electronic states, are the dominant factor in suppressing autoionization. Thus electronic states of symmetry A_1 or A_2 may be worthy of close study in this context, because they do not undergo Jahn-Teller coupling.

3) Photoionization

Introduction

Crystal field theory successfully accounts for the separations of impurity levels because these depend mainly on the electronic wave-functions of the impurity and a few parameters which can be found experimentally.

To calculate these parameters it would be necessary to consider in detail the interactions between the impurity atom and the atoms of the surrounding lattice. It is largely these interactions which determine the binding energies of impurity electrons with respect to the crystal bands, so that the energy required to ionize a transition metal impurity is much less than for the free atom or ion.

The covalency mixing of impurity and crystal wavefunctions greatly influences binding energies. The effect of this has to be disentangled from the results on experimental data of dielectric screening due to the bulk medium. The interpretation of details such as spin-orbit splittings which might enable the relative influence of these effects to be

determined is hampered by the presence of perturbations such as Jahn-Teller coupling.

Calculations on the Anderson hamiltonian [82,117] may lead to a full understanding of impurity properties, and of binding energies in particular. However these models are at an early stage; for example neither of the references cited above includes the effects of crystal fields.

To proceed with this approach much more relevant data is required. Chapter seven indicates some materials and impurities that have been studied in order to find ionization energies. Most transition metal systems have not been studied in detail. Even in the case of nickel, about which perhaps most is known, there is often uncertainty in the literature about the exact threshold energy, or even about which crystal band is involved.

Results

As has been shown in this thesis the measurement of optical absorption bands associated with photoionization can remove at least the first of these problems. Since Lucovsky derived a formula for the absorption cross section of deep impurities [118] several authors have sought to improve his model. References to these are to be found in a recent paper by Grimmeiss and Ledebo [119]. It appears that the Lucovsky model, using a δ-function potential is quite accurate for deep levels, although a core region of non-zero width gives better agreement for shallower levels. All models derive simple power laws for the absorption cross-section close to threshold.

In ZnSe:Ni (d^8) and ZnS:Ni (d^8) bands corresponding to photo-ionization transitions are seen with absorption, σ, close to threshold given by

$$\sigma \alpha (E-E_I)^{3/2} \qquad (4)$$

Thus the ionization energies were found quite simply.

Previous workers suggested that these transitions involve the valence band of the host crystal,

$$d^8 + h\nu \rightarrow d^9 + (\text{hole}) \qquad (5)$$

but did not give completely certain proof [63-6,84]. In this present research it has been found that the photoionization band seen in material containing nickel (d^8), is not present in conducting n-type ZnSe:Ni. Instead a band appears at lower energy, again described by equation (4) but with a different value of threshold.

This latter band has been studied by Szawelska and Allen using photocapacitance and it is seen to involve a transition to conduction band states [83]. In addition the internal transition of nickel (d^9) is seen.

The energies of the two ionization thresholds found when nickel is present as (d^8) in heavily nickel-doped ZnSe or as (d^9) in n-type ZnSe add up to only 0.1 eV more than the band gap. This is consistent with the weak phonon coupling seen in the photoionization band of nickel (d^8), which is therefore identified as being due to the transition of equation (5) above A similar ascription is made for ZnS:Ni (d^8).

One effect of phonon coupling is to produce an Urbach-like absorption tail below threshold, in ZnSe:Ni at least. The reason for this is not clear: models have recently appeared which predict a different form for the phonon-coupled absorption [71,72,120,121]. The agreement with experiment of these models is said to be good, but in fact is rather weak in the region below threshold, which is where they should be most critically tested. It will be interesting to study other systems to clear up this problem.

A model of photoionization has been developed which shows that the shape of an absorption band may be strongly affected by the parity of

the initial localised electronic state [69]. For a pure d-state there should be a difference in the power dependence of absorption cross-section on energy above threshold, for transitions to valence or conduction bands. In the case of ZnSe:Ni this has not been seen. Parity is not a good quantum number for impurity d-states because of mixing with crystal states.

The fine structure seen in ZnSe:Ni (d^8) and ZnS:Ni (d^8) near ionization threshold had been published previously by other workers, who ascribed it to bound hole-states, with binding energies of some 150 meV. In the present work the identification of the photoionization bands supports this, but the binding energies are found to be appreciably smaller, and more typical of hydrogenic acceptor levels. Phonon coupling to these states is much stronger than for the ionization bands, and is typical of more localised charge distributions.

Summary

It has been shown that measurements of photoionization can lead to accurate values of ionization energies for deep impurities. The interpretation of data is quite simple, although absorption measurements on their own are not sufficient to determine the sign of the charge transfer.

There is much useful work to be done merely gathering this type of data, which should lead to a better understanding of the properties of deep impurities. The role of phonon coupling is another interesting problem which remains to be solved.

APPENDIX

REVIEW OF REPORTED PHONON ENERGIES

Phonon Energies

The energies of critical point phonons and the shapes of dispersion curves may be found in several different ways. These frequently produce conflicting results, although it seems that inelastic neutron scattering can produce the least ambiguous data.

Tables 1 and 2 give the results of several studies on ZnSe and ZnS. The most recent assignments are believed to be correct, and the energies accurate to within 5%.

It is important to note that the vibronic peaks seen in absorption or emission impurity spectra do not involve exclusively phonons from the critical points of the host lattice. This may lead to wide phonon sidebands, with peak energies characteristic not just of the host, but also depending on the specific impurity. This may be seen by comparing the energies of phonon sidebands in a few materials: ZnS:Mn [124], ZnS:Co [122], ZnS:Ni [35,61] and ZnS:Cu [125,126]. See also reference [127].

ZnSe: Table 1

Symmetry point	Mode	Energy (cm^{-1})					
X	LA	190	194			149	140[1]
	TA	70	70			70.5	69[1]
	LO	223	213			225	224[1]
	TO	206	219			210	208[1]
L	TO	206					
	LO	244	234				
	TA[2]	58	57				
	LA	181	166				
Γ	TO	207	213	204	211		205
	LO	250	253	254	257		250
	PDS[3]		70				
		160	170				
		206					
		220	230				
Reference		(c)	(d)	(a)	(a)	(a)	(b)
Temperature (°K)		300	300	300	80	21	300

1. These values are arrived at by applying the method of (a) to analyse the data. Thus the second order peak at 364 cm^{-1} is ascribed to LO + LA
   " 138 cm^{-1} " 2TA
   " 415 cm^{-1} " 2TO
   " 219 " LA + TA

2. Vallin et al. [129] give TA(L) = 49 cm^{-1}.

3. PDS stands for "Peak in the one-phonon Density of States".

References for ZnSe

(a) Infra-red absⁿ and reflection:

A.Hadni, J.Claudel and P.Strimer, Phys.Stat.Sol.26,241 (1968).

(b) Raman scattering: 1st and 2nd order:

W.Taylor, Phys.Lett. 24A, 556 (1967).

(c) 2nd order Raman scattering:

J.C. Irwin and J.Lacombe, Can.J.Phys. 50, 2596 (1972).

(d) Inelastic neutron scattering:

B.Hennion, F. Mousa, G.Pepy and K.Kunc,

Phys.Lett. 36A, 376 (1971).

ZnS: Table 2

Symmetry point	Mode	Energy (cm^{-1})					
X	LA	210	222	215	155	190	211
	TA	90	93	92	93	115	88
	LO	330	304*	331	339	339	333
	TO	320	338*	318	298	298	306
L	TO	290	342*				297
	LO	340	312*				339
	TA	70	73				70
	LA	195	179				193
Γ	TO	280	271		312		271
	LO	350	352		377		352
PDS		80					
		200					
		300					
		300					
Reference -		e	f	g	h		i
Temperature (°K)		300	300	300	300		-

* The optic frequencies and assignments are not reliable.

References for ZnS

(e) Inelastic neutron scattering:
N.Vagelatos, D.Wehe and J.S.King, J.Chem.Phys.60,3613 (1974).

(f) Inelastic neutron scattering:
L.A.Feldkamp, G.Venkataraman and J.S.King,
Sol.State Comm.7, 1571 (1969).

(g) Infra-red absorption (2 phonon spectrum):
E.A.Kuasniewski, E.S.Koteles and W.R.Datars,
Can.J.Phys. 54, 1053 (1976).

(h) Infra-red absorption:
R.Marshall and S.S.Mitra, Phys.Rev. 134, A1019 (1964).

(i) Analysis of Raman and infra-red spectra:
J.C.Irwin, Can.J.Phys.48, 2477 (1970).

References

References

1. J.C. Phillips, Bonds and Bands in Semiconductors. (New York:London,1973).
2. R.Boyn and G.Ruszczynski, Phys.Stat.Sol.(b) 48,643 (1971).
3. K.Kocot and J.M.Baranowski, Phys.Stat.Sol.(b)59,K11(1973).
4. A.M. Hennel, Phys.Stat.Sol.(b)72,K9 (1975).
5. E.M. Wray and J.W. Allen, J.Phys.C4, 512 (1971).
6. D.H.Martin, Magnetism in Solids (London,1967).
7. D.S.McClure, Sol.State Phys.9,399 (1959).
8. J.S.Griffith, The Theory of Transition Metal Ions (Cambridge, 1964).
9. A.D. Liehr and C.J.Ballhausen, Ann.Phys.6,134 (1959).
10. A.M.Stoneham, Theory of Defects in Solids (Oxford, 1975).
11. J.W.Allen and G.L.Pearson, Transition Metal Impurities in Semiconductors (Stanford Electronics Laboratories: Technical Report No.5115-1, June 1967).
12. R.C. Newman, Infra-red Studies of Crystal Defects (London,1973).
13. R.Englman, The Jahn-Teller Effect in Molecules and Crystals (London,1972)
14. Y.Toyozawa, J.Lum.1,2, 732 (1970).
15. D.B. Fitchen, in Physics of Colour Centres, ed.W.B.Fowler, (Academic Press, 1968).
16. M.D. Sturge, Sol.State Phys.20,91 (1967).
17. J.F. Cornwell, Group Theory and Electronic Energy Bands in Solids (London:North-Holland, 1969).
18. H.A. Jahn and E.Teller, Proc.Roy.Soc.A161, 220 (1937).
19. U.Opik and M.H.L. Pryce Proc.Roy.Soc.A238, 425 (1957).
20. M.D.Sturge, pp 114-115 of Sol.State Phys.20, 91 (1967).
21. K.K. Rebane, Impurity Spectra of Solids (trans.) (London,1970).
22. E.D. Trifonov, Sov.Phys.Sol.State 6, 366 (1964).
23. C.H.Henry and C.P.Slichter, in Physics of Colour Centres, ed. W.B.Fowler (Academic Press, 1968).
24. F.S.Ham, Phys.Rev. 138, A1727 (1965).

25. J.A. Sussmann, J.Phys.Chem.Solids 28,1643 (1967).

26. H.von Buttlar, Nuclear Physics (Academic Press, 1968)
S. Gasiorowicz. Elementary Particle Physics (John Wiley, 1966).

27. D.R.Herrick and O.Sinanoglu, Phys.Rev.A11,97 (1975).
L.Lipsky and M.J.Conneely, Phys.Rev.A14, 2193 (1976).

28. U.Fano, Phys.Rev.124, 1866 (1961).

29. J.Friedel, Can.J.Phys.34,1190 (1956).
" Journal de Physique 19, 573 (1958).
" Journal de Physique 23, 692 (1962).

30. M.J.Taylor, Phys.Rev.Lett.23, 405 (1969).
F.Cerdeira, T.A.Fjeldly and M.Cardona, Phys.Rev.B8, 4734 (1973).

31. V.Narayanamurti and R.O.Pohl, Rev.Mod.Physics 42, 201 (1970).

32. M.Aven and H.H.Woodbury, App.Phys.Lett.1, 53 (1962).

33. R.Boyn, J.Dziesiaty and D.Wruck, Phys.Stat.Sol.(b) 42,K197 (1970).

34. A.Rosenfeld, R.Boyn and G.Ruszczynski, Phys.Stat.Sol.(b) 70,601(1975).

35. U.G. Kaufmann and P.Koidl, J.Phys.C7, 791 (1974).

36. K.Cho, J.Phys.Soc.Japan 25,1372 (1968).

37. M.Caner and R.Englman , J.Chem.Phys.44, 4054 (1966).

38. K.Huang and A.Rhys, Proc.Roy.Soc.A204, 406 (1950).

39. Y.Toyozawa and M.Inone, J.Phys.Soc.Japan 21, 1663 (1966).

40. A.Fukuda, S.Makishima, T.Mabuchi and R.Onaka, J.Phys.Chem.Solids 28
1763 (1967).

41. M.D.Sturge, H.J.Guggenheim and M.H.L. Pryce, Phys.Rev.B2, 2459 (1970).

42. A.S.Barker, Phys.Rev.165,917 (1968).

43. V.V.Artamonov, M.Ya.Valakh and G.S.Oleinik, Opt.Spect.40,583 (1976).

44. M.Ya.Valakh, M.P.Lisitsa, N.E.Novoseletskii and A.M.Yaremko, Sov.
Phys.Sol.State 14,702 (1972).

45. R.Beserman, C.Hirlimann and M.Balkanski, Sol.State Comm:20,
485 (1976).

46. N.D. Stramm in Proc.Conf.Light Scattering Spectra in Solids, New York, 1968 (p455).

47. J.Ruvalds and A.Zawadowski, Phys.Rev.B2, 1172 (1970).

48. J.M. Baranowski, J.M. Langer and S.Stefanova, Proc.11th Int.Conf. on Physics of Semiconductors, Warsaw (PAN Warsaw, 1972).

49. K.Nasu and T.Kojima, Prog.Theo.Physics 51, 26 (1974).

50. S.Shionoya, T, Koda, K.Era and H.Jufiwara, J.Phys.Soc.Japan 19, 1157 (1964).

51. I.B.Ermolovich, G.I.Matvievskaja and M.K.Sheinkman, J.Lum 10, 58 (1975).

52. E.W.Williams and C.T.Elliott, J.Phys.D2,1657 (1969).

53. S.Iida, J.Phys.Soc.Japan 25, 177 (1968).

54. S.Brandt and P.Jaszczyn-Kopec, J.Lum 11, 381 (1976).

55. G.Jones and J.Woods, J.Phys D6, 1640 (1973).

56. P.W.M. Jacobs and S.A.Thorsley, J.Lum 8, 391 (1974).

57. J.M.Langer and J.M.Baranowski, Phys.Stat.Sol(b) 44,155 (1971).

58. H.A. Weakliem, J.Chem.Phys.36,2117 (1962).

59. R.K.Watts, Phys.Rev.188, 568 (1969).

60. W.C.Holton, J.Schneider and T.L.Estle, Phys.Rev.133, A1638 (1964).

61. U.G.Kaufmann, P.Koidl and O.F.Schirmer, J.Phys.C6,310 (1973).

62. R.Loudon, Proc.Phys.Soc.84,379 (1964).

63. S.A.Kazanskii and A.I.Ryskin, Opt. and Spec.31,325 (1971).

64. " " Sov.Phys.Sol State 13,3153 (1972).

65. " " Sov.Phys.Sol.State 13, 3065 (1972).

66. " " Sov.Phys.Sol.State 14, 1571 (1972).

67. S.A.Permogorov, A.N.Reznitskii and V.A.Kazennov, Opt.and Spec.32, 392 (1972).

68. Ya.I.Vertsimakha, Yu.P.Gnatenbo and A.Kh.Rozhko, Sov.Phys.Sol.State 16, 2236 (1975).

69. J.W.Allen, J.Phys.C2, 1077 (1969).

70. H.Kukimoto, C.H.Henry and F.R.Merritt, Phys.Rev.B7, 2486 (1973).

71. A.A.Kopylov and A.N.Pikhtin, Sov.Phys.Semicon.10 7 (1976).

72. " " Sov.Phys.SollState 16, 1200 (1975).

73. M.Z. Cieplak, M.Godlewski and J.M.Baranowski, Phys.Stat.Sol.(b) 70, 323 (1975).

74. A.Baldereschi and N.O.Lipari, Phys.Rev.B9, 1535 (1974).

75. G.Sperlich and H.Muller, Phys.Stat.Sol..(b) 71, 305 (1975).

76. H.H.Woodbury and M.Aven, Phys.Rev.B9, 5195 (1974).

77. P.Lavaetz, Phys.Rev.B4, 3464 (1971).

78. S.P.Gaur, J.F.Vetelino and S.S.Mitra, J.Phys.Chem.Solids 32, 2737 (1971).

79. J.J.Hopfield, J.Phys.Chem.Solids 10, 110 (1959).

80. H.Frohlich, H.Pelger and S.Zienan, Phil.Mag.41,221 (1950).

81. T.C.Lee and W.W.Anderson, Sol.State.Comm.2, 265 (1964).

82. F.D.M. Haldane and P.W.Anderson, Phys.Rev.B13,2553 (1976).

83. H.R.Szawelska and J.W.Allen, J.Phys.C. (to be published).

84. S.A.Kazanskii and A.I.Ryskin, Opt. and Spec.33, 146 (1972).

85. J.M.Langer, Phys.Stat.Sol.(b) 47 , 443 (1971).

86. Y.Tanabe and H.Kamimura, J.Phys.Soc.Japan 13, 394 (1958).

87. S.Sugano and Y.Tanabe, J.Phys.Soc.Japan 13,880 (1958).

88. R.S.Anderson, Phys.Rev.164,398 (1967).

89. F.S.Ham, W.M.Schwarz and M.C.M. O'Brien, Phys.Rev.185, 548 (1969).

90. P.Koidl, Phys.Stat.Sol.(b) 74, 477 (1976).

91. B.Helperin, J.Phys.C9, 4139 (1976).

92. M.Bacci, A.Ranfagni, M.P.Fontana and G.Viliani, Phys.Rev.B11, 3052 (1975).

93. G.E.Stedman, J.Phys.C9, 535 (1976).

94. V.A.Arkhangelskaya and P.P.Feofilov, Opt. and Spec.28, 657 (1970).

95. M.J.Taylor, Phys.Rev.Lett.23, 405 (1969).

96. J.P.van der Ziel and L.G. van Uitert, Phys.Rev. B8, 1835 (1973).

97. T.Iida and M.Aegerter, Phys.Stat.Sol.B69, 527 (1975).

98. F.Cerdeira, T.A.Fjeldly and M.Cardona, Phys.Rev.B8, 4734 (1973).

99. M.Jouanne, R.Beserman, I.Ipatova and A.Subashiev, Sol.State Comm.16, 1047 (1975).

100. F.Cerdeira, T.A.Fjeldly and M.Cardona, Phys.Rev. B9, 4344 (1974).

101. M.Balkanski, K.P.Jain, R.Beserman and M.Jouanne, Phys.Rev.B12, 4328 (1975).

102. H.R.Chandrasekhar, A.K.Ramdas and S.Rodriguez, Sol.State Comm.18, 405 (1976).

H.R.Chandrasekhar, A.K.Ramdas and S.Rodriguez, Phys.Rev.B14, 2417 (1976).

103. J.Friedman and R.M.Hochstrasser, Chem.Phys.Lett.32,414 (1975).

104. N.Ohta and M.Ito, J.Chem.Phys.65, 2907 (1976).

105. P.L.Taylor, A Quantum Approach to the Solid State (Englewood Cliffs, N.J. 1970).

106. T.P.Martin, Phys.Rev.170, 779 (1968).

107. C.H.Henry and J.J.Hopfield, Phys.Rev.B6, 2233 (1972).

108. V.P.Srivastava and G.S.Verma, Phys.Rev.B10, 219 (1974).

F.S.Ham and G.A.Slack, Phys.Rev.B4, 777 (1971).

109. E.S.Pysh, S.A.Rice and J.Jortner, Phys.Rev.Lett.15, 289 (1965).

110. F.Bassani, G.Iadonisi and B.Preziosi, Rep.Prog.Phys.37, 1099 (1974).

F Bassani, G. Iadonisi and B.Preziosi, Phys.Rev.186, 735 (1969).

C.H.Henry, J.Lum.12/13, 47 (1976).

111. A.Onton, Phys.Rev.B4, 4449 (1971).

112. J.J.Hopfield, P.J. Dean and D.G.Thomas, Phys.Rev.158, 748 (1967).

113. M.Altarelli, Phys.Rev.B11, 5031 (1975).

114. V.A.Kiselev, B.V.Novikov, M.M.Pimonenko and E.B.Shadrin, Sov.Phys. Sol.State 13, 926 (1971).

115. A.Shibatani and Y.Toyozawa, J.Phys.Soc.Japan 25,335 (1968).

116. G.Gruner and A.Zawadowski, Rep.Prog.Phys.37,1497 (1974).

117. V.N.Fleurov and K.A.Kikoin, J.Phys.C9,1673 (1976).

118. G.Lucovsky, Sol.State Comm.3, 299 (1965).

119. H.G.Grimmeiss and L.-A.Ledebo, J.Phys.C8, 2615 (1975).
see also
R.A.Chapman and W.G.Hutchison, Phys.Rev.157,615 (1967).
J.W.Walker and C.T.Sah, Phys.Rev.B8, 5597 (1973).
W.J.Brown, D.A.Woodbury and J.S.Blakemore, Phys.Rev.B8,5664 (1973).

120. S.F.Timashev, Sov.Phys.Sol.State 14,2267 (1973).

121. L.A.Bakaleinikov, S.V.Bulyarskii, N.S.Grushko and A.A.Gutkin, Sov.Phys.Semicon.10,216 (1976).

122. P.Koidl, O.F.Schirmer and U.G.Kaufmann, Phys.Rev.B8,4926 (1973).

123. T.Ray and J.R.Reguard, Phys.Rev.B9,2110 (1974).

124. D.Langer and S.Ibuki, Phys.Rev.138, A809 (1965).

125. H.Maier and U.Scherz, Phys.Stat.Sol.(b)62,153 (1974).

126. T.Yamaguchi and H.Kamimura, J.Phys.Soc.Japan 33, 953 (1972).

127. M.Zigone, R.Beserman and M.Balkanski, J.de Physique C3,153 (1974).

128. J.M.Hollas, Symmetry in Molecules (Chapman and Hall, London 1972).

129. J.T.Vallin, G.A.Slack, S.Roberts and A.E.Hughes, Phys.Rev.B2, 4313 (1970).

130. J.C.Irwin and J.La Combe, Can.J.Phys.50,2596 (1972).

131. D.Beaglehole, Phys.Rev.B14, 314 (1976).

132. D.G.Thompson, A.Hibbert and N.Chandra, J.Phys B7,1299 (1974).

133. P.G.Burke and D.L.Moores, J.Phys B1,575 (1968).

134. R.E.Huffman, Y.Tanaka and J.C.Larrabee, J.Chem.Phys.39,902 (1963).

135. T.W. Ludwig and H.H.Woodbury, Solid State Physics 13, 223 (1962).

136. R.Bottcher and J.Dziesiaty, Phys.Stat.Sol.(b) 57 , 617 (1973).

137. R.K.Watts, Phys.Letts.27A, 469 (1968).

138. P.A.Slodowy and J.M.Baranowski, Phys.Stat.Sol.(b) 49, 499 (1972).

139. S.A. Kazanskii, A.J.Ryskin and G.J.Khil'ko, Sov.Phys.Sol.State 10, 1899 (1969).

140. R.Parrot, C.Naud and F.Gendron, Phys.Rev.B13, 3748 (1976).

141. B.Lambert, T.Buch and A.Geoffroy, Phys.Rev.B8, 863 (1973).

142. H.A.Bethe, Ann.Physik 5, 133 (1929).

143. M.C.M.O'Brien, J.Phys C4, 2524 (1971).

144. M.C.M.O'Brien, Phys.Rev.187, 407 (1969).

145. J.T. Vallin, G.A. Slack, S.Roberts and A.E.Hughes, Phys.Rev.B2, 4313 (1970).

146. B.Bacci, M.P.Fontana, A.Ranfagni and G.Viliani, Phys.Letts.50A, 405 (1975).

147. M.Bacci et al., Phys.Rev.B11, 3052 (1975).